12-1-2017

Surface Hydrologic Modeling and Analyzing Watershed Hydrologic Response to Landcover Change

Roshan Poudel
University of Nevada, Las Vegas, roshanlaiemail@gmail.com

SURFACE HYDROLOGIC MODELING AND ANALYZING WATERSHED HYDROLOGIC RESPONSE TO LANDCOVER CHANGE

By

Roshan Poudel

Bachelor of Science in Civil Engineering (Specialization: Hydropower)
Kathmandu University
2013

A thesis submitted in partial fulfillment
of the requirement for the

Master of Science in Engineering – Civil and Environmental Engineering

Department of Civil and Environmental Engineering and Construction
Howard R. Hughes College of Engineering
The Graduate College

University of Nevada, Las Vegas
December 2017

UNLV | GRADUATE COLLEGE

Thesis Approval

The Graduate College
The University of Nevada, Las Vegas

August 18, 2017

This thesis prepared by

Roshan Poudel

entitled

Surface Hydrologic Modeling and Analyzing Watershed Hydrologic Response to Landcover Change

is approved in partial fulfillment of the requirements for the degree of

Master of Science in Engineering – Civil and Environmental Engineering
Department of Civil and Environmental Engineering and Construction

Haroon Stephen, Ph.D.
Examination Committee Chair

Kathryn Hausbeck Korgan, Ph.D.
Graduate College Interim Dean

Sajjad Ahmad, Ph.D.
Examination Committee Member

Jacimaria Batista, Ph.D.
Examination Committee Member

Ashok Singh, Ph.D.
Graduate College Faculty Representative

ABSTRACT

Urban flooding is the most frequently occurring disaster in rapidly urbanizing cities. Rapid urbanization in general, is characterized by an increase in the total impervious surface area, which means less soil cover for the stormwater to infiltrate and a greater volume of runoff from the area in case of a storm event. This increased volume of surface runoff, if not drained, results in urban flooding. Urban flooding can cause serious economic and environmental damages by disrupting transportation and spreading pollution. It is therefore, essential to understand the cause, behavior and effects of urban flooding so as to minimize the risks and costs associated with urban floods.

Hydrologic models are useful tools for understanding hydrologic processes and for designing urban stormwater drainage infrastructure to reduce the risks of floodings. This research aims to study urban hydrology by estimating surface runoff from an urban area using an event based distributed parameter hydrologic model. In this research, an event-based distributed parameter hydrologic model is developed, which uses Green-Ampt infiltration model to estimate the surface runoff from a given catchment. The developed model is tested on two small catchments. The 'rainfall-runoff modeling' part of the developed model is calibrated for the rainfall events of May 22, 2017 and, May 24, 2017 over the Moores Run study area, and, validated for the rainfall event of April 17, 2017. The 'flood-modeling' part of the developed model is validated for the rainfall event of Sep 11, 2012 over the Parking-lots area at UNLV. The results of the rainfall-runoff simulation and flood depth and extent estimation for different land-cover change scenarios over the Parking-lots catchment is also provided.

The testing on Moores Run study area resulted in calibration at 30-m resolution DEM and a hydraulic conductivity value of 0.19 cm/hr. for soil group D. The error in the model's estimation of the catchment area is 7.75%. The model over-predicted the runoff volume from the catchment for the first rainfall event while under-predicted the runoff volume from the catchment for the second rainfall event. The average error in estimation of the runoff volume is 1.8%. The model also over-predicts the 'time-to-peak' and under-predicts 'peak runoff' in both cases. The average of RMSE between the predicted hydrograph and actual hydrograph for the two rainfall events is 0.0071 m^3/s in calibration, and, 0.011 m^3/s in validation. The testing on UNLV Parking-lots area resulted in calibration at 10-m resolution DEM. For the rainfall event of Sep 11, 2012, the model predicts over predicts the peak flood depth and under-predicts the maximum extent of flooding. The error in flood depth estimation is found be 12.9%. From watershed hydrologic response to landcover change analysis, it is observed that Manning's roughness coefficient doesn't affect the total volume of runoff, however, the time to peak is significantly delayed for landcover with higher values of Manning's roughness co-efficient.

This research provides an insight into surface hydrologic modeling. It also provides an overview of calibration against DEM resolution and hydraulic conductivity values. Finally, it provides an understanding of watershed hydrologic response to different landcovers with various Manning's roughness values.

DEDICATION

I would like to thank Dr. Haroon Stephen for guiding me throughout my research and for helping me to write this thesis. I also express my appreciation towards Dr. Sajjad Ahmad, Dr. Jacimaria Batista, and, Dr. Ashok Singh. I want to express my gratitude to Masih Edalat for his continuous help in my research. I also want to express my gratitude to Cabel Shrestha for his guidance and support throughout my graduate studies. Further, I would also like to thank my family and friends. I wouldn't be where I am without their help.

TABLE OF CONTENTS

LIST OF TABLES

LIST OF FIGURES

CHAPTER 1: INTRODUCTION

The study of water fluxes in urban watersheds has gained importance in recent years because of growing concerns about water sustainability and droughts in urban areas with subsequent economic, public-health and flooding impacts. Flooding in urban areas is a serious and growing problem. According to Khan et al. (2011), every year floods cause serious loss of human lives and severe economic damages throughout the world. The National Weather Service (US Department of Commerce) reported 373 flood fatalities and an estimated economic loss of about $20 billion from 2010 to 2015 in the USA alone. The city of Las Vegas experienced unusually severe flash flood storms on 8 July 1999 (J. Li, 2003) - around 70 mm of rainfall, which amounts to 35%–70% of the average annual precipitation (100 mm or 4 in) within a brief period of 60–90 min. The intense downpour caused one of the worst flooding in Las Vegas resulting in the deaths of two people and property damage of about $20 million (J. Li, 2003).

Hydrologic models are increasingly used to simulate hydrologic processes and study floods in complex watersheds (Todini, 1988). In urban areas, they are commonly used as a management tool and for designing stormwater drainage infrastructure. Hydrologic models are simplified representations of hydrology, primarily used for understanding underlying processes and simulate potential scenarios. Hydrologic processes include precipitation, interception, depression storage, surface runoff, subsurface runoff, evapotranspiration, channel flow, and groundwater flow. Hydrologic models are classified based on the aspect of the hydrological cycle they address e.g. rainfall-runoff models. Runoff models are the mathematical models that describe the rainfall-runoff relations of a rainfall catchment area. Runoff models can be used to predict increment in

the surface runoff from an urban area due to change in factors governing the surface water flux. The conceptualization of the water fluxes is essential for understanding the hydrological behavior of an urbanized catchment. Hydrologic models can simulate various fluxes (runoff) from a watershed for different real and hypothetical scenarios of rainfall events. This information is vital in understanding and devising plans to reduce floods. Further, they can also be used to analyze the capacity of the existing stormwater drainage infrastructure in an urban area.

Modeling of stormwater runoff in urban areas is complex because of heterogeneous landcover and changing overland flow paths due to newer constructions. However, recent advances in remote sensing and computing power have resulted in increased use of distributed numerical models to understand and study floods (Hunter, 2007). Typically, two types of hydrologic models - lumped models and distributed models, are used to model a flood. Distributed models allow the simulation of flood in 'as realistic as possible' manner (Gomes-Pereira, and, Wicherson 1999, Beven, 2001). Such models coupled with a long time-series of historical data that relates stream flows to measure past rainfall events are used to produce the discharge hydrographs from catchments. For example, a distributed model based on Green-Ampt infiltration equation and Continuity equation could be applied to estimate runoff from some selected catchments within the Back River watershed. Lumped models, however, are limited in their capacity to map the spatio-temporal behavior of floods in urban watersheds (Kilgore, 1997). They lack the capability to incorporate a variety of spatially varying data from different datasets on high resolution precipitation, soil characteristics, land use etc. (Carpenter et. al., 2006). A universal model applicable in all types of catchment would be difficult to create as hydrologic process vary with region and even within the same region at different times.

Hydrologic processes in different catchments vary because of the difference in catchment properties like soil surface roughness, land cover, and, hydraulic conductivity. Precise estimation of such catchment properties is imperative for the models to be able to correctly simulate the affected hydrologic processes (Zhang et al. 2010b). In particular, Manning's roughness coefficient for different land covers of a catchment is an important catchment property. All hydraulic computations involving flow require an understanding of the roughness characteristics of the surface over which the flow occurs (Barnes, 1967). Manning's roughness coefficient is needed to determine overland flow and flow in channels. While other equations like Darcy-Weisbach equation can also be used to calculate overland flow, it is seldom used in streamflow calculation and overall Manning's equation is preferred (Hessel et al. 2003).

This research aims to study urban hydrology by estimating surface runoff using an event-based distributed parameter hydrologic model. The hydrologic model is developed using a combination of Green-Ampt infiltration equation, Manning's equation for shallow flows, and Continuity equation. It is used to produce discharge hydrograph at the outlet of small catchments in Baltimore. The developed model is also used to analyze the change in surface runoff volume due to land cover change.

1.1) Research Motivation:

This research is undertaken for following reasons:

1. To identify the urban hydrological modeling practices.

Hydrological process in urban catchments are different from those in natural catchments because of the changes brought about by urbanization. Natural hydrological processes, such as infiltration and overland flow are altered, and new processes such as anthropogenic stormwater drainage flow, flow through manholes appear. Such alterations lead to a complex spatio-temporal interactions among hydrological processes. This research aims to understand some of the modeling practices and identify the practices that will reduce the uncertainties associated with hydrological modeling of urban watersheds.

2. To develop a simple physically based hydrologic model capable of simulating rainfall-runoff process.

Rainfall-runoff models have been used to produce hydrographs and peak discharge values for design purposes in medium to large watersheds (Pilgrim, 1986). However, recent rainfall-runoff models are complex in their structure due to the requirement of being physically based (Knapp et al., 1991). Todini (1988) found that the applications of several models have surpassed their limits of usability and more complex structure are being applied to the models for improved methods of representing model inputs. But at present, compared to the available data the level of model sophistication is significantly more developed (McPherson and Zuidema, 1977; Shafer and Skaggs, 1983; Pilgrim, 1986; Todini, 1988) rendering them cost ineffective and unnecessarily increasing their complexity. This research aims to develop a physically based model that is simple in its structure yet efficient enough to correctly simulate the rainfall-runoff process for the given a watershed.

1.2) Research Objectives:

The goal of this study is to understand flooding in urban areas. The main objectives of this research are as follows:

1. To develop a distributed parameter hydrologic model capable of simulating the rainfall-runoff process of an urban catchment.
2. To determine the relationship between Manning's roughness coefficient of urban surface and surface runoff using the model developed through Objective 1.
3. To provide a workflow for developing a Green-Ampt infiltration equation based on distributed parameter hydrologic model for urban catchments.

1.3) Research Approach:

1. Research approach for achieving Objective# 1:

The first objective of model development is achieved by developing a hydrologic model that simulates the rainfall-runoff event for an urban catchment. A physically based distributed parameter hydrologic model is developed, using the Green-Ampt infiltration equation to predict the infiltration within a given catchment for a given storm event. Moreover, combination of the continuity equation and Manning's equation is used to estimate overland flow. Only one runoff generation mechanism – the surface runoff is considered to determine the discharge from the catchment. This hydrologic model uses gridded DEM to delineate the catchment and identify the pour-point. The rainfall event and computational time is divided into a number of smaller time steps. The outflow from each grid cell for each time step is then computed by the hydrologic model

and the outflow from the pour-point cell is plotted against time to obtain a discharge hydrograph from the catchment.

2. Research approach for achieving Objective# 2:

This objective is achieved by changing the Manning's roughness values associated with selected pixels/regions of the catchment corresponding to different landcover change scenarios. Some examples of landcover change scenarios are changing the landcover from concrete to grassland and transformation of a residential area into a park. For each of the scenarios, discharge hydrographs is to be produced and compared to determine the relationship between Manning's roughness and surface runoff from the urban catchment.

1.4) Thesis Outline:

This thesis is organized as follows:

- Chapter 1 provides an introduction to the research problem, motivation and objectives of the research.
- Chapter 2 is the literature review and provides a description of the studies reviewed to conduct this research.
- Chapter 3 provides a description of the study area and the data used in this research.
- Chapter 4 includes the methodology for developing the Green-Ampt infiltration equation based hydrologic model.

- Chapter 5 highlights and explains the results for discharge hydrographs obtained from the developed hydrologic model.
- Chapter 6 summarizes the thesis by providing conclusions and recommendations for future study.

CHAPTER 2: LITERATURE REVIEW

This chapter includes a review of the studies consulted to conduct this research. As the first objective of this research is to develop a distributed parameter hydrologic model based on Green-Ampt infiltration model, the first part of this review discusses studies on urban hydrologic modeling and the use of Green-Ampt infiltration based hydrologic models, which is followed by an overview of the studies on the causes of urban flash flooding. A brief history of flash flooding in the two study sites of this research is also provided.

2.1) Urban hydrologic modeling

Hydrologic models are the watershed models that are used to study the rainfall-runoff relation of a watershed in connection to geography and geology. Watershed models have been extensively used from early times for flood control and drainage of stormwater. Recent advances in the field of satellite technology and remote sensing, GIS and database management systems have significantly improved the ability of urban watershed models to predict urban hydrology. These improvements in urban watershed models have made them an increasingly attractive tool to manage urban water systems for public health and sanitation, flood protection and more recently, for environmental protection. Despite the advances, many important challenges in urban watershed modeling still remain unresolved. The global trend of urbanization has meant that water management paradigms have evolved from the simple objective of just securing the water supply and flood protection, to a combined management strategy of the various urban water system components i.e. water treatment, distribution, recycling, sewerage and storm drainage etc. (Bach

et. al., 2014). Thus, there is a need for the newer urban watershed models to be able to address these management strategies while also ensuring that the models are reliable, usable, affordable, resilient, and, adoptable to address the uncertainties of climate change and urbanization (Ahmad and Simonovic, 2004).

Modern urban hydrologic models act a tool for providing an integrated water management solution. Integrated water management strategies use a multi-dimensional approach centered on the need for water, the policy to meet the needs and management strategies (Ahmad and Simonovic, 2006). The first dimension may consist of water elements encompassing various aspects of water quantity and quality. The second dimension may consist of water uses which includes agriculture, water supply, energy generation, industry etc. Other dimensions may consists of policy to balance the supply of water amongst different users. Usable water is limited in its availability and depends on the environmental systems such as atmosphere, hydrosphere, ecosphere etc. of a particular area (Dawadi and Ahmad, 2012).

The practice of managing environmental systems as a cohesive whole is a recent phenomenon and needs further research. Traditionally, water management strategies have lacked an integrated approach and considered all components independent of each other in a fragmented manner (Ahmad and Prashar, 2010, Bach et al., 2014). Development of watershed models has progressed along the same path as management. Various models are available for different parts of the urban water system, each capable of addressing some water system components to a great detail, but lacking the capability to interact with the surrounding environment (Bach et. al., 2014). Therefore, the focus in recent times has been more towards the development of integrated

watershed models that are capable of addressing issues related to integrated water resources management.

2.1.1) Historical and Current practices

The main idea behind the development of urban watershed models was to come up with a tool that can help understand the hydrological behavior of urbanized catchments. The primary hydrological needs of urban population are availability of clean water and management of waste-water/sewage. The initial development of hydrologic models was mainly guided to address these two particular issues – drainage of excess stormwater and proper evacuation of waste. As the technology related to hydrologic models grew, so did the capabilities of the models. Issues related to safety i.e. flood prediction, pollution risk assessment etc. were also addressed by the hydraulic and transport models (Price, 2011; Elga et al., 2015), which were developed at a later stage.

The need for proper drainage of stormwater and wastewater was felt by the people from the earliest civilizations of the Mediterranean and the Middle East (Delleur, 2003). Historical evidences suggest that Habuba Kabira, a fourth century B.C. town, in the old Mesopotamia is the first urban layout with drainage (Vallet, 1997; Delleur, 2003). There are also evidences to suggest existence of city scale drainage systems in the prehistoric Indus valley (Delleur, 2003). The concept of a single drainage structure for the combined drainage of rainwater and sewage first arose in Medieval Europe (Delleur, 2003). The current urban drainage practices are based on the concepts of urban drainage developed in European and American cities in the early 1800s (Delleur, 2003). As urban population centers started growing in sizes, the need for more sophisticated means

of management of urban stormwater and sewage drainage led to the birth of urban hydrologic models.

The origin of hydrologic modeling in the broad sense started with the Rational Method by Mulvaney (1850), and has modernized to the recent physically based distributed hydrologic models (Todini, 2007). Within the same time frame, input-output models, now known as data-driven models, starting from the Unit Hydrograph (Sherman, 1932; Todini, 2007), have evolved into Artificial Neural Network (ANN) models and Data Based Mechanistic (DBM) models (Todini, 2007). The Rational Method proposed by Mulvaney (1850) estimated only peak flow but not flood volume, while Sherman's Unit Hydrograph (UH) model was capable of producing flood hydrographs for a rainfall event sampled at constant time intervals. The introduction of Instantaneous Unit Hydrograph (IUH) by Sherman led to the separation of hydrologic models into two groups - physically meaningful models, and, data driven models (Todini, 2007). In physically meaningful models, the physical processes to be simulated by the model are pre-defined by the modeler. Data driven models, on the other hand, are based on machine learning and require a large amount of data (Ahmad et. al., 2010). Data driven models can spot connections and correlations between input and output, not pre-defined by the user, based on the data alone. The extension of IUH to larger catchments caused problems needing subjective choices like the determination of excess rainfall by separating storm runoff from base flow, on top of the existing difficulties of physical interpretation (Ahmad and Simonovic, 2004). To get an improved physical inference of catchment response, different models were developed throughout the 1960s in all of which, each individual components of the hydrological cycle were represented by interconnected conceptual elements. Each of these conceptual elements represented, the response of a particular subsystem:

Rockwood, 1964 – SSARR; Dawdy and O'Donenell, 1965, Crawford and Linsley, 1966 – Stanford Watershed IV; Burnash et al., 1973 – Sacramento; Sugawara, 1967, 1995 – Tank, etc. In all these models, parameters such as the storage coefficients, the roughness coefficients etc. were physical entities inferred from the physical and geographical characteristics of the catchments, and, needed to be optimized. This was a serious flaw of these models as the optimized parameter values sometimes were unrealistic and the conditions of observability (sufficient data for the determination of the parameter values) were not possible for all types of catchments (Singh and Woolhiser, 2002; Todini 2007). Basically, these models could be categorized as data-driven.

By late 1970s, newer type of lumped models were introduced. These lumped models were based on the idea that the rainfall-runoff process is mainly influenced by the dynamics of saturated areas. These models relied on the Dunne assumption - that all precipitation enters the soil and surface runoff arises only after the saturation of the upper soil layer (Todini, 2007). Though characterized by few significant parameters, these models (Zhao, 1977 - Xinanjiang), (Moore and Clarke, 1981 – PDM) were not dynamically meaningful (Todini, 2007). By late 1990's, models like VIC model (Liang et al., 1994, 1996 a,b), ARNO (Todini 1996, 2002a), etc. were developed which considered two parameter distribution function curve representing the relation between the total volume of water stored in the soil and the extension of the saturated areas (Todini, 2007). However, the parameterization of this curve was also based on empirical formulas.

One of the first physically-meaningful distributed model, TOPMODEL, was developed by Beven and Kirkby in 1979. Further advances in physically representing the rainfall-runoff process were made by Wooding (1965 a, b, 1966), and, Woolhiser and Liggett (1967) by conducting the

study of small urban basins using kinematic models, while Freeze and Harlan (1969), though just as a proposal, argued for the creation of a numerical model based on the knowledge of surface and sub-surface phenomena (Todini, 2007). By late 1980's, distributed models capable of catchment scale predictions, were developed (Todini, 2007), the examples for which are SHE (Systeme Hydrologique European) model developed by the Danish Hydraulic Institute (DK), the Institute of Hydrology at Wallingford (UK) and SPGREAH (France) (Abbott et al., 1986 a, b). MIKE-SHE (Refsgaard and Storm, 1995) and SHETRAN (Ewen et al., 2000) are the updated version of SHE. The limitations of SHE such as the requirement of large volumes of data and computational time (Ahmad and Simonovic, 2009), however, limited its usability and thus propelled development of physically meaningful distributed hydrologic models such as DHSVM (Wigmosta et al., 1994), TOPKAPI (Todini, 1995), LISFLOOD (De Roo et al., 2000), WATFLOOD (Kouwen, 2009), etc. that had simpler parameterization.

2.1.2) Classification of contemporary hydrologic models

Recent hydrologic models are grouped into various categories based on the modeling approach used. Melone et al. (2005) stated that watershed-scale modeling approaches are distinguished based on - the algorithm employed (empirical, conceptual, or physically-based) to develop the model, the approach used for model input or parameter specification (stochastic or deterministic), and, the spatial representation (lumped or distributed). Ever since the development of the Stanford Watershed model (1966), a number of hydrologic models have been developed (Singh, 1989). Different types of models were developed for different purposes. While many models share structural similarity, some are different. Singh (1995) classified the hydrologic models into different groups as follows:

2.1.2.1) Process based classification

A hydrologic model has five components – 1) system (watershed) geometry, 2) input, 3) initial & boundary conditions, 4) governing equations, and 5) output as shown in figure 2.1-1.

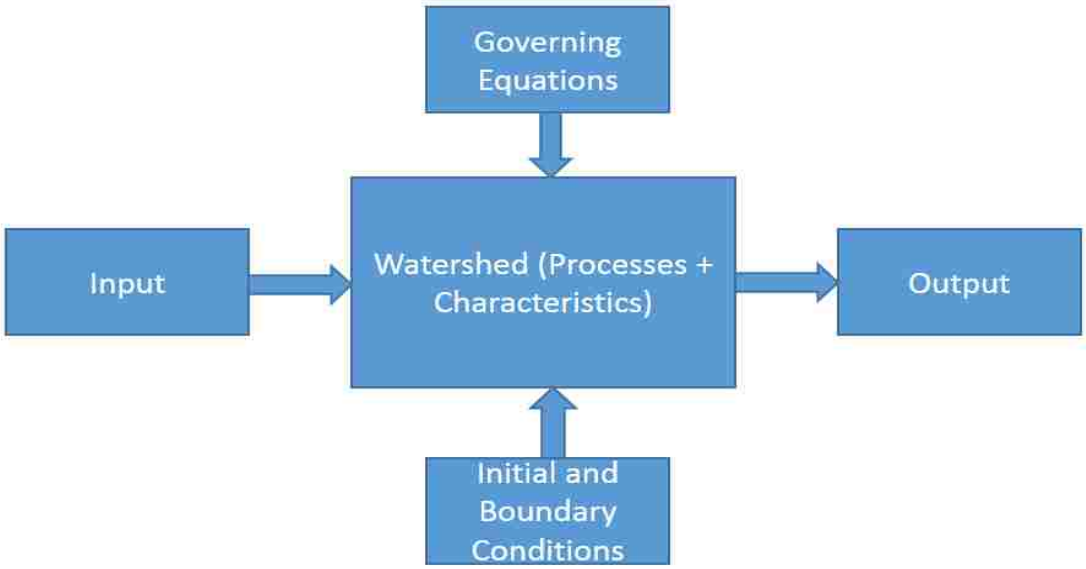

Figure 2.1-1: Components of a hydrologic model.

Different combination of model components are done to produce different types of models. The fifth component (output) is affected by the watershed processes and characteristics. Watershed processes include all the hydrologic process that affect the output. Based on the watershed processes and characteristics, the models are described as lumped or distributed, deterministic or stochastic, or mixed as shown in figure 2.1-2.

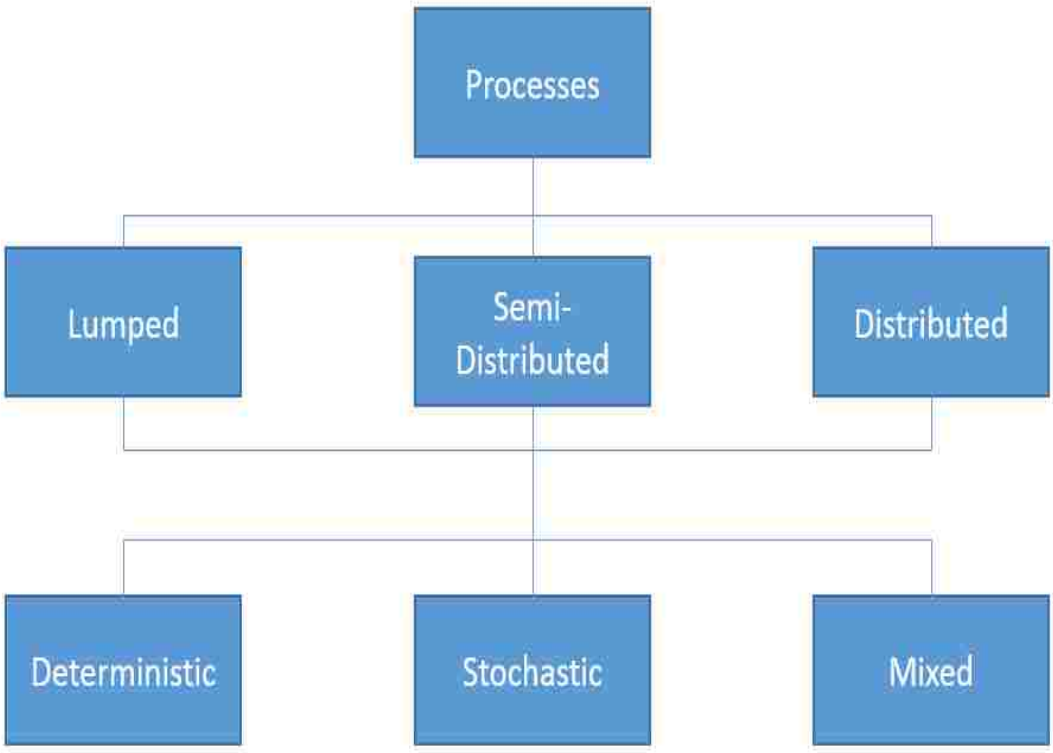

Figure 2.1-2: Classification of hydrologic models based on process description.

In lumped models, the watershed is delineated as a single entity and the spatial variability of the processes within it aren't taken into account. Some examples of lumped models are HYMO (Williams and Hann, 1972), RORB (Laurenson and Mein, 1983), tank model (Sugawara, et al., 1984) etc. In general, the governing equations of lumped model are expressed as ordinary differential equations. Distributed models, on the other hand, take into account the spatial variability of the process, inputs and boundary conditions (Carpenter et al., 2006). In some models, many of the processes and watershed characteristics are lumped together, but some of the processes that affect the output directly such as rainfall-runoff process, are considered to be distributed. Such models are semi-distributed models. Some examples of distributed models are SWMM (Metacalf and Eddy, Inc. et al., 1971), SHE (Abbott et al., 1986a, 19886b) etc.

2.1.2.2) Time-scale based classification

Sometimes hydrologic models are classified as 1) continuous-time or event model, 2) daily, 3) monthly, and 4) yearly models, based on the temporal scale of the models. Diskin and Simon (1979) defined the temporal scale as a combination of two-time intervals – one of which is used for input and internal computations, while the other is used for output and calibration.

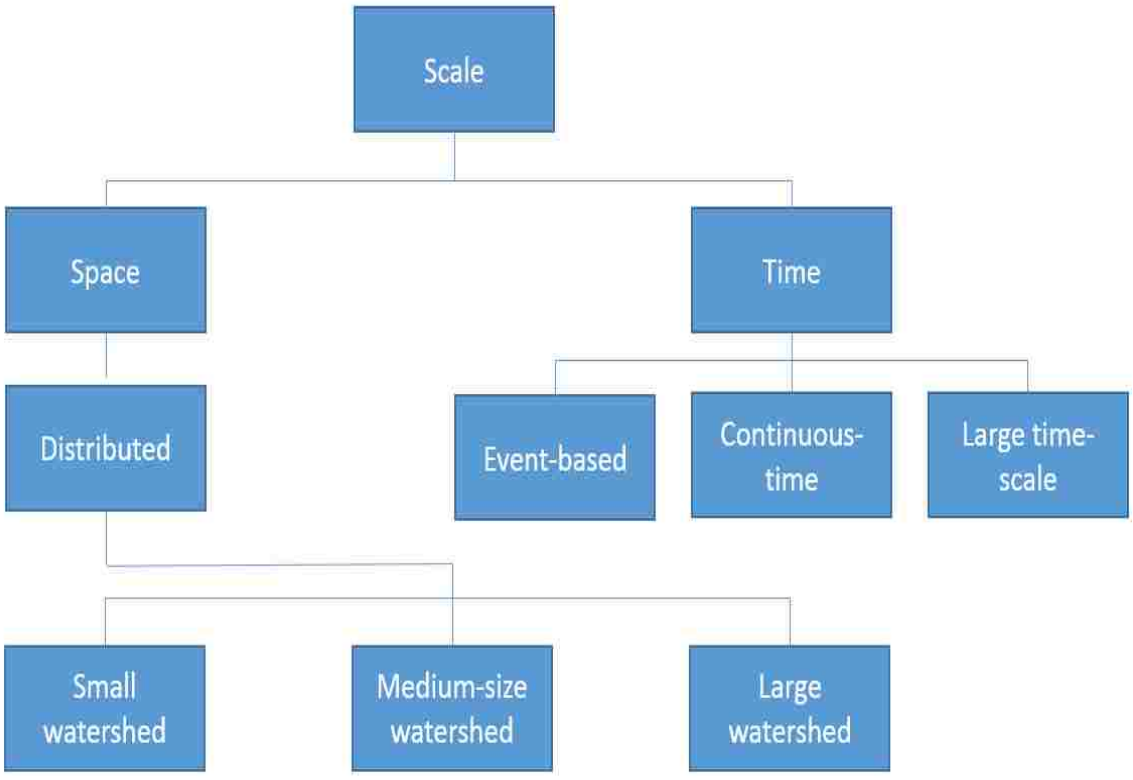

Figure 2.1-3: Classification of hydrologic models based on spatio-temporal scale.

Hydrologic models are also classified as small-watershed models, medium-watershed models, and large-watershed models based on the spatial scale. Singh (1995) has stated that watershed with an area of 100 km^2 or less are small watersheds while those with an area greater than 10000 km^2 are larger watershed.

2.1.2.3) Land-use based classification

Singh (1995) has classified watersheds models as - 1) coastal, 2) agricultural, 3) urban, 4) desert, 5) forest and range land, 6) mountainous, 7) wetlands, and 8) mixed, based on the land use. Generally, larger models have mixed land use.

2.1.2.4) Model-use based classification

Hydrologic models are classified as – 1) planning models, 2) management models, and 3) prediction models, based on their use. Planning models are primarily used for river systems management strategies (Singh, 1995).

2.1.2.5) Solution-technique based classification

Based on the solution-techniques, hydrologic models are classified as numerical models – which provide the approximate solution, and, analytical models – which provide the exact solution.

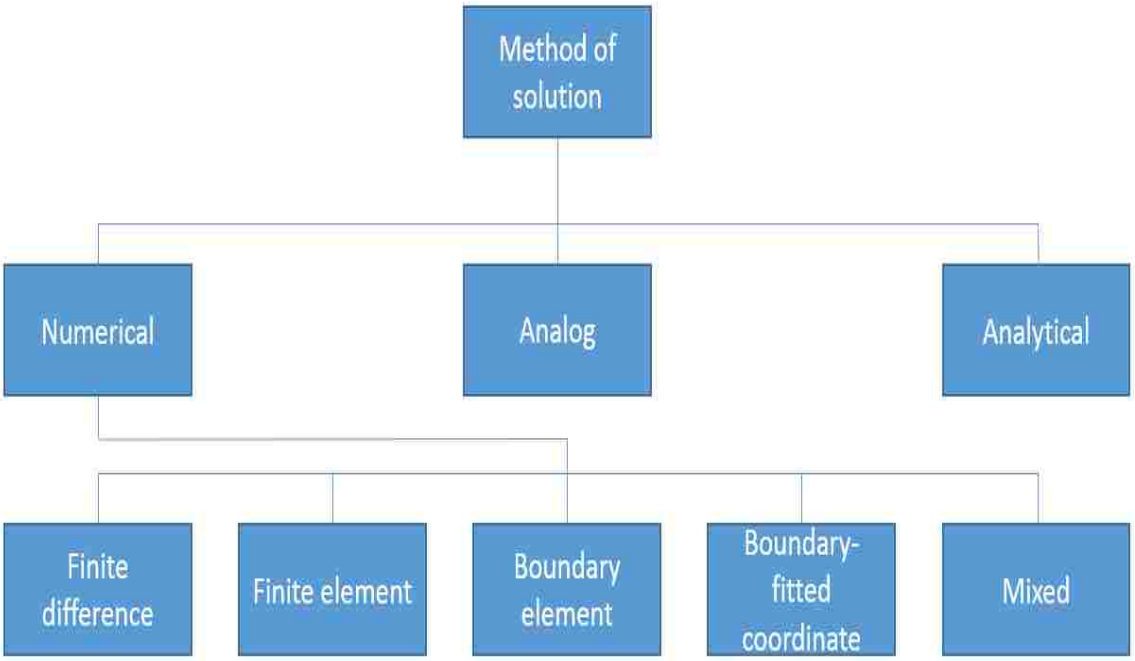

Figure 2.1-4: Classification of hydrologic models based on solution technique.

System dynamics approach (Sterman 2000; Mirchi et al., 2012) has also been used to model floods and water resources systems. Some applications include flood management (Ahmad and Simonovic 2000, 2001, 2006), river flows (Dawadi and Ahmad 2012), Urban water system planning and management (Dawadi and Ahmad 2013; Shrestha et al., 2011, 2012; Qaiser et al.,2011, 2013), regional water system planning (Chen et al., 2017; Wu et al., 2013) hydrology (Zhang et al., 2017) and water quality management (Amoueyan et al., 2017; Rusuli et al., 2015; Venkatesan et al., 2011a and 2011b).

2.1.3) Shortcomings of contemporary hydrologic models and modeling practices

To assess the current status of urban hydrological modeling, a study on the recent findings and review papers on hydrologic models was done. Based on literature review, the following

limitations of contemporary hydrologic models and shortcomings in modeling practices are identified.

Urban hydrologic modeling is still dominated by a surface hydrology perspective (Dawdy, 1982). The difficulties of defining and quantifying unsaturated flow in porous media has meant that an overwhelming majority of contemporary hydrologic models still don't properly take into account the contribution of sub-surface flow in runoff generation for urban catchments (Elga et al., 2015). Change in evapotranspiration rate due to urbanization, and losses due to evapotranspiration have not been properly quantified or taken into consideration either (Fletcher or Burns, 2012).

The spatial scales covered by urban hydrologic models are still limited to the built-up areas. The spatio-temporal scales of physical processes do not necessarily correspond to the spatio-temporal discretization of the hydrologic models (Elga et. al, 2015) as a result of which consistency of model integration at several scales is difficult (O'Loughlin et al., 1996; Mitchell et al., 2007). Elga et al., 2015 found that the most commonly used temporal resolution for modeling of urban catchments greater than 10 km^2, was 1 hour. Temporal resolution of 1 hour is not sufficient to accurately characterize the fast components of the urban fluxes (Elga et al, 2015). Some of the components of urban water systems like drinking water networks, sewers etc. have been only partially incorporated into contemporary hydrologic models. Though attempts have been made to create a universally applicable hydrologic model, still, only very models, if any, are useable for all types of urban catchments (Elga et al., 2015).

Remotely sensed data are still not sufficiently available. While more than 80% of the hydrological spatially-distributed hydrologic models are in some form, one way or the other, coupled with GIS, the use of remotely sensed data still trails behind (Elga et al., 2015). Furthermore, the uncertainties related to RS data-derived parameters are still not well understood (Todini, 2007). Difficulties in calibration and optimization of integrated urban hydrologic models still persist (Vojinovic and Seyoum, 2008). Integrated hydrologic models because of their complexity and high parameterization need vast amount of data of every urban water component represented, for calibration purpose (Hardy et al., 2005; Mitchell and Diaper, 2005). However, data availability, due to their cost, is still a limiting factor in urban hydrological modeling (Bach et. al, 2014).

Modern hydrologic models still lack the capability to fully and accurately simulate the interactions between surface and sub-surface fluxes. Furthermore, there is a growing trend to reduce the complexity of the code for model construction, so as to allow non-hydrologists to undertake significant model development (Hunter et al., 2007). However, reducing the complexity of hydraulic codes makes the model results overly reliant on user-defined values (Werner, 2004; Hunter et al; 2005b) which if not properly set, in case of certain models (1D/2D models), can cause a 'chequerboard' oscillation in the solution rendering the simulation useless (Hunter et al., 2007). Further, there is still a lack of an effective framework for model reliability and analysis of uncertainties in large-scale hydrologic modeling systems (Song et al., 2011). The uncertainties in hydrologic modeling come from four aspects in particular: uncertainties in input data and parameters, uncertainties in model structure, uncertainties in analysis method and the initial and

boundary conditions. Classical analysis approach to quantify these uncertainties are insufficient due to the high computational cost (Song et al., 2011).

2.2) Green-Ampt infiltration model and disadvantages of SCS CN model.

Among the various available infiltration-based hydrologic models, the Green-Ampt infiltration model is widely used in practice (Desborough and Pitman, 1998, Gusev and Nasonova, 1998). Kale and Sahoo (2011) reviewed the usefulness of the Green-Ampt infiltration model for varied field conditions. The authors examined critically the Green-Ampt infiltration model, delineated its capabilities, and, pointed out its use and limitations. According to the authors, the Green-Ampt infiltration model is the best model for assessing the cumulative infiltration and is better than Richard's infiltration model, as it requires just two parameters to define soil properties and also provides an analytical solution.

The Green-Ampt infiltration model is a physically based hydrodynamic model, and relates the rate of infiltration to measurable soil properties such as porosity, hydraulic conductivity, and, the moisture content of a soil. It uses a simplified version of the Richards equation. The Richards equation describes the movement of water in unsaturated soils. The vertical movement of water by which water on the ground surface enters the soil is known as infiltration. Among the various flow components, infiltration has the largest influence on the volume of watershed runoff (Mein and Larsson, 1973). Infiltration is a complex phenomenon that depends on a number of soil properties and climatological variables. For most rainfall events, runoff from a watershed is produced when the intensity of rainfall exceeds the infiltration capacity of the soil. In general,

there exist three distinct cases of infiltration when a rainfall of intensity 'I' is applied to a soil having a saturated conductivity 'Ks', and an infiltration capacity 'f'.

Case 1: $I < Ks$

In this case, no runoff from the watershed is produced, as all the rainfall gets absorbed into the soil as shown in figure 2.2-1. However, since the moisture content of the soil is changing, the rainfall is taken into consideration for designing the hydrologic model. Line A in the figure 2.2-1 shows this situation.

Case 2: $Ks < I < f$

All the rainfall infiltrates into the soil in this case as well. During this stage, as water infiltrates into the soil, the capacity of the soil to absorb the water keeps on decreasing as shown in figure 2.2-1. Line B of the curve BC in the figure illustrates this case.

Case 3: $Ks < f \leq I$

In this case, some rainfall gets absorbed into the soil while the rest contribute to runoff. Curve C and curve D represent this in figure 2.2-1.

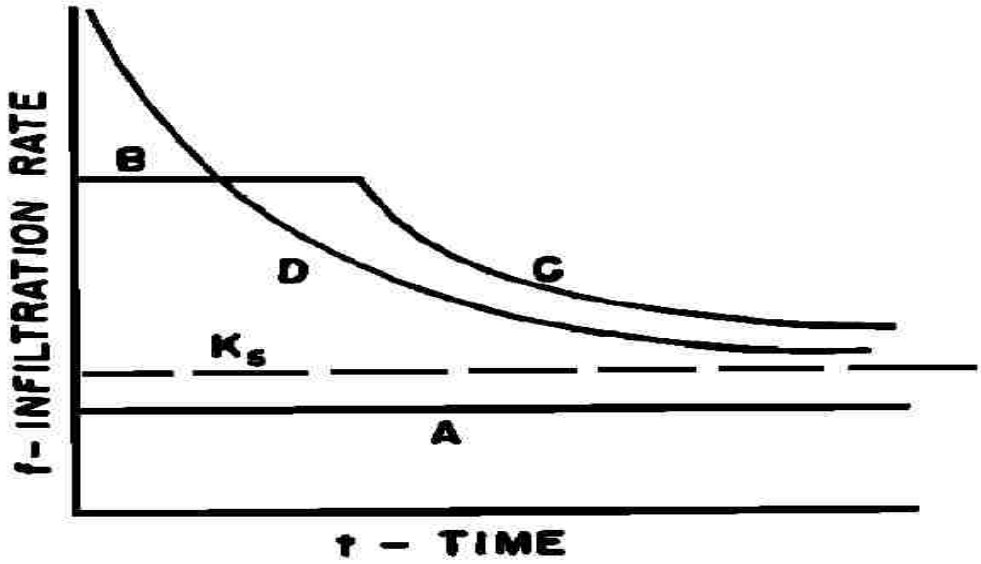

Figure 2.2-1: Different cases of infiltration behavior under rainfall. (Source: Mein and Larson, 1973)

The simplicity and accuracy of Green-Ampt infiltration model allows for its use in infiltration computation in rainfall-runoff modeling.

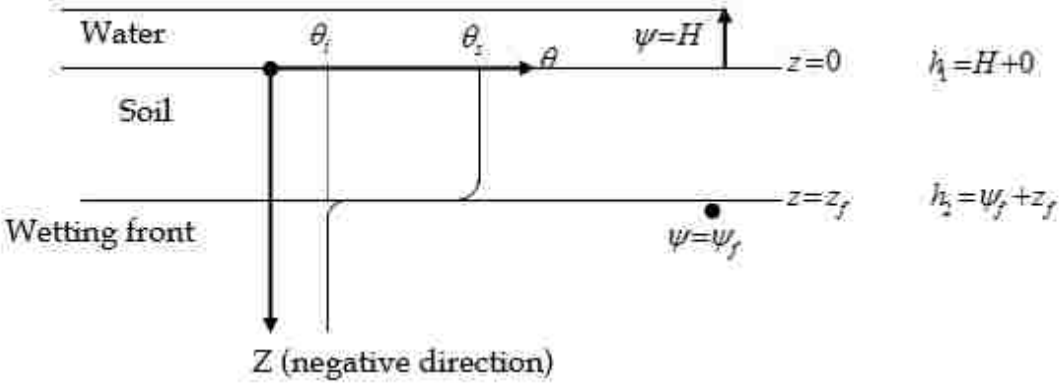

Figure 2.2-2: Infiltration profile for the Green-Ampt model.

In Green Ampt method of infiltration estimation, instantaneous infiltration rate is defined as a function of hydraulic conductivity of the given soil (K) , soil suction head (ψ), and the initial amount of infiltrated water already present in the soil (ΔΘ) as given in equation (1).

$$f_t = K\left(\frac{\psi.\Delta\Theta}{I_t} + 1\right) \ldots (1)$$

where f_t is the rate of infiltration in cm/hr. at time t, K is the effective hydraulic conductivity of the transmission zone in cm/hr., ψ is the wetting front suction head in cm, ΔΘ is the available soil moisture content and I_t is the cumulative infiltration in cm.

The advantages of the Green-Ampt infiltration model are:

1. Wetting front location can be computed because of the availability of analytical solution.
2. Soil properties can be characterized by using less numbers of parameters i.e. only two.
3. It is a widely tested infiltration model. Further, it is simple and self-sufficient to handle various field conditions.
4. "The model is sufficient to represent the soil spatial heterogeneity in a lumped manner." (Kale and Sahoo, 2011).
5. It is the most suitable model for assessing cumulative infiltration.

Though widely used for runoff estimation from rainfall, Ponce and Hawkins (1996) criticized the conceptual basis of the curve number method and stated that the SCS method is more suitable for lumped model than for distributed modeling. Further, Woodward et al., (2003) found that the initial abstraction ratio of 0.05 gave better estimates of runoff for hundreds of rainfall-runoff data from 307 watersheds in the USA. Lim et. al (2006) also, suggested that an initial abstraction ratio of 5%, rather than the traditional 20%, is more appropriate for urbanized

watersheds to reflect the developed conditions. The main disadvantages of the SCS Runoff Curve number method highlighted by the authors are as follows:

1. Sensitivity of the method to Curve Number (CN) values.
2. Difficulty in fixing the initial abstraction ratio.
3. Lack of clarity about how to vary Antecedent Moisture conditions (AMC).

Based on these reviews, it is concluded that Green-Ampt infiltration based hydrologic model is the more preferable hydrologic model for urban areas.

2.3) Causes of urban flash flooding

Floods are the most commonly occurring natural disaster in urban areas. It occurs when the capacity of stormwater drainage structure is overwhelmed by an intense or a prolonged rainfall. The intensity of flooding has increased in recent years (Genovese, 2006). Genovese (2006) identified multiple interrelated reasons for the increment in flooding intensity in urban areas, however, attributed flooding in urban areas primarily to two main factors: i) urbanization and ii) climate change.

USGS (2003) reported that urbanization generally increases the size and frequency of urban flooding in the USA. The report showed the hydrological effects of urban development. Ntelekos et al. (2009) described the impact of urbanization on future flooding in the USA. The author examined the results from global and mesoscale climate change models along with urbanization rate and economic growth statistics to draw conclusions about future flood costs for different emission scenarios. The Weather Research and Forecasting model (WRF V2.2) was used

to predict the number of days that will exceed 60mm of rainfall. The predicted number of days with excess rainfall was used to find the coefficients of Sun et al. (2007), which are used in a cost function to directly estimate the future monetary damages due to flooding. The authors found that there will be an increase in the expected annual damages (EAD) from floods in the future. The authors also found that growth rate coefficients have greater effect on the predicted EAD than coefficient of climate change.

Several other studies have also been conducted to demonstrate the impacts of urbanization on flooding. Feyen et al. (2008) assessed the impacts of global warming and change in land use pattern on future floodings in Europe. The authors used 'LISFLOOD' hydrologic model in combination with HIRHAM climate model to predict future flood depths and extents for SRES A2 greenhouse emission scenario. Monetary damages were estimated using flood depths-damage function and land use information. The authors predict that many European countries will as well face an increase in EAD in the near future. The authors also pointed that compared to the global climate change, the effect of urbanization is more significant on local urban flooding.

Huong & Pathirana (2003) conducted a study on the combined effects of climate change and urban growth on urban flooding system. The authors found that climate change contributed in sea level rise whereas urbanization affected local rainfall patterns. After running simulations for various scenarios, the authors concluded that urban rainfall intensities is a major factor in causing a localized flooding and so, the impact of urbanization is greater than that of climate change in urban flooding.

Based on the literature review, it is found that urban flooding is caused by both urbanization and climate change. However, urbanization has a major impact on localized flood. So, only urbanization has been considered as a crucial factor for urban flooding in this research. Although recent studies (Sagarika et al. 2014; Dawadi and Ahmad, 2012; Forsee and Ahmad, 2011) indicate that climate change also impacts floods significantly, climate change impacts is not considered to be within the scope of this research and hence is not taken into consideration to develop the hydrologic model.

2.4) Flooding in Baltimore

The state of Maryland, which consists of Baltimore city, has a long history of flooding. The first recorded flooding event in Maryland, however, occurred in Baltimore on May 11, 1860 incurring heavy damage to the city's business district and bridges over Jones Falls (Joyce and Scott, 2010). From 1860 to 2005, Maryland has witnessed 54 major flood events (Joyce and Scott, 2010). In recent years, the flood event of September 2003 due to Tropical Storm Isabel caused over $8 million worth of property damages in Maryland (FEMA, 2012).

Figure 2.4-1: Flooding in Pratt Street, downtown Baltimore on Sep 19, 2003. (Source: Amy Davis/ The Baltimore Sun)

The city of Baltimore lies near the head of the Patapsco River. The entire city of Baltimore is drained by four main watersheds: the Gwynns Falls, the Jones Falls, the Herring Run, and the Inner Harbour. The four Baltimore city watersheds are all part of the larger Chesapeake Bay watershed. The city's elevation ranges from sea level at the harbor to 150m in the northwest corner near Pimlico. The Chesapeake Bay watershed consists of forested areas as well as urban and industrial areas.

Baltimore city is one of the flashiest city in the contiguous US (Smith, 2015). The city receives an average annual rainfall of 41.94 inches, with the peak rainfall occurring on the months

of July and August, making it one of the rainiest cities in the USA. In recent years, there has been an increase in the number of flash flood events in and around the Baltimore city. The severe thunderstorms of July 30, 2016 over Ellicott City in Baltimore County caused significant damage and led to the loss of lives of two people (Britto, 2016). The thunderstorms dumped an estimated 6 inches of rainfall within just two hours triggering flash flood that inflicted severe damage to the area, primarily the Main Street, destroying several houses, businesses, sidewalks, and, the city's landmark clock tower (Britto, 2016).

2.5) Flooding in Las Vegas

Las Vegas experiences flash floodings on a regular basis. Though floodings in Nevada have been observed from late 1800's, the first official account of flooding in Las Vegas is that of July 15, 1905 (USDA, 1977). Since then, the U.S. Soil Conservation Service has documented a total of 184 flood events in Las Vegas between the years 1905 and 1975 (CCRFCD, 2013). Of them, 12 floods have resulted in economic losses of more than $1 million (CCRFCD, 2013). Flash floods have also reoccurred in Vegas almost every year since 1990, with most of them occurring between July and August (CCRFCD, 2013).

Figure 2.5-1: Flooding at Northwest Las Vegas Valley on Aug. 25, 2013. (Photographer: Heather Aguilera)

"Las Vegas Valley lies in a region characterized by a series of northward-trending mountain ranges and intervening valleys" (Purkey, 1994). The valley soils are rich in eroded sediments, mainly, calcium carbonate (USGS, 2000). Calcium carbonate is the main ingredient of limestone, which on mixing with moisture and the drying, results in the formation of impervious layer of caliche (Skinner and Porter, 1992). The combination of widespread caliches and lack of adequate stormwater drainages structures in Las Vegas Valley has meant that high volumes of runoff is produced from even relatively moderate precipitations increasing the likelihood of flooding.

"Las Vegas is the driest metropolis in the United States with an average annual rainfall of less than 5 inches" (Marlow, 2011). Despite this, the area often experiences small bursts of intense rainfall in the form of high intensity thunderstorms and subsequent floods (CCRFCD, 2013). While flash flood can and do occur year round, the flooding of 1975 is considered to be one of the worst, with estimated economic damages of around $4.5 million (Randerson, 1976).

Figure 2.5-2: Flooding near Caesars Palace, July 3, 1975. (Source: CCRFCD)

A study by Randerson (1976) on the flash floodings of July 3, 1975 in Las Vegas, found that rapid urbanization of the city without proper upgradation of the stormwater drainage infrastructure was one of the main reasons for the flood event of July 3. The heavy rainfall of about 3 inches (70% of the annual average) resulted in 4.19×10^7 m^3 of water spread over an area of 550 km^2. The total amount of runoff was estimated to be 2.3×10^7 m^3, which means infiltration losses

were less than 45%. This excess runoff volume resulted in flooding in the Valley, and, areas in and around the central business district were affected the most. Las Vegas valley experienced another major flooding on July 8, 1999, with property damages amounting to $20 million and 369 destroyed homes (Manning, 1999). Two fatalities - one by drowning in Flamingo Wash and the other in a traffic accident (Schoenmann, 1999) were also attributed to the floodwaters.

Flash flooding of September 11, 2012, resulted in 80 instances of property damage and one death at the Desert Rose Golf Course. Recently, another major flood event occurred in Las Vegas on September 07, 2014. According to the authors of CCRFCD 2014-2015 annual report, tropical moisture associated with Hurricane Nobert generated intense rainfall over a large section of Clark County causing intense flooding in and around the Moapa area. The findings of the report are summarized below:

- As per the NWS, the rainfall total over a 30 square mile area near Moapa, may have exceeded even 6 inches of rainfall (150% of the annual average).
- Large sections of I-15 near mile marker 92 were damaged which resulted in the closure of the highway for days.
- The Clark County Department of Public Works estimated damages in excess of $1 million to County maintained roadways and infrastructure as a result of this event. NDOT estimated $5 million in damages to I-15.

Figure 2.5-3: Photo of a damaged section of I-15 due to the flood events of Sep 07, 2014. (Source: CCRFCD)

2.6) Summary of Literature review

Through the reviews, it is concluded that there is a lot of scope in regards to improving the existing hydrologic models. It is also concluded that Green-Ampt infiltration model based hydrologic models are preferable to other hydrologic models because of their simplicity, wide acceptance, and, sufficiency to test variety of field conditions. Further, it is also concluded that both Baltimore and Las Vegas are prone to occasional flash floodings. Flash flooding in Las Vegas can be attributed to the city's high rate of urbanization. Hence, to reduce the risk of flash flooding

in Las Vegas either the urbanization needs to be checked or the drainage system needs to be upgraded. This research investigates the possibility of developing a hydrologic model applicable to such small watersheds.

CHAPTER 3: STUDY AREA AND DATA

This chapter provides a detailed description of the study area chosen for the research along with an explanation for how and why the study areas are selected. Further, the sources and attributes of the data used in the research are also explained.

3.1) Study Area

The study areas for this research consists of the catchment area of Moores Run tributary within the Back River watershed, and, UNLV Parking-lots area within Las Vegas Wash watershed in Nevada, as shown in figure 3.1-1.

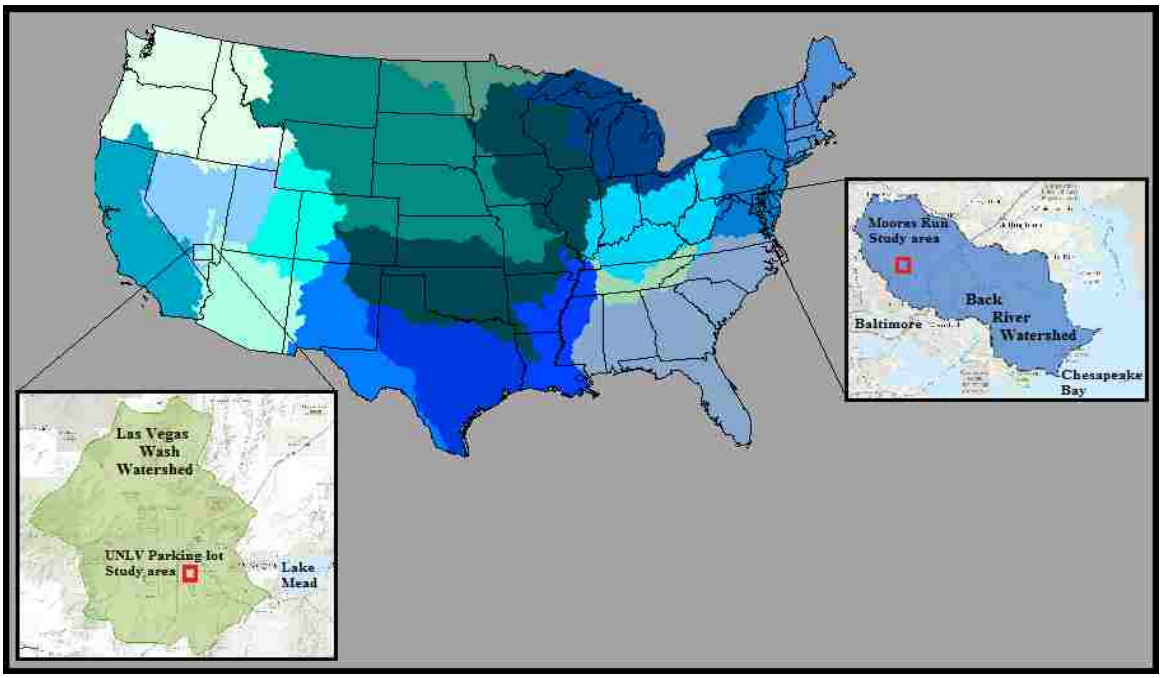

Figure 3.1-1: Location of the study areas.

Back River watershed (USGS Hydrological Unit Code 02060003), is located between the latitudes 39.22° to 39.41° N, and, longitudes 76.19° to 76.37° W. It has an area of approximately 158.13 km^2. The watershed consists of Moores Run, which is a tributary of the Back River and ultimately drains into the Chesapeake Bay. Las Vegas Wash watershed (USGS Hydrological Unit Code 15010015), is located between the latitudes 35.76° to 36.72° N, and longitude 114.85° to 115.7° W. It has an area of approximately 4,854.7 km^2. The watershed encompasses the Las Vegas Wash which discharges into the Colorado River at Lake Mead. Smaller catchments within the Back River watershed, and, the Las Vegas Wash watershed are chosen as the study areas for this research for two reasons:

1. They consist of both urbanized and undeveloped areas.
2. Availability of the data.

The hydrologic model developed in this research is tested on two small catchments lying within the Back River watershed and the Las Vegas Wash watershed. A small catchment consisting of the parking areas in UNLV, as shown in figure 3.1-2, is chosen to test the 'flood modeling' part of the developed model, whereas, the drainage area of stream gage of tributary of Moores run in North East Baltimore, as shown in figure 3.1-3, is chosen to test of the 'rainfall-runoff modeling' part of the developed model. The Parking-lots area in UNLV is situated at a latitude of 36°06'08" N and a longitude of 115°8'41''W. The Parking-lots including the Tropicana Garage area have a total area of approximately 0.114 km^2. The stream gage for Moores run tributary lies at a latitude of 39°20'12.1" N, and, a longitude of 76°32'26.2''W. The drainage area for the stream gage is provided as 0.5434 km^2 (USGS, 2017).

Figure 3.1-2: UNLV Parking-lots area. Study area (in red) for the validation of the 'flood-modeling' part of the hydrologic model.

Figure 3.1-3: Moores Run study area. Study area for the validation of the 'rainfall-runoff modeling' part of the hydrologic model.

The small catchment of the Parking-lot areas (the entirety of front parking lot of Thomas and Mack Centre, Blacklot parking area, Red lot parking area, and, Tropicana parking garage) in UNLV is chosen as the study area for the validation of the flood model because of the following reasons:

1. The confined nature of the catchment area.

The Parking-lots area considered as the study area for this research is surrounded by high features on all sides (elevated sidewalks with trees on western and southern side, and, buildings on northern and eastern side) and without subsurface flow, which ensures that water from neighboring catchments doesn't enter into the chosen catchment, and, also water from the chosen catchment doesn't outflow into the neighboring catchments because of flooding.

2. Ease of access to confirm the type and number of drainage inlets within the study area.

The Parking-lots area within UNLV is chosen as the study area for this research because of accessibility issues. To validate the model, the number of outlets of the catchment needs to be known. The selected catchment area has only 1 drainage inlet below the 'Tropicana Parking Garage', which acts as the outlet of the catchment area. A visual confirmation of the existence of no more than 1 drainage inlet (catchment outlet), within the study area, was done.

3. Availability of the data required for the soft validation of the developed hydrologic model.

The Parking-lots area is chosen as the catchment to validate the 'flood-modeling' part of the hydrologic model because of the availability of the flood depth data (photos), needed to compare the actual flood extent and depth during the flood event of Sep 11, 2012 with the flood extent and depth predicted by the hydrologic model.

4. Size of the catchment compared to the depth of flooding.

This research only deals with localized flooding in small catchments. Flooding in large-sized catchments is beyond the scope of this research.

The drainage area of the Moores Run tributary in North Las Vegas, is chosen as the catchment for the validation of the 'rainfall-runoff modeling part' of the developed model because of the following reasons:

1. Availability of both rainfall data and the stream discharge data from the catchment for the corresponding rainfall.
2. Size of the drainage area.

For validation purposes, the model developed in this research is supposed to simulate the 'rainfall-runoff' process from a single rainfall event only, and, simulation of rainfall-runoff event from multiple rainfalls within a catchment is beyond the scope of this research because of the complexities involved in analyzing the results. Runoff from larger watersheds are generally related to multiple rainfall events i.e. different rainfalls in two or more places within the same catchment at the same time or at different times. Further, runoff from the farthest corners of larger watershed take days to get recorded at the stream gage station, and, a significant quantity of the runoff from the upstream areas of the watershed may be stored in detention basins. This makes it complex to analyze what volume of the rainfall gets converted into runoff in the given watershed. The drainage area for Moores Run trib. stream gage at 0.544 km^2, is one of the smallest among the watersheds in the USA for which USGS stream gage data is available. The smallest watershed is chosen to minimize the possibility of multiple rainfall events contributing to produce the runoff from the catchment, and also, to avoid the possibility of runoff getting stored in detention basins,

or, release of water from detention basins contributing to the runoff being recorded at the stream gage station.

3.2) Data

The remote sensing data and hydrological data used in this research are described in the following sub-sections.

3.2.1) Remote Sensing Data

The remote sensing data utilized in this research are as follows:

3.2.1.1) '10-m DEM' for UNLV Parking-lots area.

In this research, a 10-m resolution DEM, derived and resampled from 1-m LiDAR data of the study area is used as the elevation data for the Parking-lots catchment area. The 1-m resolution LiDAR data (2008 version) for the study area is downloaded from The National Map (TNM) website (https://viewer.nationalmap.gov/basic/) in '.las' format. A single '.las' file is converted into a 1-m resolution raster, in ArcMap using 'Single return' and 'Last of many return' filters, which is then resampled to 10-m DEM of the study area.

3.2.1.2) '30-m DEM' of Moores Run Study area.

A 30-m DEM, derived and resampled from 1-m LiDAR data of the study area is used as the elevation data for the Moores Run Study area. The 1-m resolution LiDAR data (2008 version) for the study area is downloaded from The National Map (TNM) website in '.las' format. Three downloaded '.las' files of the study area are patched together and converted into a single 1-m resolution raster file, which is then resampled to 30-m DEM of the study area.

3.2.1.3) '2015 version NAIP imagery (1m resolution)'

The National Agriculture Imagery Program (NAIP) acquires aerial imagery during the agricultural growing seasons in the continental United States. The image file of UNLV Parking-lots study are is downloaded from W.M. Keck website (http://keck.library.unr.edu/searchresultsnew.aspx?q=36115A2). 2 Tiff files named - Las Vegas SW (3611563) and Las Vegas SE (3611564) of 1m resolution are downloaded in total, to cover the entire study area and mosaicked together to create a single image file. The resulting mosaic is projected in NAD 1983, Zone 11 UTM coordinate system. Similarly, the image file of Baltimore city is downloaded from the National Resources Conservation Services website (https://nrcs.app.box.com/v/naip/1/18274612871) in '.zip' format. The file named 'Ortho_1-1_1n_s_md005_2015_1.zip' is extracted to obtain a '.sid' image file of the study area. The so-obtained image file is projected in NAD 1983, Zone 18 UTM coordinate system. The default spectral resolution for both the images is RGB.

3.2.2) Hydrological Data

Hydrological data used in this research are rainfall data, surface hydrological soil group information data, and, values for some properties of soil.

3.2.2.1) Rainfall Data

Rainfall data for LVW watershed for the duration of the study period is available on the Clark County Regional Flood Control District (CCRFCD) website (http://www.ccrfcd.org/rainguages.htm). CCRFCD provides reliable real-time weather information and rainfall data of relatively higher temporal resolution (5 mins) and hence is selected as a data source.

i) Rainfall data for the rainfall event of Sep 11, 2012 over the UNLV Parking-lots area

The rainfall data used for the validation of the 'flood modeling' part of the developed hydrologic model is downloaded from CCRFCD website in '.csv' format with filename 'gagestation_4574'. 15 minute interval precipitation data of September 11, 2012 for rain gage station '4574' is chosen as the rainfall data. The rainfall event lasted for 90 mins duration. However, rainfall data in the model is provided as cumulative rainfall as shown in the figure 3.2.2-2.

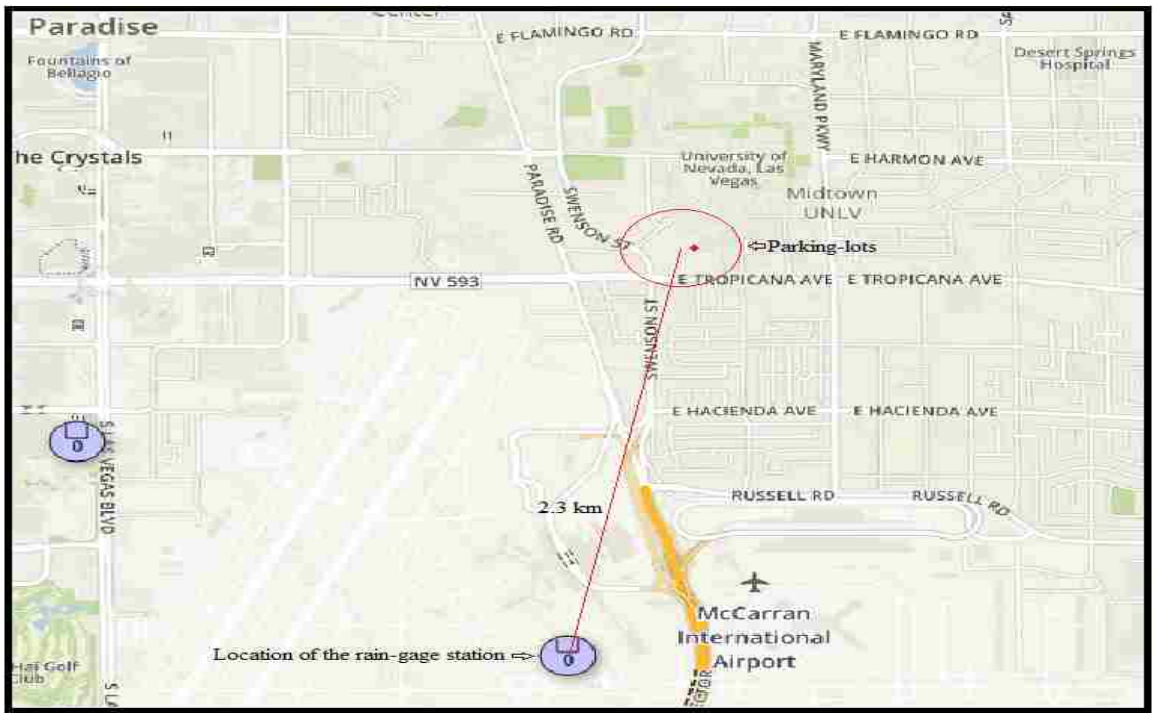

Figure 3.2.2-1: Location and the distance of the rain-gage station from UNLV Parking-lots area. (Location of the drainage inlet for Parking-lots area shown by the red dot).

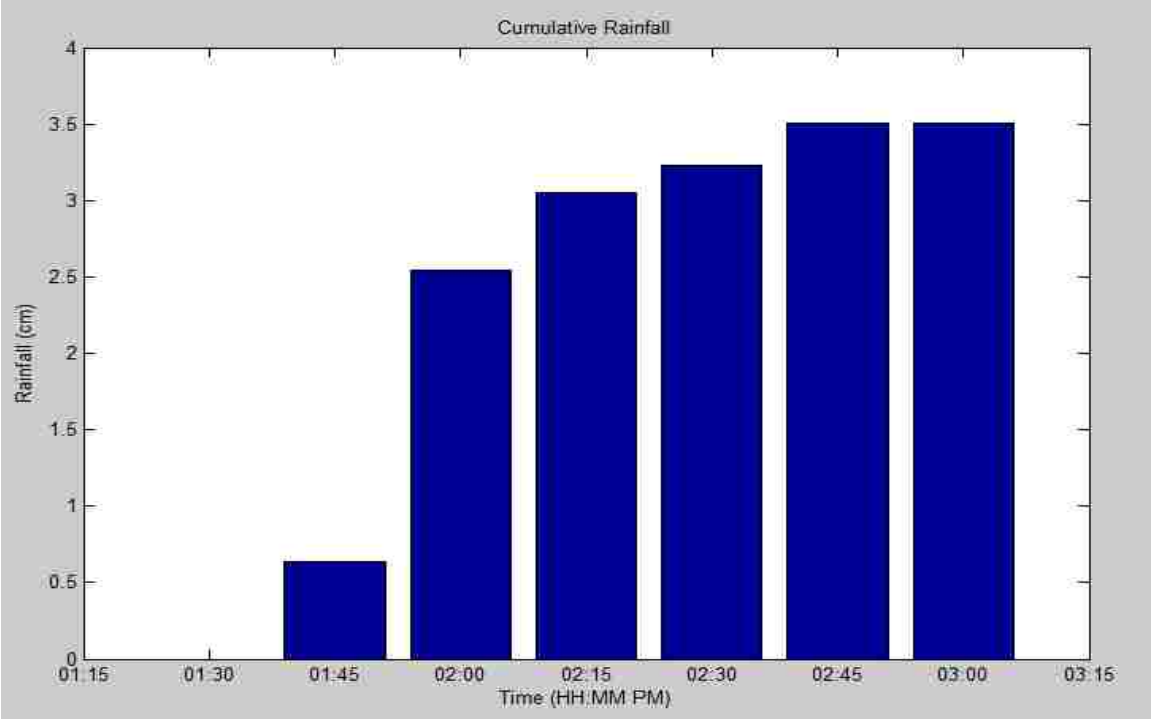

Figure 3.2.2-2 Rainfall hyetograph of September 11, 2012 over UNLV.

ii) Rainfall data over the Moores Run study area.

The rainfall data used for the validation of the 'rainfall-runoff modeling' part of the developed hydrologic model is obtained from the Wunderground website (https://www.wunderground.com/personal-weather-station/). Among the five rain-gage stations located around the watershed, the rainfall data of May 22, and, May 24 (all 2017) from the rain-gage station in Hazelwood Farms (KMDBALTI136), nearest to both the watershed and the stream-gage, is selected for the validation of the model.

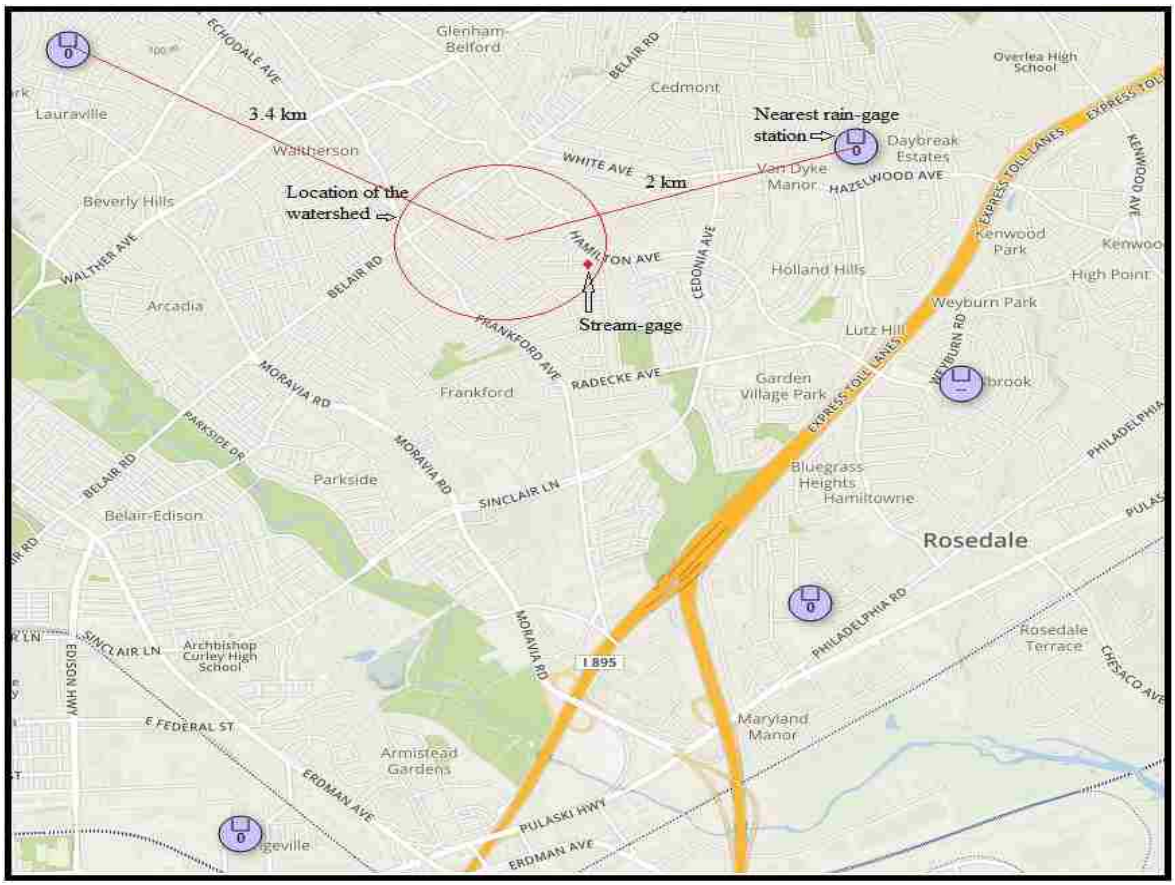

Figure 3.2.2-3: Location and the distance of the rain-gage stations from the Moores Run watershed.

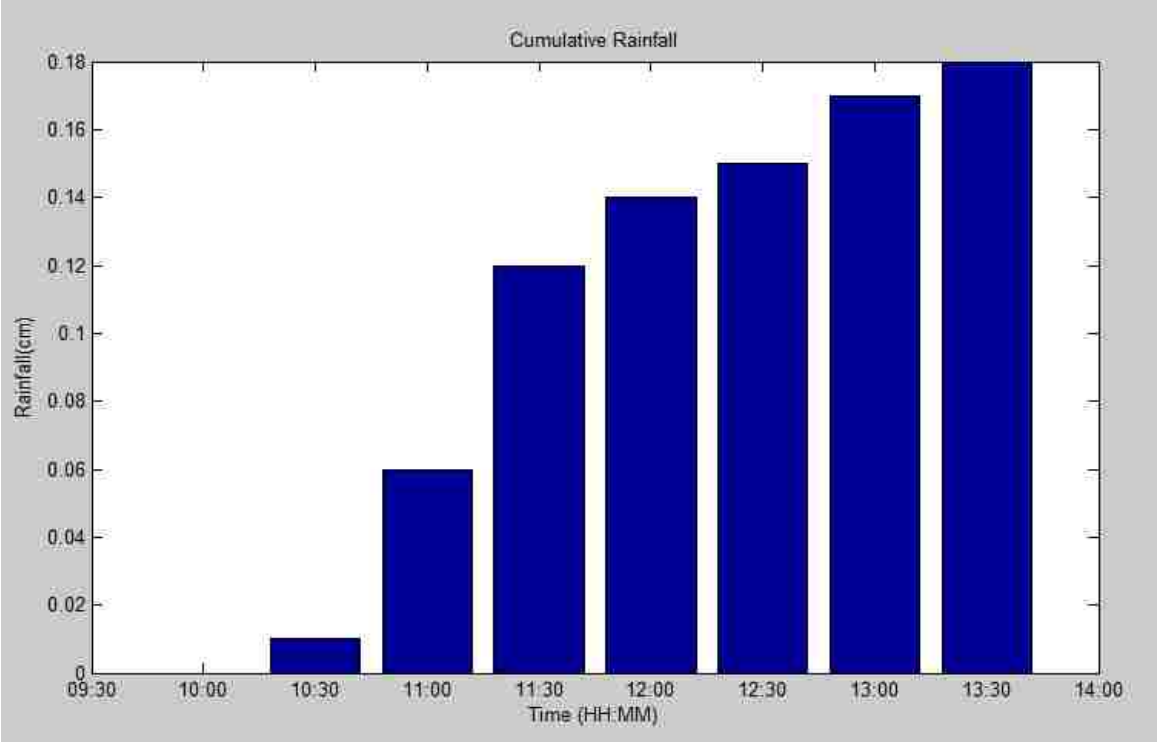

Figure 3.2.2-4: Rainfall hyetograph of April 17, 2017 over Moores Run Study area.

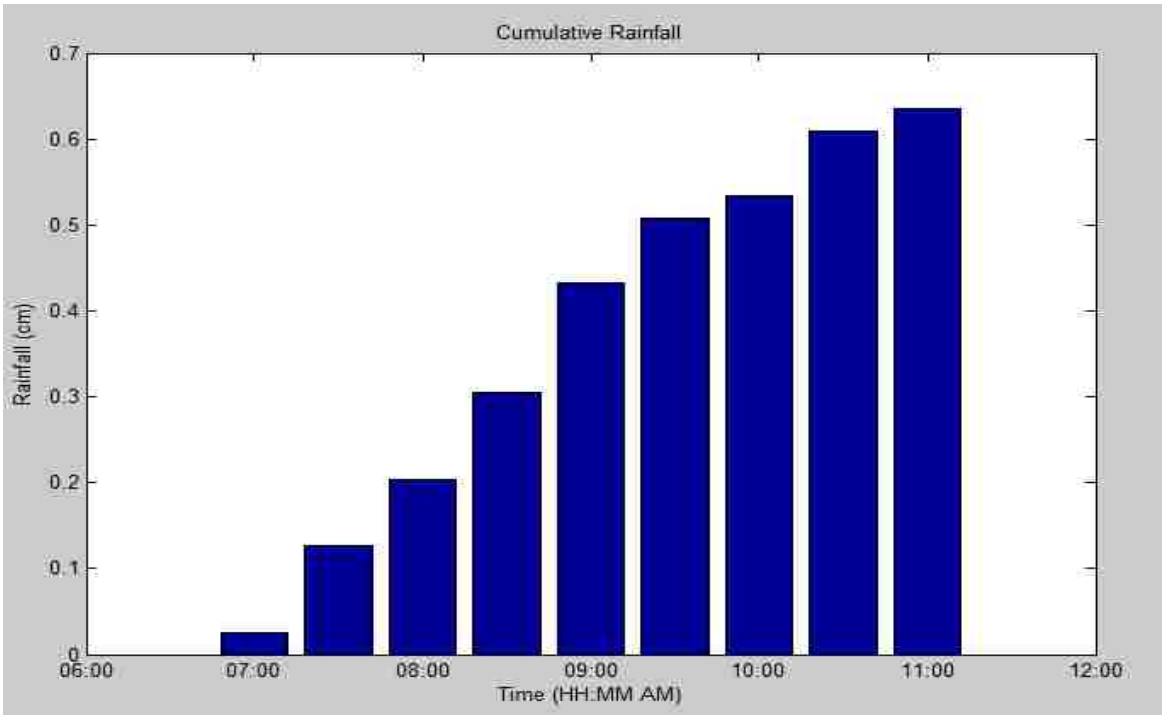

Figure 3.2.2-5: Rainfall hyetograph of May 22, 2017 over Moores Run Study area.

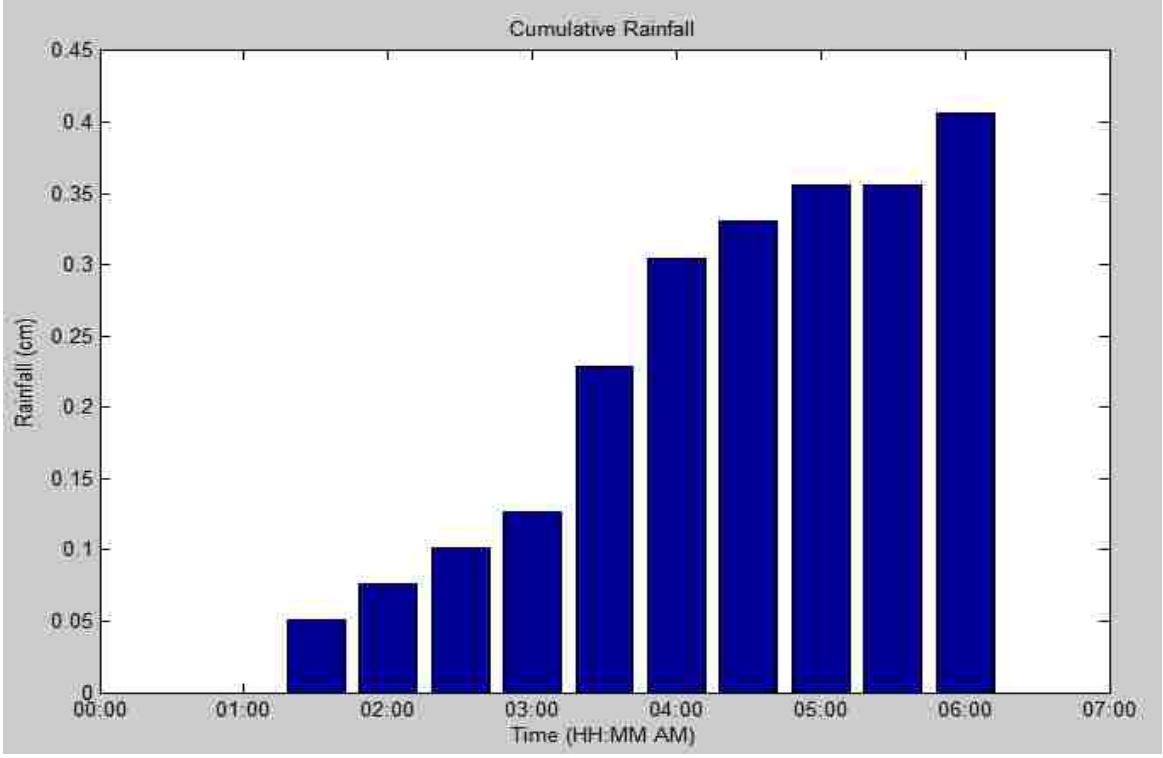

Figure 3.2.2-6: Rainfall hyetograph of May 24, 2017 over Moores Run Study area.

3.2.2.2) Soil group data

Soil is classified into Hydrological Soil Group (HSG) (Cronshey, 1986) based on infiltration rates. Cronshey (1986) categorized soils into 4 groups as per their infiltration rates, namely: A (sandy), B (silty), C (sandy clay), and, D (silty clay). Group A has a high infiltration rate while Group D has a low infiltration rate. From figure, it can be observed that Moores Run study area consists of all 4 types of soil groups. HSG data are collected from Soil Survey Geographic (SSURGO) Database that is maintained by the Natural Resources Conservation Service (NRCS) of the United States Department of Agriculture (USDA).

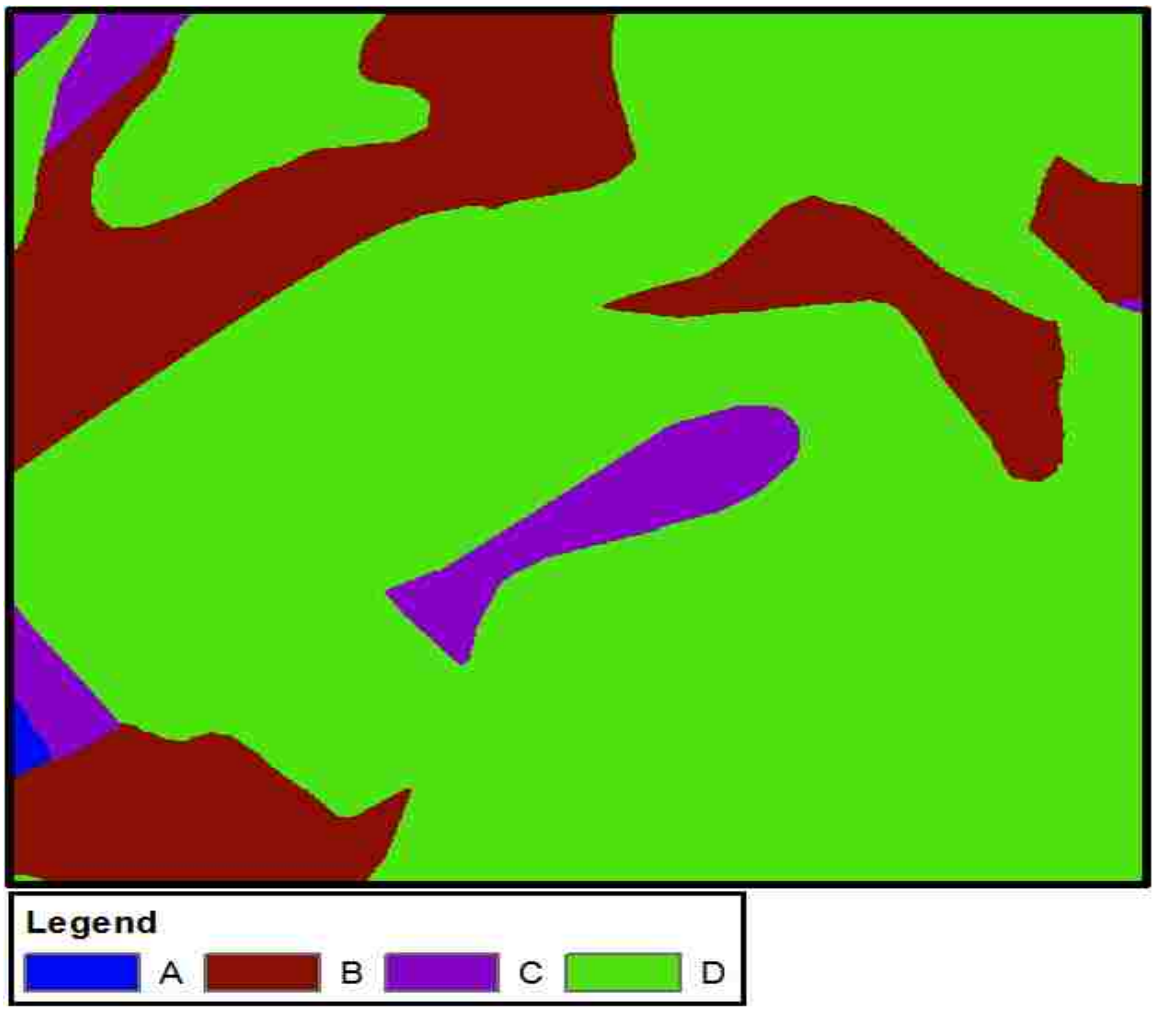

Figure 3.2.2-7: Soil group map of Moores Run study area.

The HSG data is downloaded from Web Soil Survey website (http://websoilsurvey.sc.egov.usda.gov/App/HomePage.htm) that contains SSURGO database. The HSG data for Nevada and Maryland are downloaded as raster datasets. The dataset contains many other physical and engineering properties of the soil groups as well. The HSG information are extracted from the downloaded data to create a HSG map. This HSG map is then extracted for the study area to create the soil map.

3.2.2.2.1) Properties of soil

The hydraulic model developed in this research requires various soil properties data as input. The soil properties that need to be input as data into the models along with their units are described below:

3.2.2.2.1.1) Hydraulic conductivity (K)

Hydraulic conductivity of a porous medium is defined as the ratio of velocity of water through the medium to its hydraulic gradient, indicating permeability of the porous media. A literature review on the values of hydraulic conductivity for different groups of soil suggested the following values of hydraulic conductivity:

Table 3.2.2-1: Values of hydraulic conductivity for different soil textures

Texture	Minimum 'K' (m/s)	Maximum 'K' (m/s)	Average (m/s)
Sand	2.55*10^-5	5.35*10^-4	2.8*10^-4
Silt	1*10^-8	5*10^-6	2.5*10^-6
Sandy clay	5*10^-9	5.5*10^-6	2.7*10^-6
Silty clay	5*10^-10	5*10^-8	2.52*10^-8

Source: Geotechdata.info, http://geotechdata.info/parameter/permeability.html

3.2.2.2.1.2) Manning's roughness coefficient (n)

The 1-m NAIP imagery of the study area for this research is classified into 7 landcover classes. Based on literature review for the Manning's roughness co-efficient for different

landcovers, the ‘Mn’ value for the 7 landcovers used in the landcover classification of the study area are assigned as follows:

Table 3.2.2-2: Manning’s roughness coefficient (n)

Landcover	Range	Recommended ‘n’ (Set 1)
Asphalt	0.010 – 0.013	0.012
Bare soil	0.010 – 0.016	0.018
Concrete	0.010 – 0.013	0.012
Grass	0.010 – 0.480	0.035
Vegetation	0.025 – 0.160	0.023
Residential area		0.014
Wetland (Water inundated land)	0.012	0.012

Source: Chow, 1959.

3.2.2.2.1.3) Porosity, effective porosity, and, wetting front suction head (ψ).

The values of porosity, effective porosity, and, wetting front suction head used in the model are as follows:

Table 3.2.2-3: Soil properties

Soil type	Porosity	Effective porosity	Suction head (cm)
A	0.437	0.417	4.95
B	0.501	0.486	16.68
C	0.430	0.321	23.9
D	0.479	0.423	29.2

Source: Rawls, Brakensiek, and, Miller (1983)

CHAPTER 4: METHODOLOGY

This chapter includes the description of the methods and procedures followed to develop and validate the model. The model proposed in this research is conceptually not very different from existing rainfall-runoffs models. Rainfall-runoff models take rainfall along with various geological data as the input to produce runoff from a given watershed as the output. The methods followed to develop and verify the model to achieve the first objective can be divided into five components, namely: 1) Data preparation, 2) Modeling, 3) Calibration and Validation, 4) Simulation, and 5) Error analysis. The first two components together make up the model development part while the rest constitute up the model verification part. To achieve the second objective, different landcover change scenarios for the UNLV Parking-lots area is analyzed using the developed model.

4.1) Hydrologic modeling

4.1.1) Data preparation:

This section describes the procedures followed to prepare the data to be input into the hydrologic model. The inputs into the model include elevation data of the study area and rainfall data. The elevation data of the study area is necessary to identify the pour-points and delineate the watershed. Various other datasets such as flow direction matrix, slope matrix etc. are also derived from the elevation data.

4.1.1.1) Elevation data

In the developed model, the elevation data for the study area is provided as an input matrix. A 30-m resolution DEM is used for Moores Run study area, and, a 10-m resolution DEM is used for UNLV Parking-lots area, the image for both of which are provided in the results chapter. DEM of different resolutions are used for the two study areas based on suitability of DEM resolutions given the difference in size of the study areas.

4.1.1.2) Flow-direction and watershed delineation.

The developed model derives the flow direction matrix from the input DEM using the 8-neighborhood connectivity model based on the terrain analysis. Flow direction of water from a cell to the adjacent cell is supposed to be in the direction of steepest descent. Flow directions from each cell are stored as compass angles from 0° to 360° as elements of matrix in a matrix of the same size as the input DEM. Flow direction of 0° represent flow from a cell to the next cell in x direction i.e. flow from (x_1, y_1) to (x_1+1, y_1).

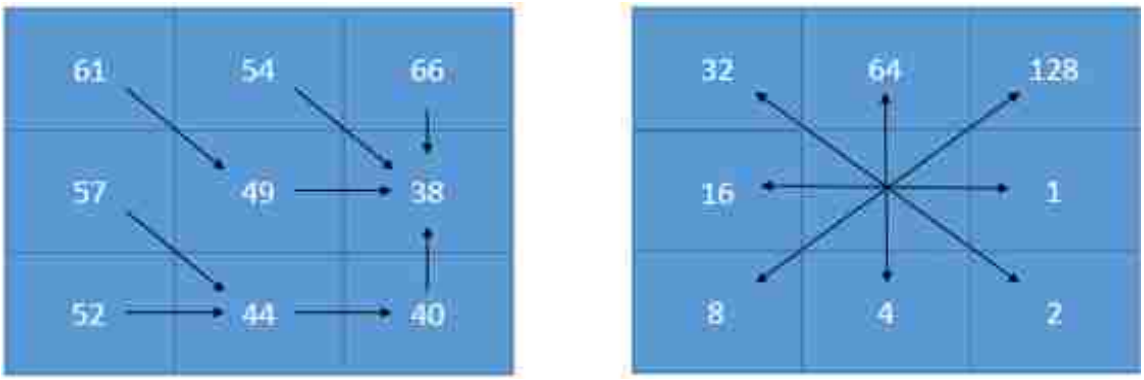

Figure 4.1-1: (left) illustration of how flow direction is determined for a sample watershed, (right) assigning value to flow direction.

Flow direction of 90° represents flow from a cell to the next cell in y-direction i.e. flow from (x_1, y_1) to (x_1, y_1+1). For calculation purpose, flow direction is stored as a number indicating the adjacent cell to which water flows, taking a value from 1 to 8 for each adjacent cell. Figure 4.1-1 shows the process to determine the flow direction. If in some cases, multiple neighboring cells have equal lowest elevation then flow is assumed to take place towards the direction of the neighbor with the lowest elevation whichever is encountered at first during the modeling process. The model delineates the watersheds within a study area based on the flow direction the results for which are provided in the results chapter.

4.1.1.3) Hydrological slope

The dataset containing the slope values of each cell is derived from the DEM using the 8-neighborhood connectivity model based on the following formula.

$$Slope = \text{atan}\left(\sqrt{\left(\frac{dZ_x}{dx}\right)^2 + \left(\frac{dZ_y}{dy}\right)^2}\right) \ldots (2)$$

Where $'dx'$ and $'dy'$ are distance the between the adjacent cells in x-axis and y-axis respectively, 'dZ_x' is the difference in elevation of the adjacent cells in x-axis, and, 'dZ_y' is the difference in elevation of the adjacent cells in y-axis. The value of slope is stored as percentages of change in elevation from 0% (flat) to 100% (vertical) in raster data layer.

4.1.2) Modeling:

The hydrologic model developed in this research is a physically based distributed rainfall-runoff model. The models governing equations are solved by an implicit finite difference method. Input to the model is precipitation. Output from the model is the simulated runoff at the watershed outlet. The model produces the outlet discharge hydrograph as a response to rainfall as input. The catchment area is discretized into different grids – a matrix of square elements, based on the resolution of DEM. Within each grid cell the topography, soil properties, and, land characteristics are considered to be uniform. Overland flow in each grid cell is estimated through an integrated implementation of Green-Ampt and Manning's equations. The flow direction field amongst grid cells is determined using 8-neighborhood connectivity model based on the terrain slope and aspect.

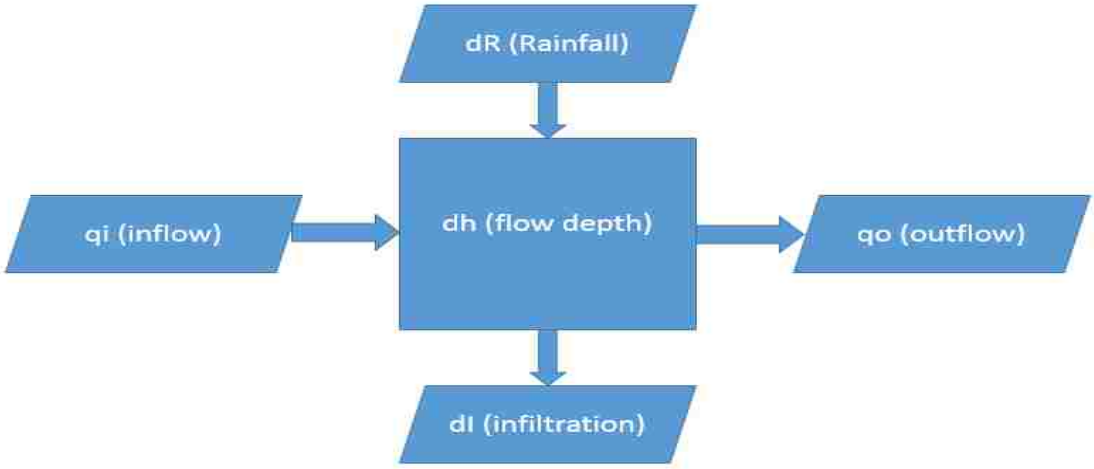

Figure 4.1-2: Cell model.

The model implementation is done iteratively over time-steps to map flow field and compute discharge hydrograph. Cell-to-cell connectivity sequence is determined by developing a computationally intense procedure (Smith, 1991). The cell-to-cell connectivity is sequenced such that outflow from one cell becomes the inflow to the next downstream cell. Thus, within each

time-step, the runoff computations proceeds from the highest elevation cell in the catchment to the outlet following a hydrologically ordered flow sequence (Palacois-Velez, 1990).

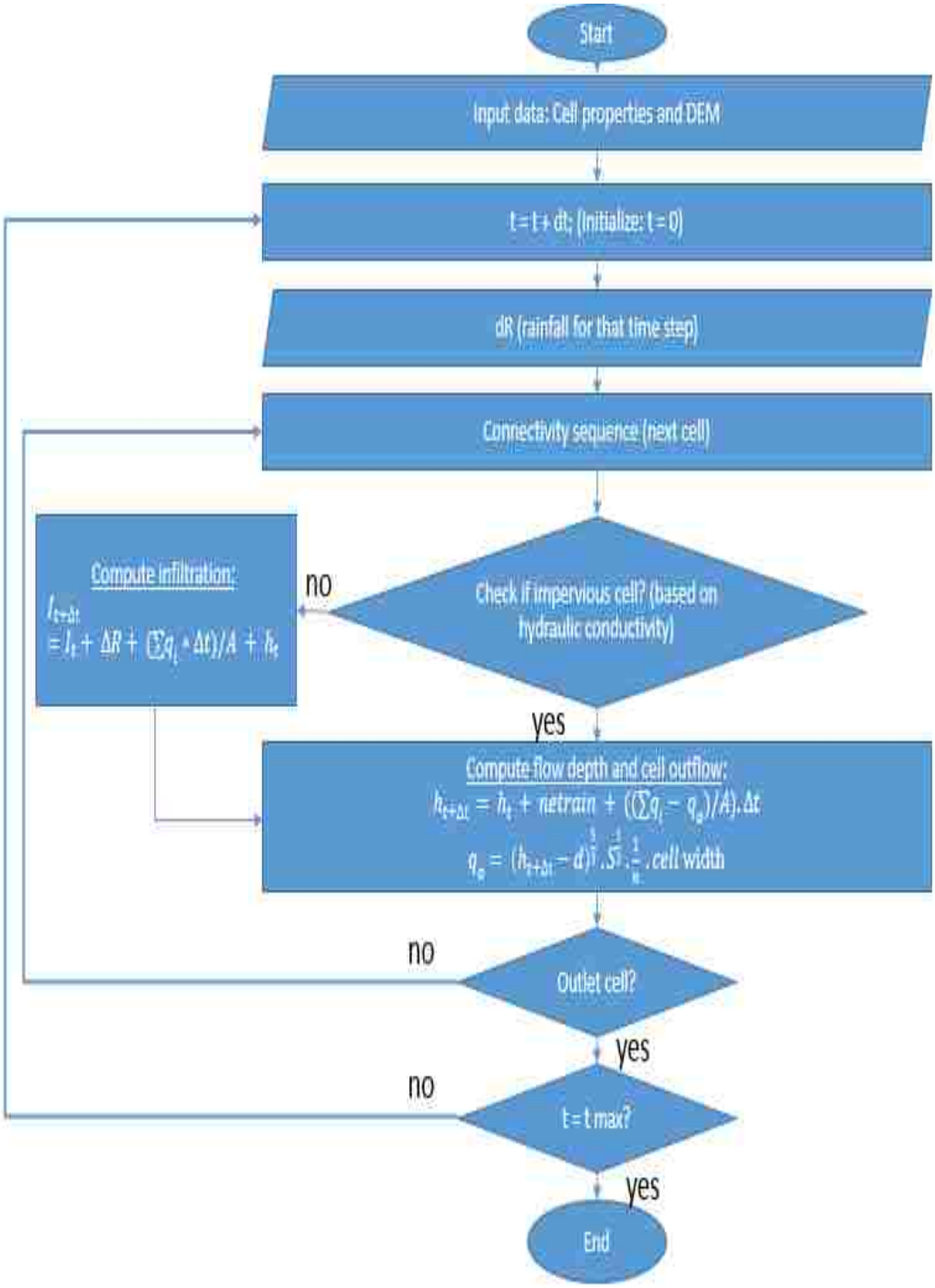

Figure 4.1-3: Generalized model structure.

The schematic diagram of the cell model is shown in figure 4.1-2. For each time-step, depth of flow in the cell 'h_2' and outflow from the cell 'q_o' is found for each cell is calculated using Continuity equation and Manning's equation respectively. Cumulative infiltration 'dI' into each cell for each time-step is predicted using Green-Ampt equation. The model hierarchy is time-step oriented as shown in figure 4.1-3. The connectivity sequence ensures that each watershed cell is recalled in the proper hydrologic order. The step-by-step description of the equations and calculation procedures are provided in the appendix chapter.

4.2) Description of the Matlab code for the developed hydrologic model

The hydrologic model developed in this research is coded in Matlab. Matlab is chosen as the programming language for the development of the hydrologic model of this research because of the following reasons:

1. The author's familiarity with the programming language used in Matlab as compared to other programming languages.
2. The suitability of 'Matlab' programming platform to develop the hydrologic model of this research.

The hydrologic model developed in this research deals with matrices and equations. Further, some of the analysis of the results of this research involves image processing. Matlab has a large database of built-in algorithms for image processing and the basic data element in Matlab is a matrix. This feature makes Matlab, the most suitable platform to develop the model of this research.

3. Ease in testing the algorithms

Matlab allows the programmers to test algorithms immediately without recompilation. The algorithm for the model can be executed line by line in Matlab. This feature allows for ease in debugging the code.

4.4) Image classification

A 3-band Sid imagery (2010) of the Moores Run study area is used to classify the landcovers in ArcMap 10.1. The three bands are: Red – Band 1, Green – Band 2, and Blue – Band 3. Supervised classification is done to classify the image into 7 landcover groups namely – grassland, water, asphalt, concrete, residential area (roof tiles), sparse vegetation and bare-soil. In supervised classification, training samples are created by the user to provide spectral signatures for which the image is classified. Different features on earth's surface like (land, water, vegetation etc.) have different spectral signatures for a particular band of wave and remotely sensed images can be processed to determine the features of the images using this property of the features. Further, the classified 1m resolution and 30 m resolution images of the study area is also provided in the results chapter.

4.5) Model calibration and validation

The developed model was supposed to be calibrated for the values of hydraulic conductivity, Manning's roughness co-efficient, and, the DEM resolution. However, for 1m, 2m,

3m, and, 5m resolution DEM of the study area, the developed model failed to simulate the rainfall-runoff process. Further, even for DEM of resolutions 10 m, and, 20 m, the relatively higher number of pixels within the study area made it difficult to obtain the results of the simulation within a reasonable and acceptable time frame. Therefore, DEM of 30m resolution is selected for this research keeping the runtime of the model in consideration. DEM of even smaller resolutions like 40 m, or 50 m, for which the runtime of the simulation process is even smaller, however, aren't preferable because the details of the landcover characteristics are lost to a great extent at such small spatial resolution. 30-m resolution DEM is therefore, considered to be the optimum resolution for the chosen study area factoring in both the runtime of the model and the accuracy of landcover characteristics that can be represented by a pixel.

The developed model is tentatively calibrated for the values of hydraulic conductivity 'K' of soil group D in Moores Run study area. Calibration of the developed model against hydraulic conductivity is carried out by producing hydrographs from the catchment for the same rainfall event but for different values of hydraulic conductivity for soil group D and comparing it with the actual stream discharge data from the catchment for the same rainfall. RMSE plots of predicted hydrograph with the actual hydrograph for different values of 'K' are drawn to determine the most preferable value of 'K' for soil group D. However, the model is not calibrated to determine the exact value of hydraulic conductivity given the limited number of trials.

The developed model was also supposed to be calibrated for the Manning's roughness co-efficient values of each landcover. However, the 'time to peak' in the hydrograph predicted by the model for all rainfall events lagged the actual 'time to peak' of the discharge from the catchment

even for the lowest Manning's roughness co-efficient values for each landcover that could be found in the literature. Therefore, only one set of Manning's roughness co-efficient values, containing the lowest Manning's roughness co-efficient value found in the literature, is used.

The hydrologic model developed in this research is validated in two parts. The 'rainfall-runoff modeling' part of the developed model is validated using the stream discharge data of the Moores Run trib. stream-gage for 3 rainfall events. The actual stream discharge hydrograph, from Moores Run trib. catchment for each rainfall event, is compared with corresponding hydrograph predicted by the model for each rainfall event. A table containing the comparison of the runoff volume, the peak runoff, the time to peak, and the hydraulic conductivity 'K' value for soil group D, is constructed. The 'flood modeling' part of the developed model is validated using the photos of Sep 11, 2012 flood event in UNLV Parking-lots area. A comparison is made between the actual extent and the depth of flooding for the flood event of Sep 11, 2012 over the UNLV Parking-lots area with the predicted extent and the predicted depth of flooding. A snapshot of the predicted depth of flooding at different time steps along with the snapshot of the peak flooding is also provided.

4.6) Model Implementation/Simulation

The simulation of the developed model is carried out in two parts – the first part consists of the simulation of the developed model over Moores Run study area, and, the second part consists of the simulation of the developed model over the UNLV Parking-lots area. The developed model is simulated to predict the surface runoff discharge hydrograph from the Moores Run study area

for the rainfall events of May 22, 2017 and, May 24, 2017, the results for which are provided in the results chapter. A time-step size of '1s' and a runtime of 550 mins is used to carry out each simulation. A hydraulic conductivity 'K' value of 0.1 cm/hr. for soil group D, is arbitrarily chosen, to carry out the first simulation. The results from the first simulation is then compared with the actual stream data and depending upon the predicted volume of runoff, the value of 'K' is altered such that the RMSE of the predicted hydrograph with the actual hydrograph becomes less and less. The RMSE of the predicted hydrograph with the actual hydrograph from each simulation for the corresponding 'K' value is then plotted in a 'RMSE vs K value' plot, the results for which are also provided in the results chapter. The developed model is simulated to predict the flooding in UNLV Parking-lots area for the rainfall event of Sep 11, 2012. A time-step size of '0.5s' and a runtime of 180 mins is used to carry out each simulation. The results of the simulation over UNLV Parking-lots area are provided in the results chapter.

4.7) Error analysis

The error analysis for the results of 'rainfall-runoff' simulations is carried out by comparing the RMSE and correlation coefficient of the predicted hydrograph with the actual stream discharge data. Plots of predicted hydrograph for different rainfall events along with the corresponding actual stream-discharge data are provided in the results chapter. The error analysis for flood modeling is done by comparing the predicted peak flood depth and maximum extent of flooding with the actual peak flood depth and actual flood extent.

4.8) Landcover change analysis

The developed hydrologic model is tested for various landcover to analyze the catchment response to such landcover change scenarios. Test runs for four landcover – bare soil, sparse vegetation, dense vegetation, and, Bermuda grass are conducted by changing the values of Manning's roughness co-efficient. A table providing the summary of the Manning's roughness co-efficient used, hydraulic conductivity values, peak flow, time to peak, peak flood depth, duration of flood, and, the total runoff volume from each land cover for the rainfall event of Sep 11, 2012 along with the surface runoff is provided in the results chapter.

4.9) Summary of methodology

This chapter provided a discussion on the methods and procedures followed to develop, calibrate and validate the hydrologic model. Further details of the data to be input into the model along with the explanation of the equations based on which the model provides output are also provided. The procedures followed to determine the time-step size for the model and for error analysis, along with an explanation for image classification and landcover change analysis are also provided. The hydrologic model developed in this research is tested on two study areas the results for which are provided in the results chapter.

CHAPTER 5: RESULTS

This chapter provides the results for the simulation of the developed hydrologic model for the three rainfall runoff events over Moores Run catchment, and, for the flood event of Sep 11, 2012 in the UNLV Parking-lots area. The results for catchment delineation, image classification, and, hydrograph prediction over Moores Run study area are described in the first sub-section. The results for catchment delineation, hydrograph prediction and flood estimation, and, the catchment response to different landcover scenarios for UNLV Parking-lots area are provided in the second sub-section.

5.1) Moores Run study area

This sub-section provides the results for the 'rainfall-runoff' modeling part of the developed hydrologic model.

5.1.1) Results for DEM resampling and watershed delineation

Figure 5.1-1 shows the resampled 30m resolution DEM of the Moores Run study area. The resampling of DEM from 1m to 30m is done in ArcMap 10.1, and, the resampled DEM raster is converted to a 'Matlab' readable format file to carry out the analysis in Matlab. From the DEM it is found that the highest elevation value within the study area is 303.3 m lying towards the north-west end, whereas the lowest elevation value is 109.2 m towards the east end. The general slope of the study area is from the north-west to the east. The 30-m resampled DEM is not smoothened

using filters but is used as it is. Filtering 30-m resolution DEM would significantly change the topography of the study area. However, the 30-m resampled DEM contained some pixels of abnormal elevations which was corrected manually based on the elevations of the neighboring pixels.

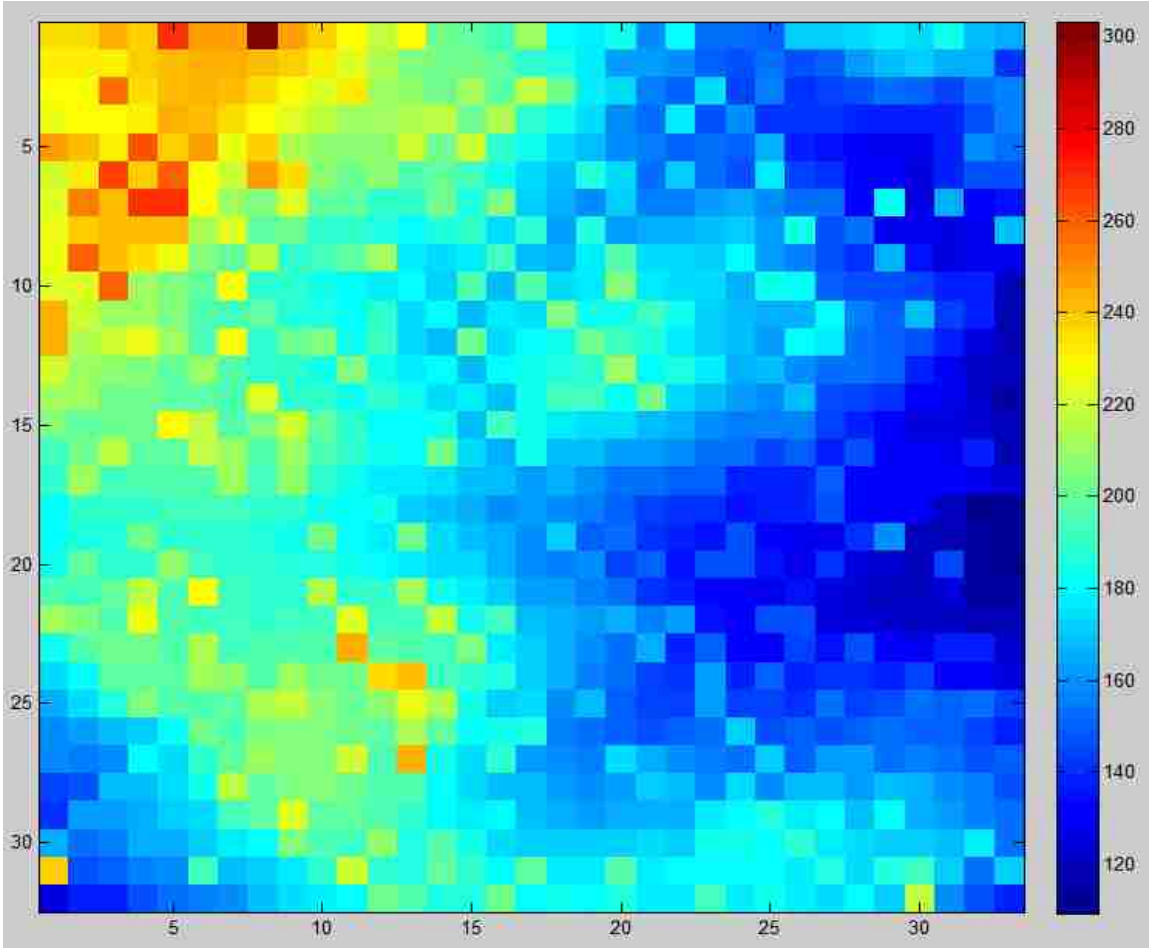

Figure 5.1-1: 30-m resolution DEM of Moores Run study area with elevation values (in meters).

Figure 5.1-2 shows the streams networks, pour-points, ditches, and, catchments of the study area. It is observed that there are 5 cells within the study area that are ditches, and, 17 cells at the boundaries are pour-points. It is also observed that the location of the 14th pour-point (20th row,

33rd column) matches with the location of the stream gage station for the Moores Run study area. It is found that 557 upstream pixel in total contribute to the pixel at 20th row and 33rd (last) column, and so, the catchment has an area of 0.5013 km^2.

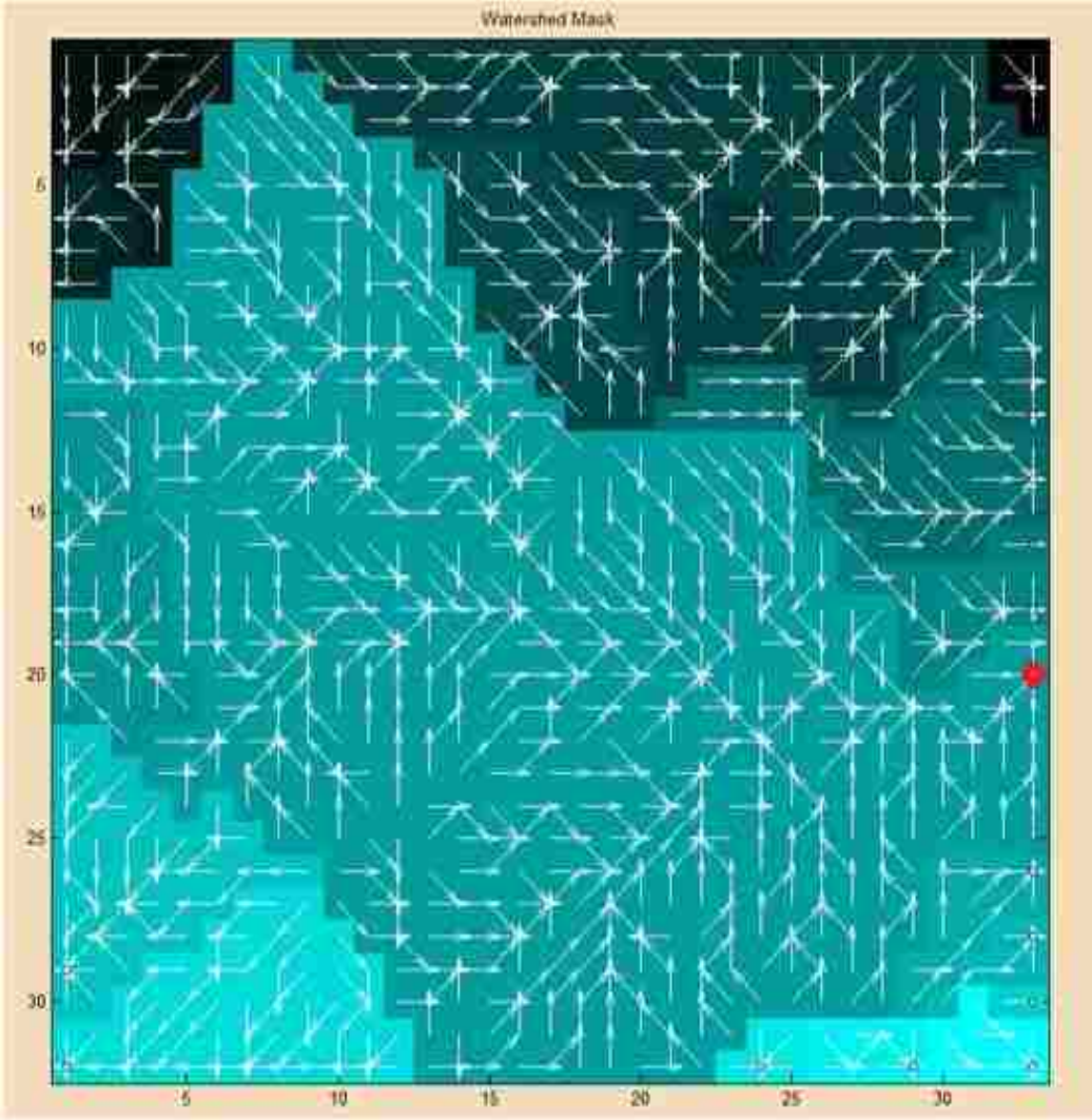

Figure 5.1-2: Catchments for Moores Run study area predicted by the model. (Pixel with red dot represents the pour-point pixel.)

5.1.2) Results for Image classification

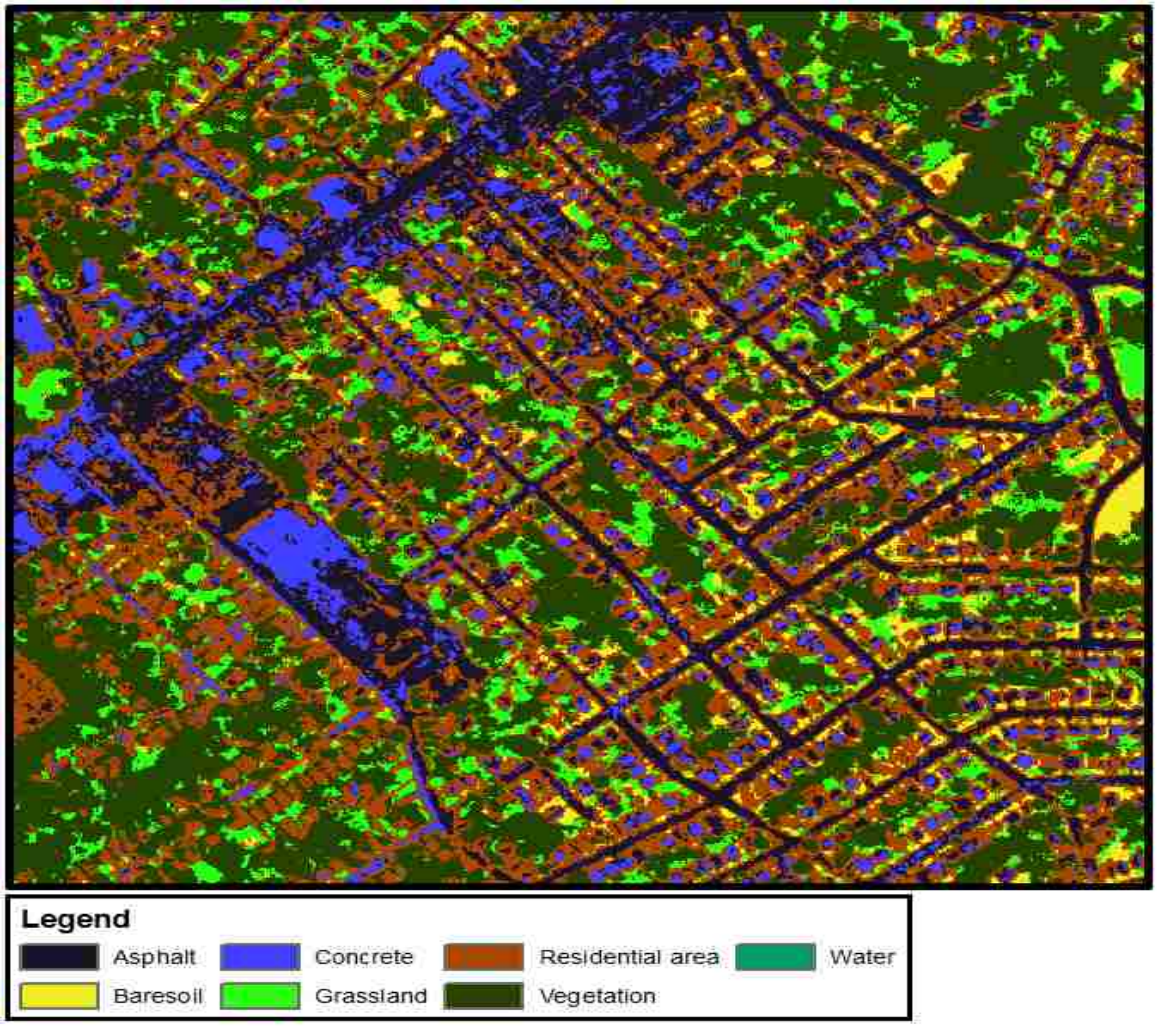

Figure 5.1-3: 1-m resolution Classified image of the Moores Run study area.

Figure 5.1-3 shows the 1m resolution classified image of the Moores Run study area. From the 1m resolution classified image of Moores Run study area, it is found that the study area consists of 32.5% Residential area, 30% Vegetation, 18% Asphalt, 8.5% Grassland, 7% Concrete, 3.99% Bare-soil, and, 0.01% Water landcover pixels. The 1m resolution classified image of the Moores

Run study area is then resampled into 30m resolution image based on ‘majority’ values. Figure 5.1-4 shows the 30m resolution classified image of the study area.

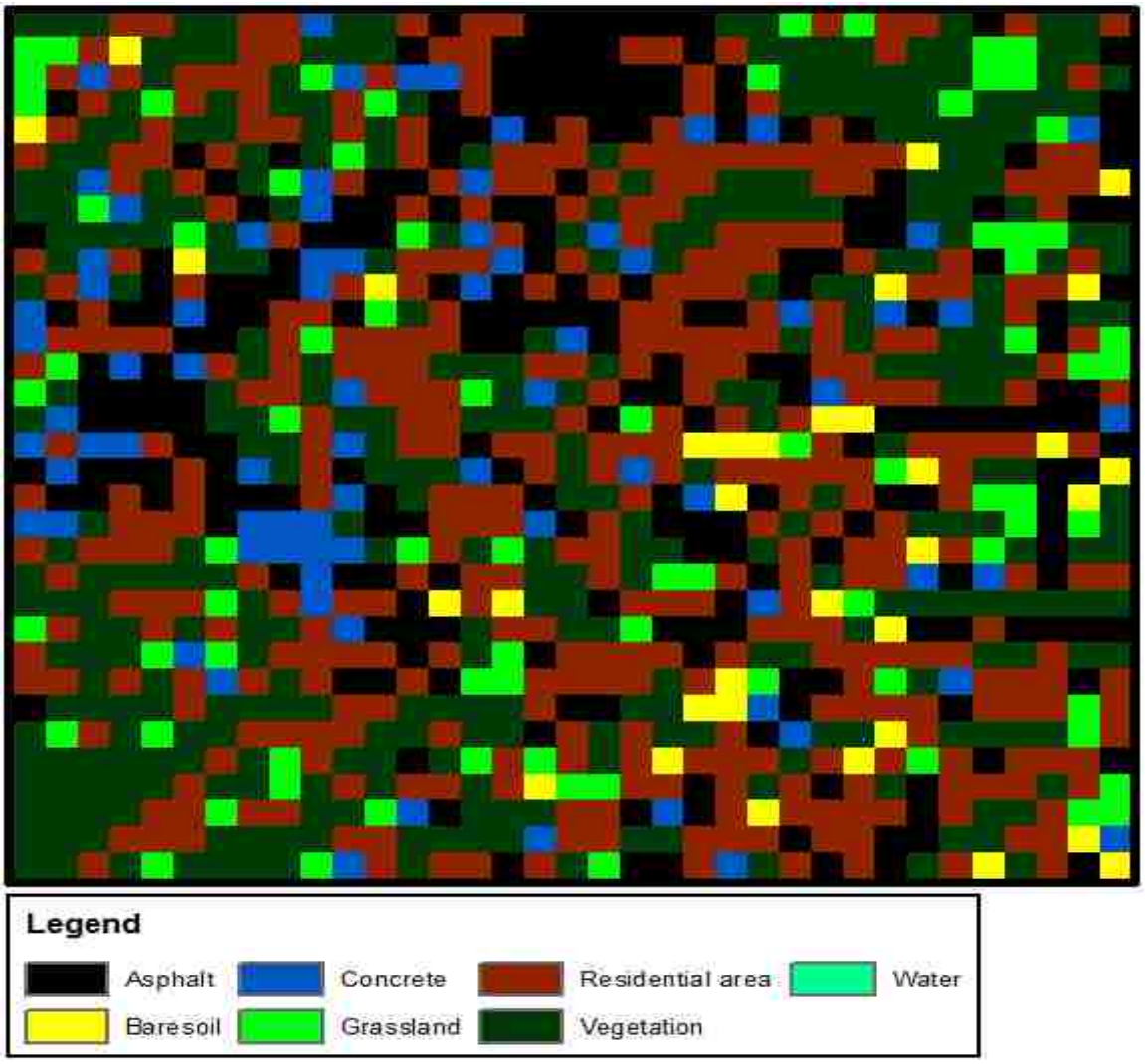

Figure 5.1-4: 30-m resolution classified image of the Moores Run study area.

5.1.3) Calibration and error analysis.

The hydrologic model developed in this research is calibrated using the stream discharge data of the Moores Run trib. stream-gage for two rainfall events as shown in the figure 5.1-5 and

figure 5.1-8 respectively. Figure 5.1-5 shows the plot of actual stream data for the rainfall event of May 22, 2017 over the Moores Run study area.

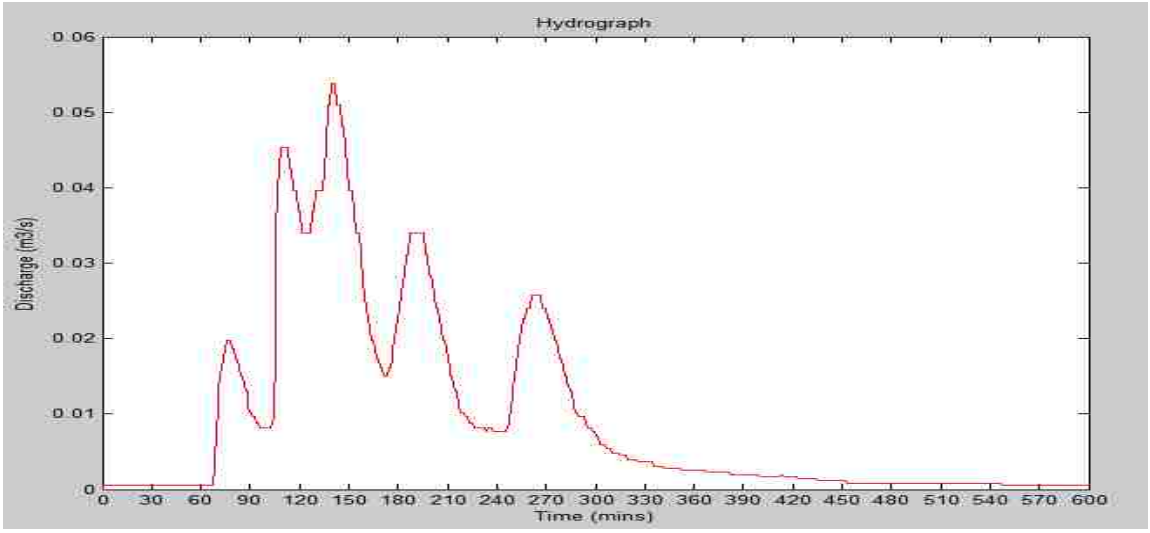

Figure 5.1-5: Actual stream discharge data for the rainfall event of May 22, 2017. (Source: USGS)

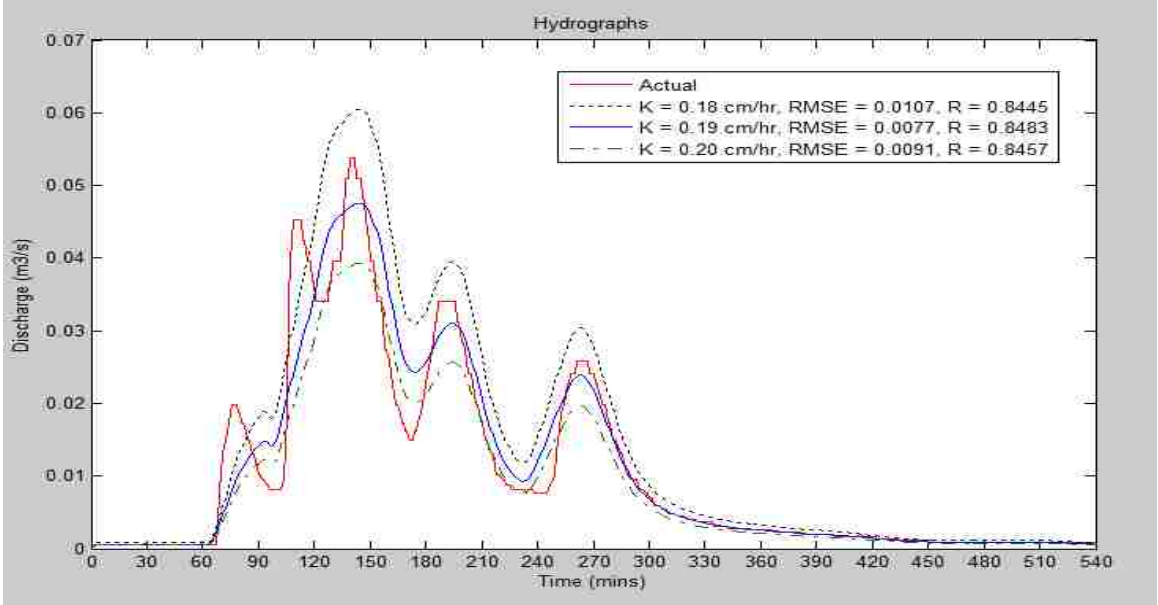

Figure 5.1-6: Comparison of the hydrographs predicted by the model for different values of K for soil group D for the rainfall event of May 22, 2017.

Figure 5.1-9 shows the plot of different hydrographs predicted by the model for the rainfall event of May 22, 2017. It is observed that the predicted hydrograph has the smallest RMSE value of 0.077 m^3/s for K = 0.19 cm/hr. The coefficient of correlation between the predicted hydrograph and actual stream discharge data is 0.8483 in this case. Figure 5.1-10 shows the 'RMSE vs K' plot. It is observed that as the value of 'K' is increased from K = 0.19 cm/hr., the RMSE between the predicted hydrograph and the actual stream discharge data keeps increasing upto K = 0.24 cm/hr. At K > 0.24 cm/hr. no runoff is produced and the RMSE remains the same for all values of K > 0.24 cm/hr.

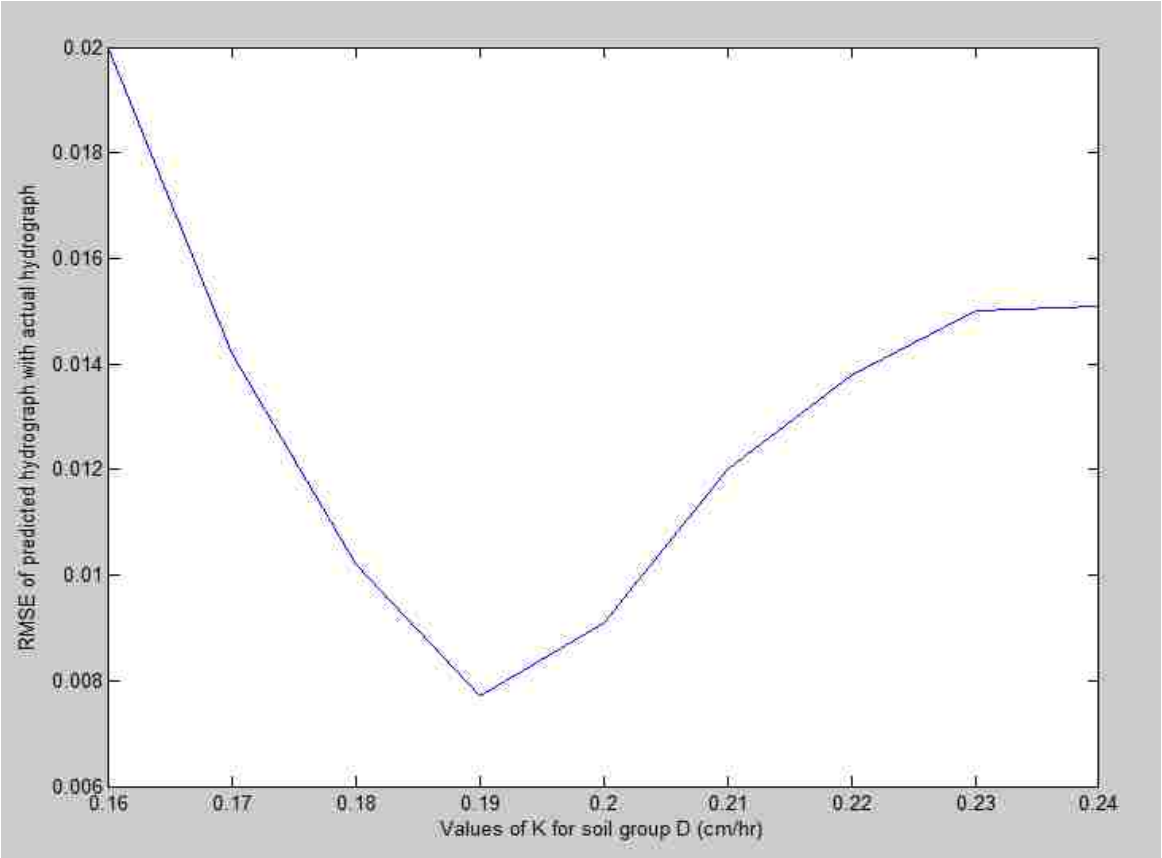

Figure 5.1-7: Plot of 'RMSE vs K' for the first calibration trial.

Figure 5.1-12 shows the plot of different hydrographs predicted by the model for the rainfall event of May 24, 2017. It is observed that the predicted hydrograph has the smallest RMSE

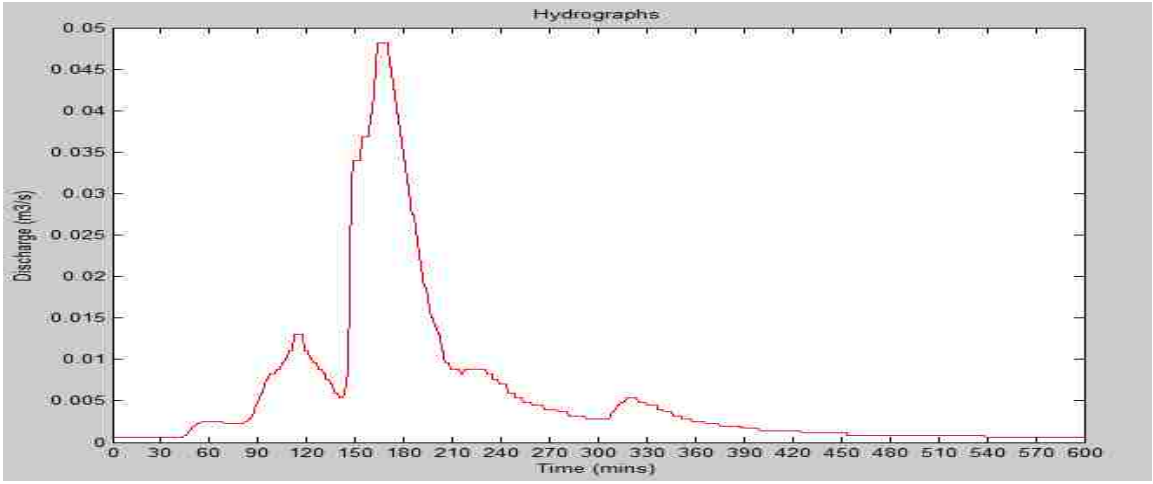

Figure 5.1-8: Actual stream discharge data for the rainfall event of May 24, 2017. (Source: USGS)

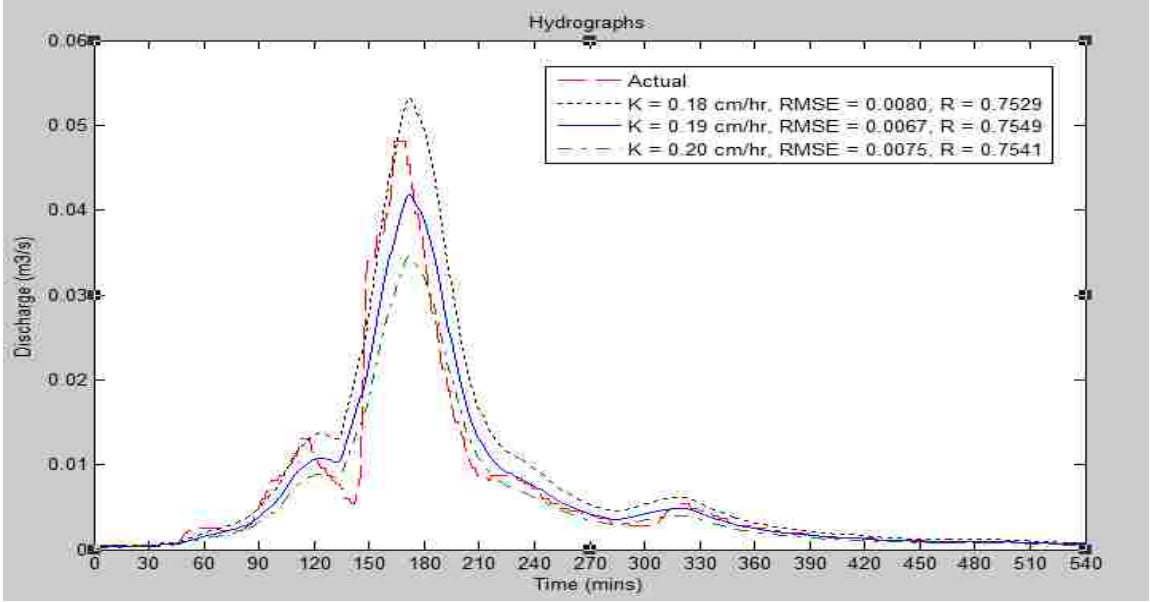

Figure 5.1-9: Comparison of the hydrographs predicted by the model for different values of K for soil group D for the rainfall event of May 24, 2017.

value of 0.0067 m^3/s for K = 0.19 cm/hr. The coefficient of correlation between the predicted hydrograph and actual stream discharge data is 0.7549 in this case. Figure 5.1-13 shows the 'RMSE vs K' plot. It is observed that as the value of 'K' is increased from K = 0.19 cm/hr., the RMSE between the predicted hydrograph and the actual stream discharge data keeps increasing upto K = 0.25 cm/hr. At K > 0.25 cm/hr. no runoff is produced and the RMSE remains the same for all values of K > 0.25 cm/hr.

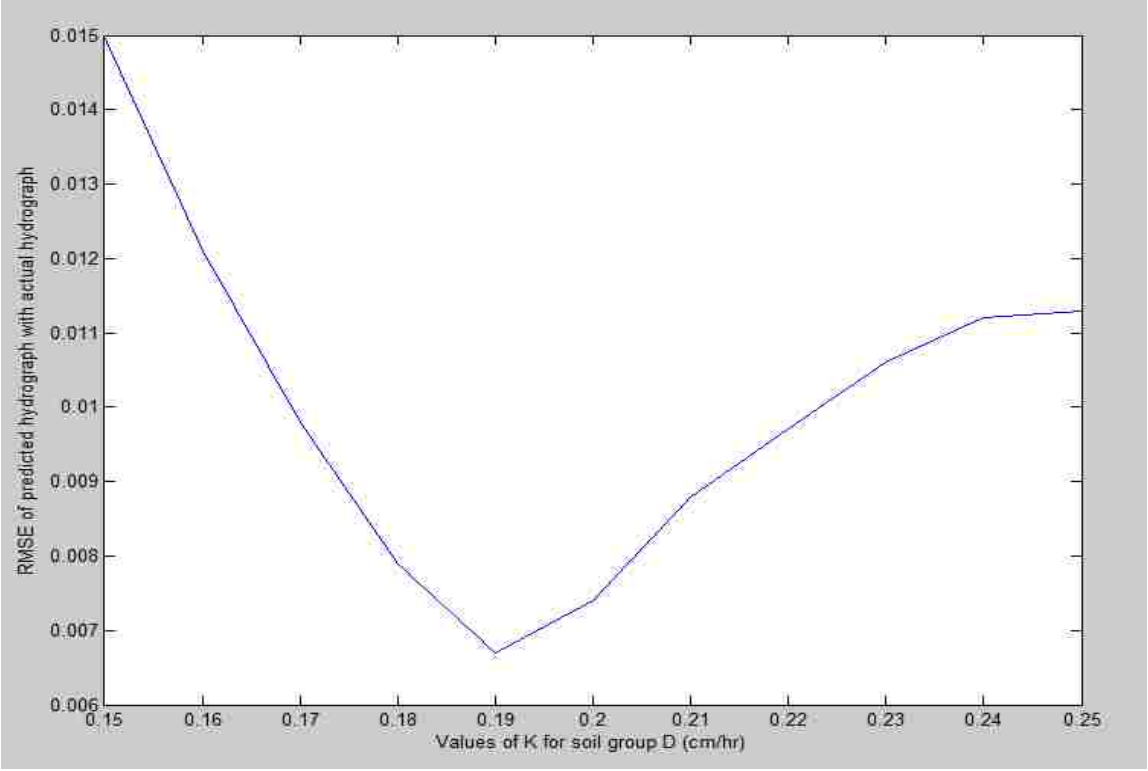

Figure 5.1-10: Plot of 'RMSE vs K' for the second calibration trial.

5.1.4) Hydrographs and validation.

The hydrologic model developed in this research is validated using the rainfall event of April 17, 2017 over the Moores Run study area and the corresponding stream discharge from the

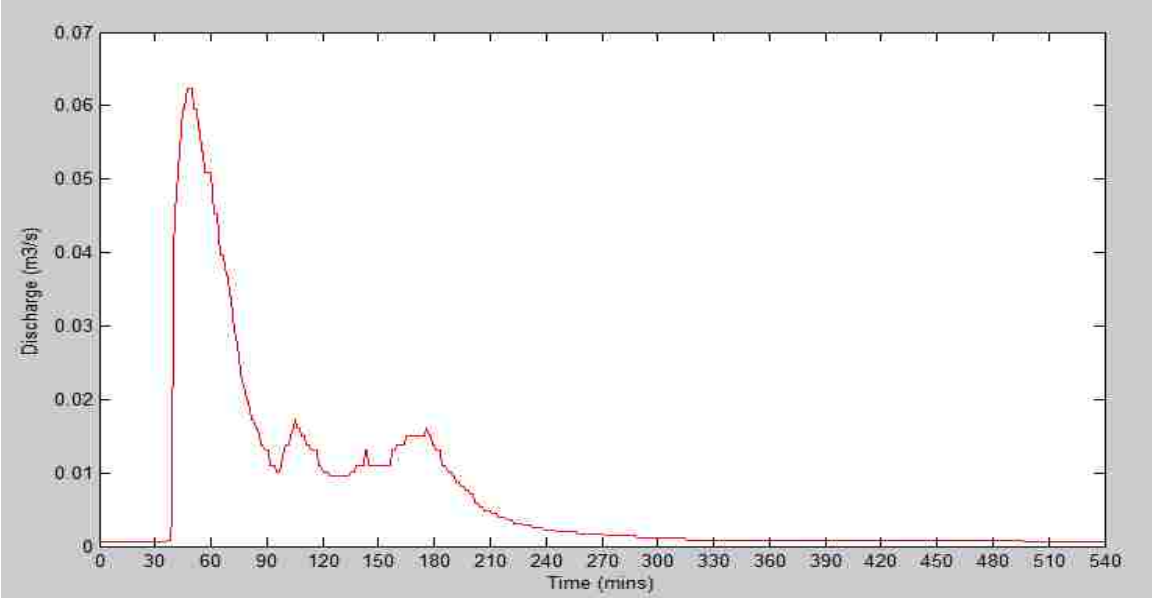

Figure 5.1-11: Actual stream discharge data for the rainfall event of May 24, 2017. (Source: USGS)

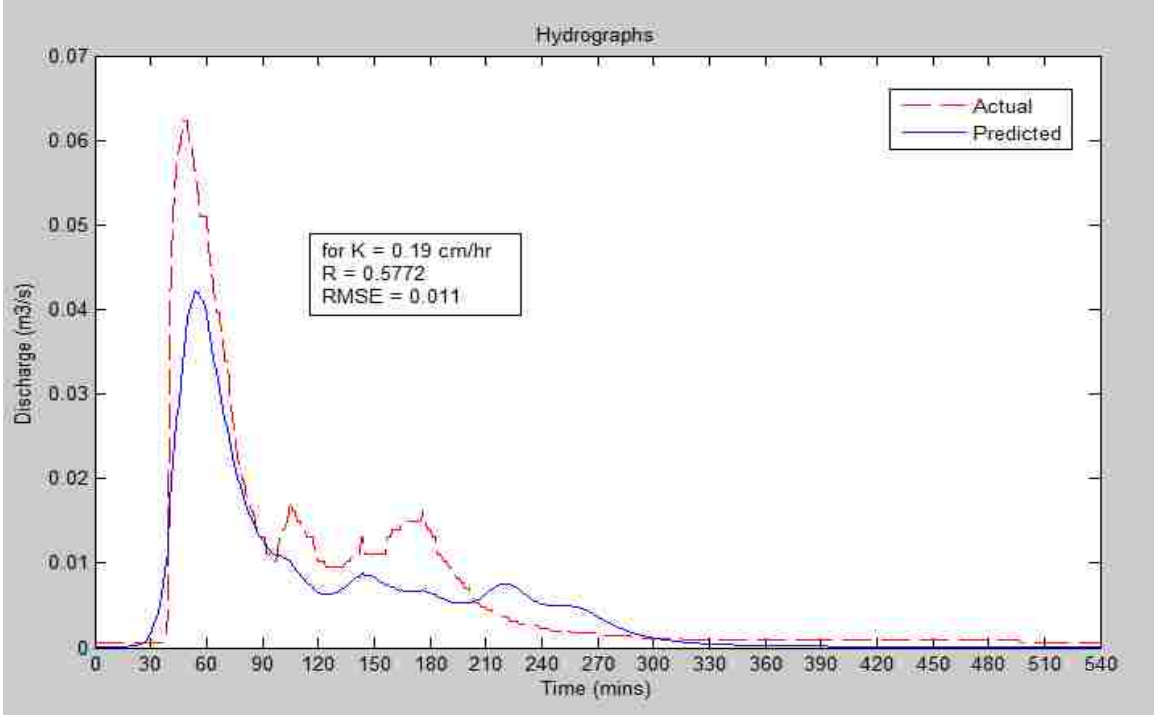

Figure 5.1-12: Comparison of the hydrograph predicted by the model for the rainfall event of April 17, 2017 with the actual stream discharge data from the catchment.

catchment as shown in figure 5.1-11. The model is validated by comparing the hydrograph predicted by the model for the rainfall event of April 17, 2017 with the actual stream discharge data from the catchment, using K = 0.19 cm/hr for soil group D.. It is found that the co-efficient of correlation between the predicted hydrograph and the actual discharge data is 0.5772. Similarly, in this case, the RMSE error between them is found to be 0.011 m^3/s.

5.1.5) Discussion

This sub-section provides the description of the results for Moores Run study area.

For the elevation data to be input into the model, DEM of resolution 1 meter was arbitrarily chosen at first. The rationale for choosing this resolution being - 1) choosing the highest possible resolution to make the stream lines and catchment area predicted by the model match the actual streamlines and the catchment area as closely as possible, and, 2) choosing the highest possible resolution so the accuracy of the landcover characteristic represented by a pixel isn't diluted. However, for the high spatial resolution of 1m, the developed model failed to simulate the rainfall-runoff process because the number of pixels on which computations needed to be carried out exceeded the computational memory space available in the model. Even for DEM of resolutions 10m, and, 20m the simulation process took too long to compute the results. DEM of 30 m resolution was therefore found to be the optimum DEM for Moores Run study area. For DEM of 30 m resolution, it is found that the catchment area predicted by the model for Moores Run trib. consists of 557 pixels in total. So, the predicted catchment has an area of 0.5013 km^2 which is pretty close to the actual drainage area for Moores Run trib. provided by the USGS as 0.5434 km^2.

The error in the model's estimation of the catchment area is found to be 7.75%, and, can be attributed to resolution of the DEM used.

Two rainfall events over the Moores Run trib. catchment are used to calibrate the model and to determine the value of hydraulic conductivity while the third rainfall event is used to validate the model. The summary of the results for the trial simulations of the rainfall-runoff events is provided in the Table 5.1-2:

Table 5.1-2: Summary of outputs for 'rainfall-runoff' analysis

Event Date	Runoff Volume (m^3)		Peak Runoff (m^3/s)		Time to Peak (mins)		K for soil group D. (cm/hr.)
2017	Actual	Predicted	Actual	Predicted	Actual	Predicted	
May-22	339.85	344.26	0.0535	0.0475	140	146	0.19
May-24	208.88	204.01	0.0481	0.0420	167	171	0.19
Apr-17	379.58	189.00	0.0652	0.0425	47	54	0.19

For the rainfall event of May-22, 2017, it is observed that the predicted runoff volume (344.26 m^3) is more than the actual runoff (339.85 m^3) produced from the catchment for 0.19 cm/hr. hydraulic conductivity value for soil group D. The error in estimation of the runoff volume is 1.29%. It is also observed that the 'time to peak' predicted by the model lags the actual 'time to peak' by 6 mins. For the rainfall event of May-24, 2017, it is observed that the runoff volume (204.01 m^3) from the catchment predicted by the model is less than the actual runoff (208.88 m^3)

produced from the catchment for 0.19 cm/hr. hydraulic conductivity value for soil group D. The error in estimation of the runoff volume is -2.33%. It is also observed that the 'time to peak' predicted by the model lags the actual 'time to peak' by 4 mins. RMSE curves of predicted hydrographs with actual hydrograph for different values of 'K' for soil group D are drawn. In all cases, it is observed that the volume of runoff from the catchment increases with the reduction in the value of K which is as expected. However, from calibration, it is also observed that while increasing the value of 'K' to reduce the error in runoff volume, the error in 'time to peak' increases slightly. From the two trials, it is assumed that the values of hydraulic conductivity for soil group 'D' for Moores Run study area is about 0.19 cm/hr., which is consistent with the values of hydraulic conductivity for soil group D found in various literature. However, more trials need to be done to ascertain the accuracy of this result. The value of K for soil group D found from calibration is used to validate the model using the rainfall event of April 17, 2017 over the Moores Run study area. Through validation, it is observed that the estimated runoff volume of 189 m^3/s is less than the actual runoff volume of 379.58 m^3/s. The error in estimation of runoff is found to be -50%. It is also observed that the 'time to peak' predicted by the model, for the first peak, lags the actual 'time to peak' by 7 mins, whereas the second peak and the third peak lag by even more.

From other trials not included in the results, it was noticed that the 'time to peak' could be adjusted by changing the values of Manning's roughness co-efficient associated with each landcover. However, the Manning's roughness co-efficient values for which the model predicted the most accurate 'time to peak' were less than the most commonly used Manning's roughness co-efficient values for different landcovers found from the literature review. Further, the developed model consistently printed out 'cell-mass imbalance' error for smaller than usual Manning's

roughness co-efficient values for time-step size of ‘5 seconds’. It is concluded that in pixels with extremely small Manning’s roughness co-efficient values, the velocity of water within the pixel becomes unrealistically high. Keeping this in consideration, only one set of Manning’s roughness coefficient values was used for the trials to validate the model. The set of Manning’s roughness co-efficient values that was used to validate the developed model contain the lowest values of Manning’s roughness for the associated landcovers that could be found from literature review.

5.2) UNLV Parking-lots area:

This sub-section provides the results for the flood-modeling part of the developed hydrologic model.

5.2.1) Results for DEM filtering and watershed delineation

Figure 5.2-1 shows the unconditioned 10m resolution DEM of the study area. The highest elevation pixel in the study area has an actual elevation of 616.3 m, and the lowest elevation pixel has an actual elevation of 590.8 m. The study area is conditioned using a
5*5 filter in Matlab so as to remove irregularities. Presence of irregularities like sinks or abnormally elevated pixels cause problem in delineating the catchment boundary. Reconditioning of the DEM leads to elimination of irregularities while preserving the overall topographic trend of the study area.

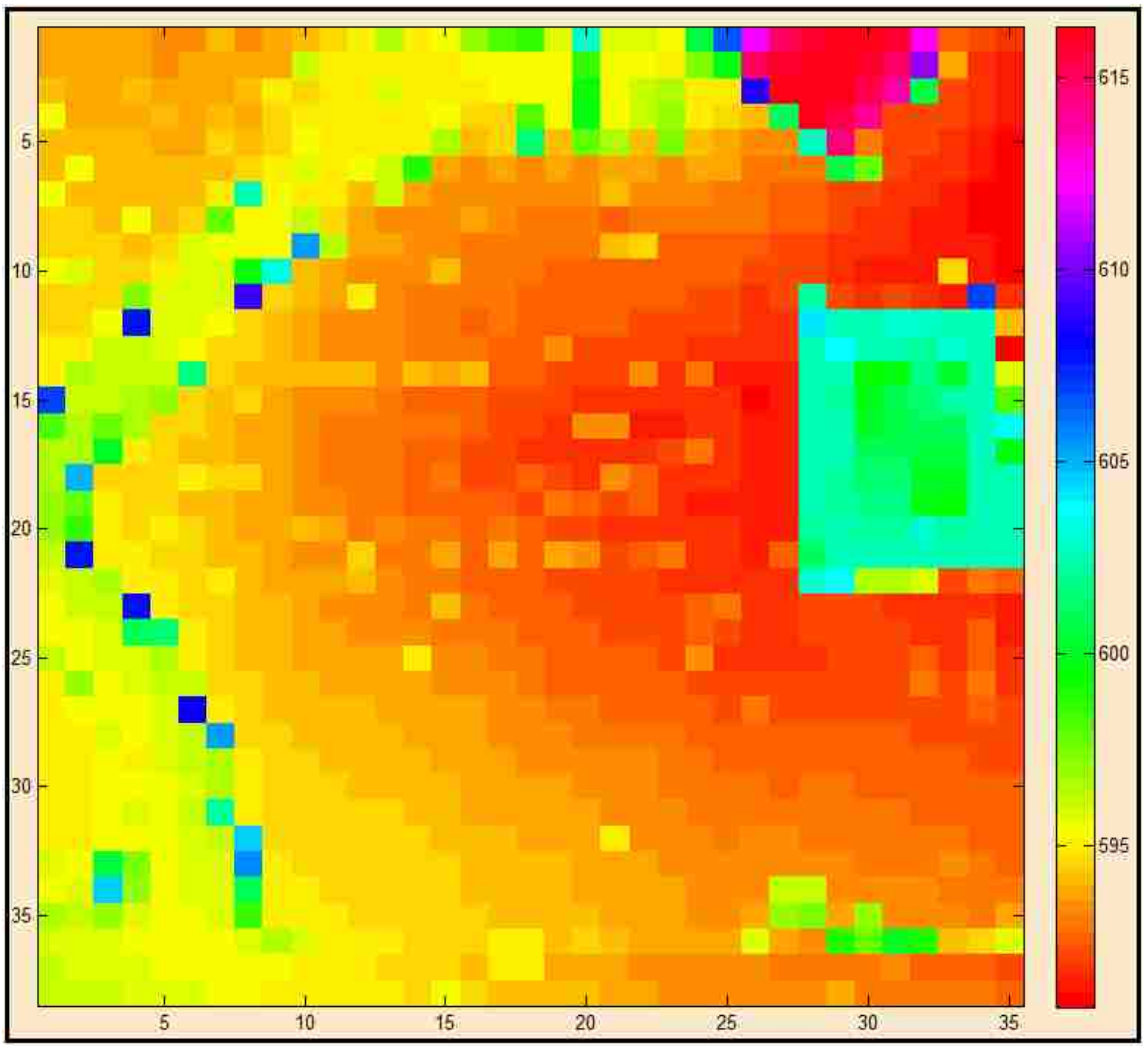

Figure 5.2-1: 10-m resolution DEM of UNLV Parking-lots area with elevation values (in meters).

Figure 5.2-2 shows the conditioned map of the study area. It is observed that the study area in general is sloping towards east with the lowest elevation pixel located at 15th row and 26th column. Reconditioning of DEM causes slight change in the elevation values of pixels depending upon the elevation values of the neighboring pixels. It is observed that, in the reconditioned DEM, the highest elevation pixel has a value of 616.2 m, and, the lowest elevation pixel has a value of

590.8 m. The reconditioned 10m resolution DEM of study area is used to delineate the catchments within the study area.

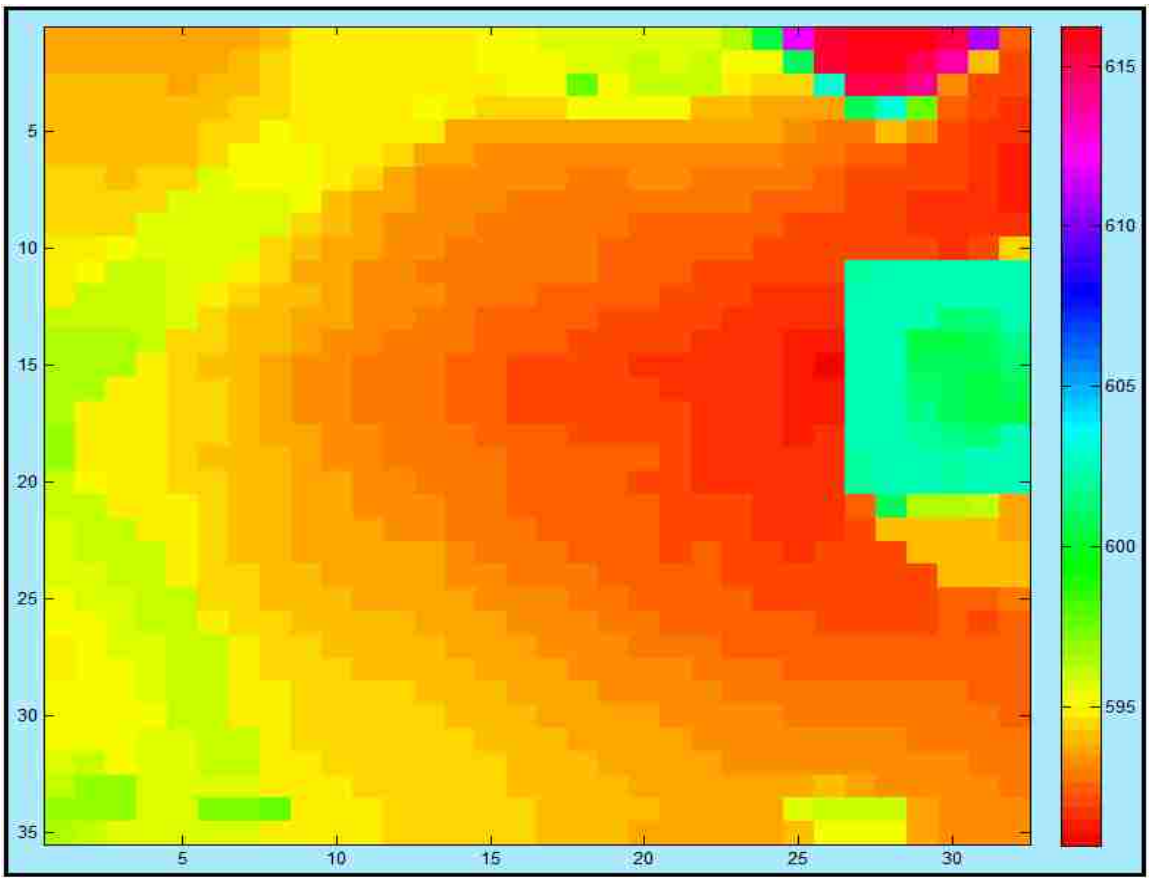

Figure 5.2-2: Reconditioned 10m DEM of UNLV Parking-lots area.

Figure 5.2-3 shows the streamlines, ditches, pour-points, and, catchments obtained by using the 'cell-ordering' function on the study area matrix in Matlab. It is observed that the developed hydrologic model identifies 7 pixels within the study area as ditches and 15 pixels at the boundaries as pour-points. It is also observed that the location of the 4th ditch pixel (15th row, 26th column) identified by the developed hydrologic model matches with the location of the drainage inlet of the Parking-lots area, located in front of the Tropicana Garage area. It is found that 757 upstream pixel in total contribute to the pixel at 15th row and 26th column, and so the

catchment has an area of 75,800 m^2. For analysis purpose, only the catchment with pixels contributing to the pixel at 15^{th} row and 26^{th} column is considered in this research and all other catchments are ignored.

Figure 5.2-3: Catchment areas within the UNLV Parking-lots study area predicted by the model. Pixel with red dot represents the pour-point pixel.

Figure 5.2-4: Location of the pour-point predicted by the developed hydrologic model as compared to the actual position of the drainage inlet.

5.2.2) Hydrographs

The developed model only identifies the cells at the boundary of the study area matrix as pour-points and hydrographs can only be plotted pour-points. However for the catchment area concerned, it is found that the drainage inlet of the study area matches with the location of the ditch pixel at 15th row and 26th column, which is not a boundary pixel. In the developed hydrologic

model, pour-points are assigned a drainage capacity of infinity and ditch pixels of zero by default. The inflow from other pixels into the ditch pixel is supposed to just raise the flow-depth in the ditch pixel until the sum of elevation of the ditch pixels and the flow-depth in the ditch pixel matches with the sum of elevations of the neighboring pixel and the flow-depth in the neighboring pixels. Once they match, then the inflow into the ditch pixel is distributed equally to raise the flow depth in the ditch pixel as well as the neighboring pixels depending on the number of neighboring pixels whose total elevation matches with that of the total elevation of the ditch pixel. However, since the ditch pixel concerned actually has a drainage inlet, a value of 0.48 m^3/s (assumed based on Urban Water Drainage Criteria Manual, 2002) is manually assigned as the drainage capacity of the concerned ditch pixel, after which the hydrologic model treats the concerned ditch pixel as a pour-point and not as a ditch pixel. Figure 5.2-5 shows the runoff hydrograph at the drainage inlet for the given rainfall.

It is observed that the peak flow occurs after just 15 mins from the beginning of the rainfall event. It is also observed that a runoff becomes less than 0.001 m^3/s after 156 mins. Figure 5.2-5 shows the hydrograph when the drainage capacity of the inlet is considered to be infinite. The model also estimates that two a peak flow of 1.6 m^3/s occurs around 33 mins for a drainage inlet of infinite capacity. The model also predicts that the runoff becomes less than 0.001 m3/s after 126 mins in this case.

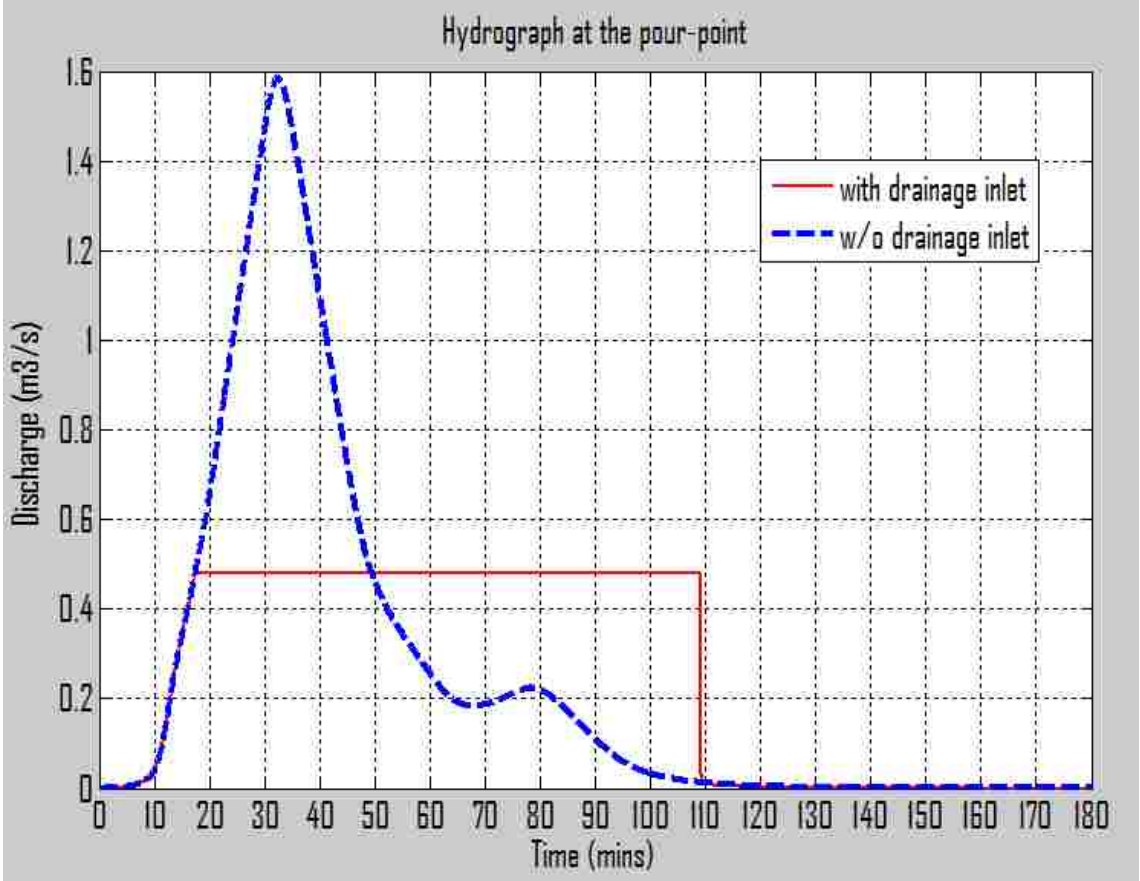

Figure 5.2-5: Predicted hydrograph at the pour-point for the rainfall event of Sep 11, 2012.

5.2.3) Inundation mapping and Estimation

Figures through 5.2-6 to 5.2-10, show the inundated pixels within the catchment at various time steps. The color bars provide the depth of flooding in meters.

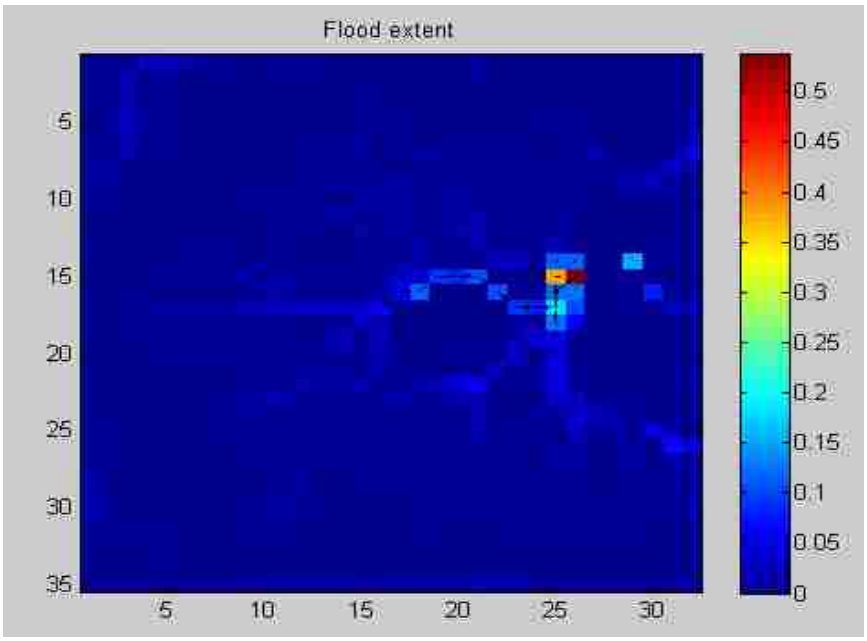

Figure 5.2-6: Inundation map of the Parking-lots catchment at 16 mins.

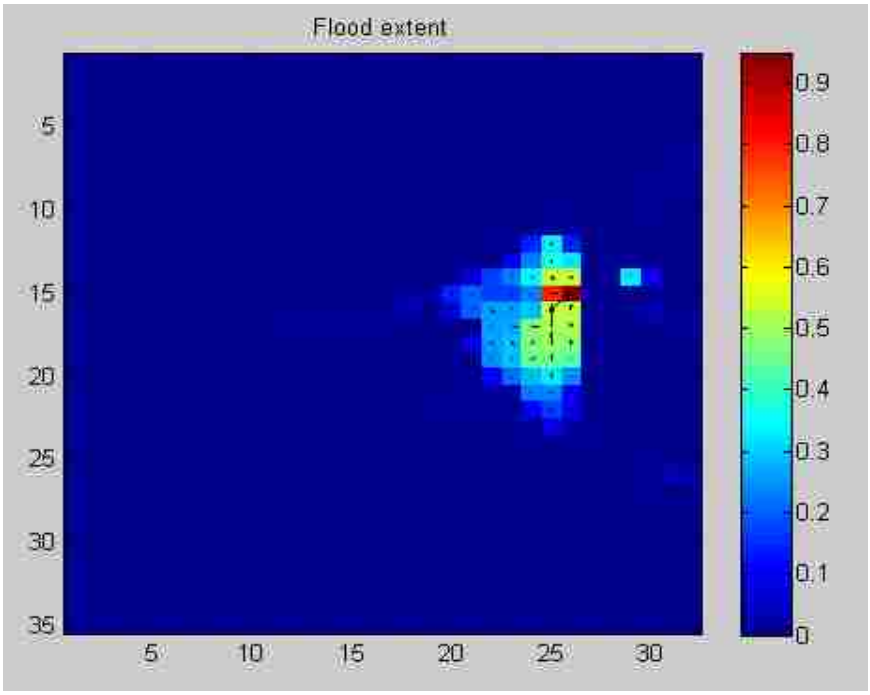

Figure 5.2-7: Inundation map of the Parking-lots catchment at 30 mins.

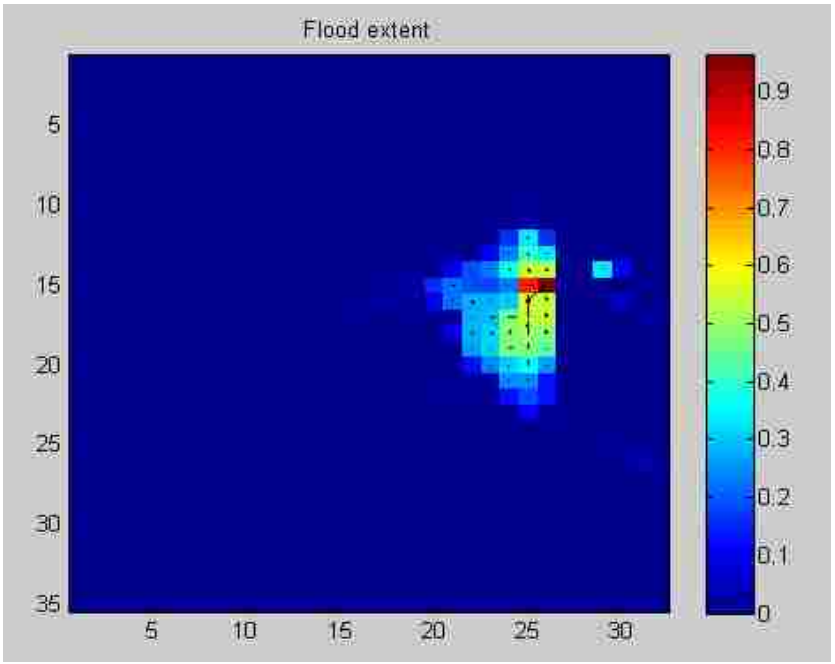

Figure 5.2-8: Inundation map at 37 mins (maximum flood depth at the inlet pixel).

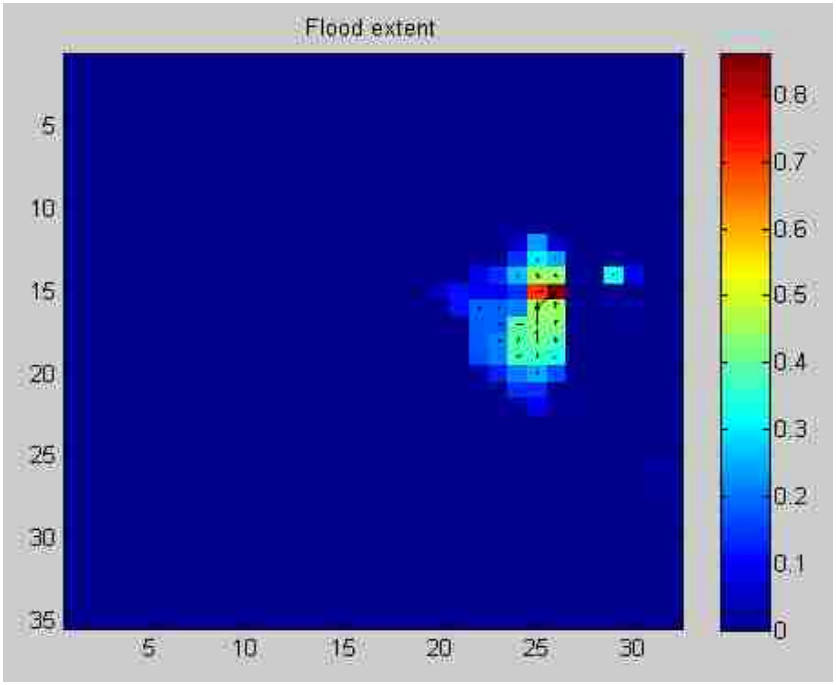

Figure 5.2-9: Inundation map of the Parking-lots catchment at 60 mins.

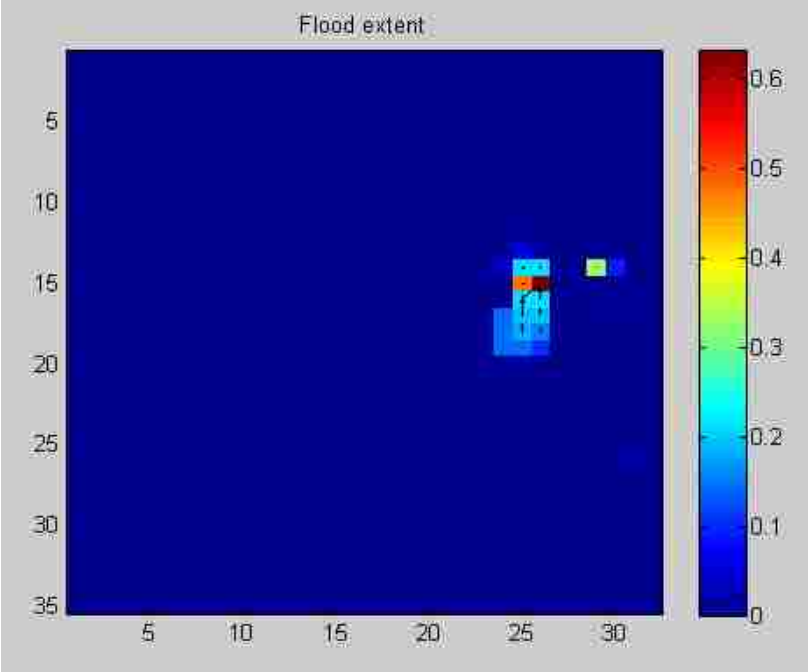

Figure 5.2-10: Inundation map of the Parking-lots catchment at 90 mins.

5.2.4) Validation of the model

The developed model is validated for only 10m resolution DEM of the study area. The validation of 'flood modeling' part of the developed model is done by comparing two parameters – flood depth and extent of flooding.

5.2.4.1) Validation for flood depth estimation

Figure 5.2.4-1 shows the image used for the validation of the flood depth estimation by the model. From the figure, it is observed that the peak flood elevation is about 0.85 m, at and around the drainage inlet. The peak flood elevation at the drainage inlet cell as predicted by the model is 0.96 m.

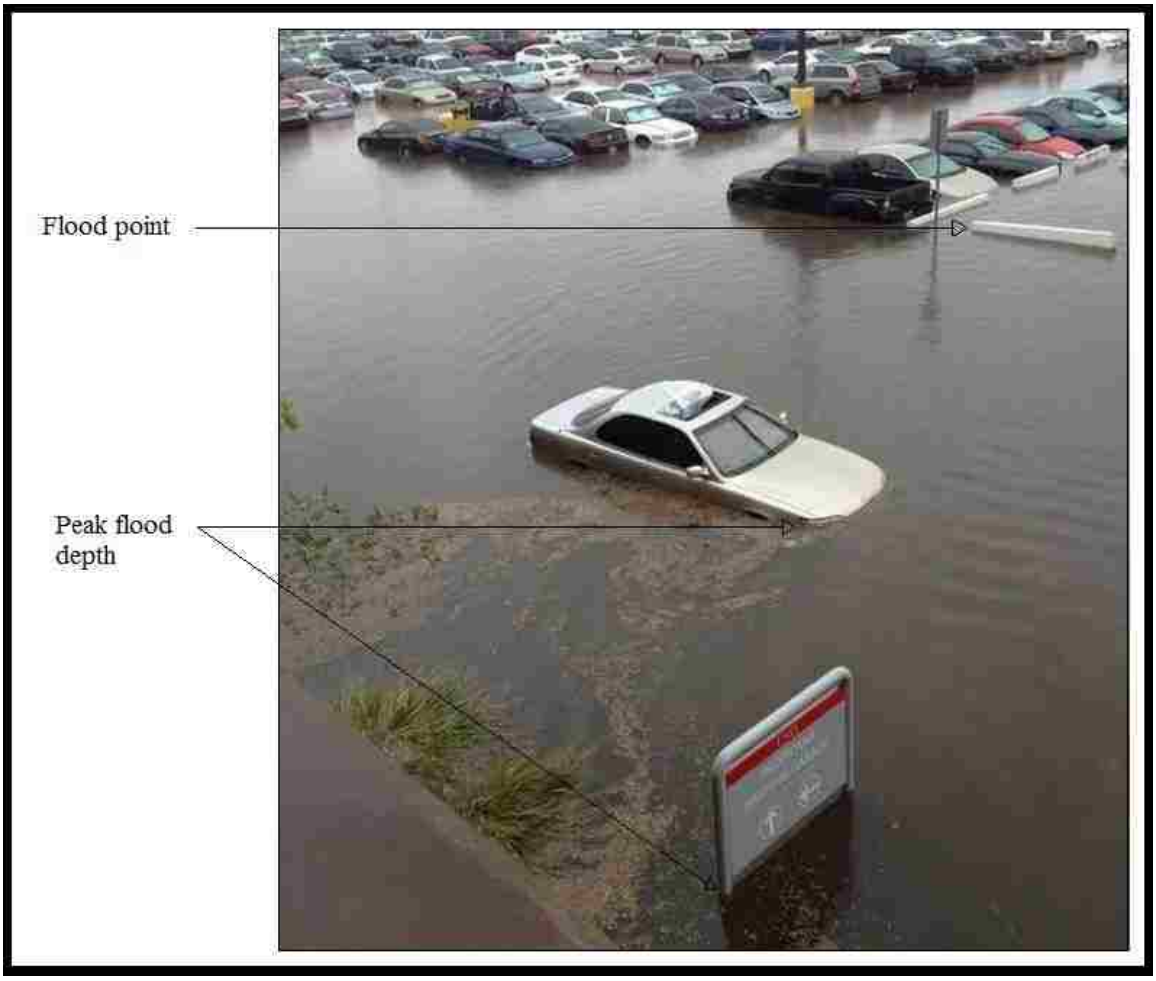

Figure 5.2.4-1: Image used for the validation of the peak flood depth. (Source: UNLV RebelYell)

5.2.4.2) Validation for flood extent estimation

Figure 5.2.4-2 shows the image used for the validation of the flooding extent estimation by the model. From the figure, it is observed that the maximum extent of flooding towards the West end from the drainage inlet is about 80.48 m. The maximum extent of flooding towards the western side from the pour-point as predicted by the model is 70 m. Pictures to validate the extent of flooding towards the South end and the North end couldn't be found.

Figure 5.2.4-2: Image used for the validation of maximum extent of flooding towards West end.

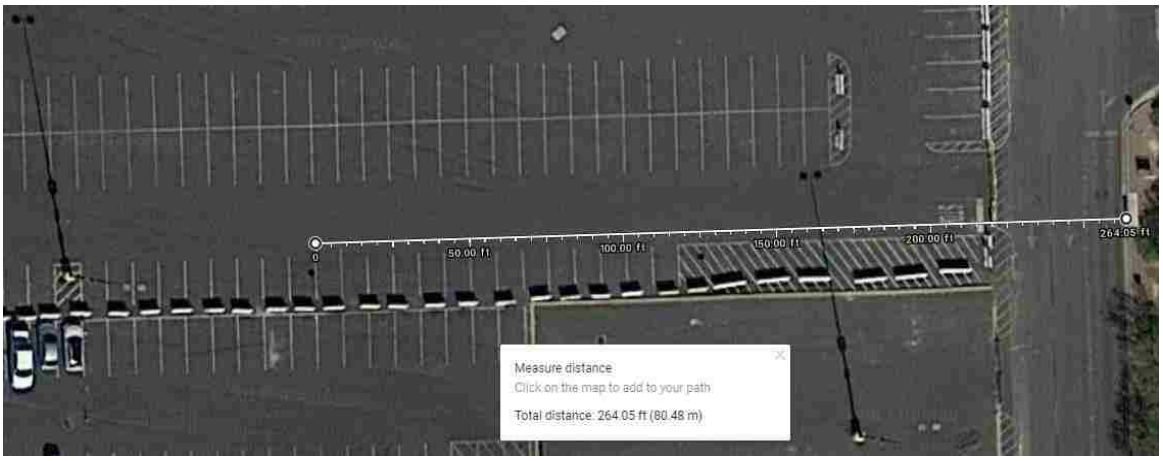

Figure 5.2.4-3: Distance from drainage inlet to the actual maximum extent of flooding towards the West end as measured in Google-Map.

5.2.5) Discussion

This sub-section provides a description of the results for model simulation run over UNLV Parking-lots area.

The 10-m resolution DEM data for the study area is derived from 1-m resolution LiDAR data in ArcMap and converted to a format usable in Matlab. DEM of higher resolutions namely 2 m, 3 m, and, 4 m for the study area were also prepared. The trial for hydrologic model was started with the highest resolution DEM available i.e. 1 m. However, it is found that the size of the study area (350m*380m) is too large for 1-m resolution DEM to be used. For 1-m resolution DEM, the study area consisted of about 133,000 pixels which meant that the results for simulations couldn't be obtained within a reasonable time frame. It is also found that 3 m, and, 4 m resolution DEMs of the study area are also unsuitable keeping in consideration the scope of this research. DEM's of resolution lower than 10m for the study area, are not considered in this research as they don't define the topography of urban watersheds accurately. Hence, 10m resolution DEM of the study area is found to be the most suitable for this research.

Using the 10-m resolution DEM of the UNLV Parking-lots study area and the rainfall event of Sep 11, 2012, the developed model predicted a peak flow of 1.6 m^3/s at around 33 mins from the beginning of the rainfall as shown in figure 5.2-6. The model also predicted that the runoff from the catchment lasts for 156 mins. However, Sayed (2014) using 5-m resolution DEM of the same study area and the same rainfall-event but SCS Curve number method found that a peak runoff of 2.91 m^3/s occurs at around 82 minutes from the beginning of the rainfall as shown in figure 5.2-7. Further, Sayed (2014) found that the runoff from the catchment ends after 203 minutes.

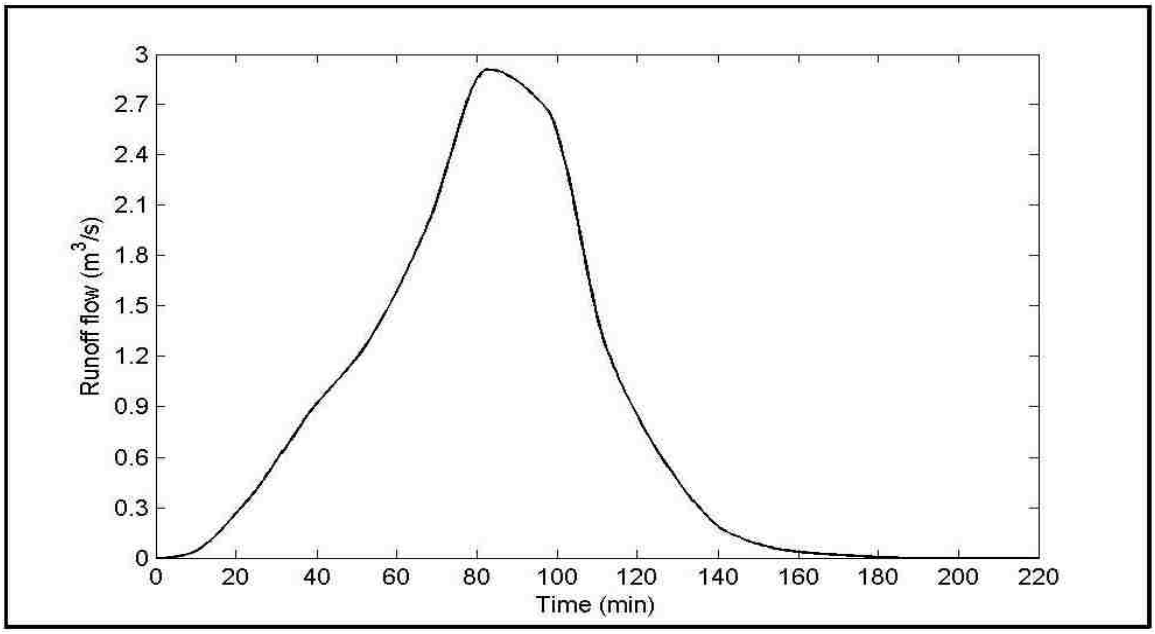

Figure 5.2.5-1: Runoff hydrograph at the drainage inlet of UNLV Parking-lots area, for the rainfall event of Sep 11, 2012 using SCS Curve number method. (Source: Sayed, 2014)

This difference in time to peak and peak runoff volume from the catchment could be due to the difference in methods used; the developed model is Green-Ampt infiltration based model, while, the model developed by Sayed was SCS Curve Number model. It may also be due to other factors like the resolution of the DEM of the study area, and/or, the resolution of rainfall used for simulation of the 'rainfall-runoff' event.

5.3) Landcover change scenarios

The developed hydrologic model is tested for various landcover to analyze the catchment response to such landcover change scenarios. Test runs for four landcover change scenarios are

conducted and the results obtained are compared with the results obtained from the actual landcover, and, an analysis of the comparison is provided.

Scenario 1: The catchment area consists of bare-soil only.

In this case, the landcover for the catchment area is considered to be bare soil by assigning the Manning's roughness coefficient value of 0.018 for all pixels within the catchment. Figure 5.3-1 shows the runoff hydrograph at the drainage inlet for the given rainfall event when the landcover of the catchment area is considered to be bare soil. It is observed that that a peak flow of 0.73 m^3/s occurs at 36 mins. Figure 5.3-1 also shows the hydrograph at pour-point when the drainage inlet is considered. It is observed that the flooding starts after 33 mins and lasts upto 49 mins.

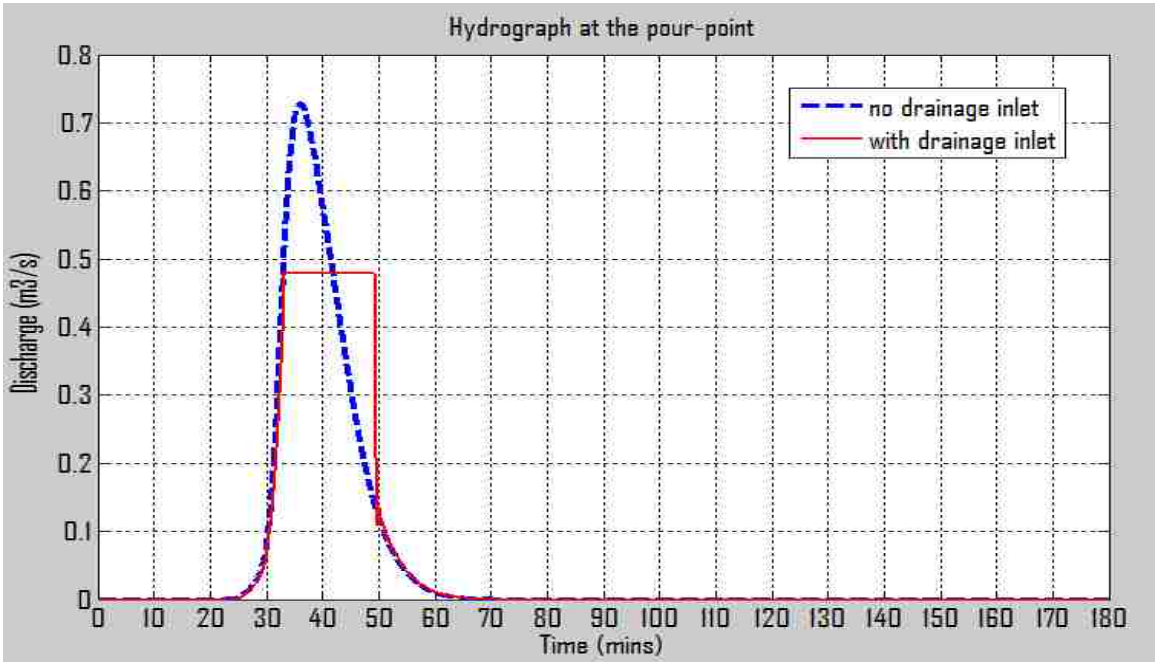

Figure 5.3-1: Runoff hydrograph at the pour-point for bare-soil.

Figure 5.3-2 shows the extent of inundation at peak flow. The model predicts that the inlet pixel is flooded to a maximum elevation of 0.75 m at 37 mins.

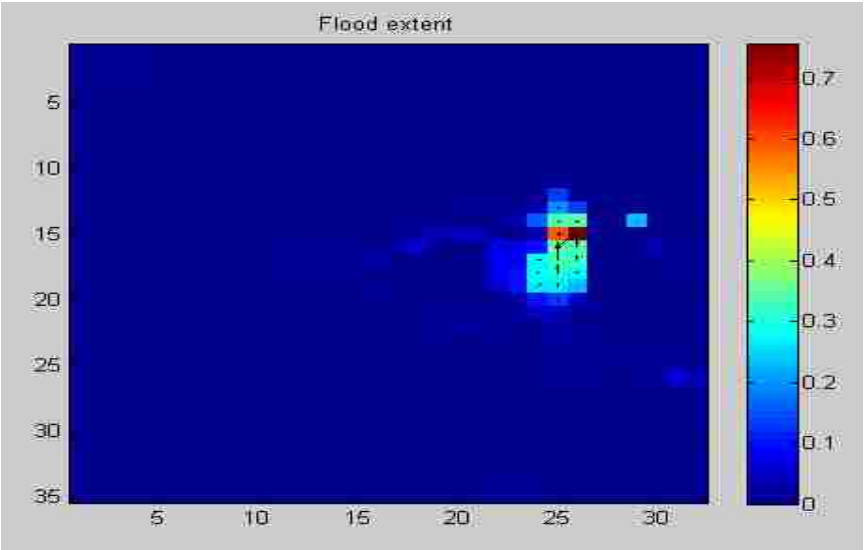

Figure 5.3-2: Inundation map at 36 mins (maximum flood depth of 0.75 m at the inlet pixel).

Scenario 2: The catchment area is covered with sparse vegetation.

In this case, the landcover for the catchment area is considered to be sparse vegetation by assigning the Manning's roughness coefficient value of 0.023 for all pixels within the catchment. Figure 5.3-3 shows the runoff hydrograph at the drainage inlet for the given rainfall event when the landcover of the catchment area is considered to be sparse vegetation. It is observed that a peak flow of 0.69 m^3/s occurs at 37 mins. Figure 5.3-3 also shows the hydrograph at pour-point when the drainage inlet is considered. It is observed that the flooding starts after 34 mins and lasts upto 49 mins.

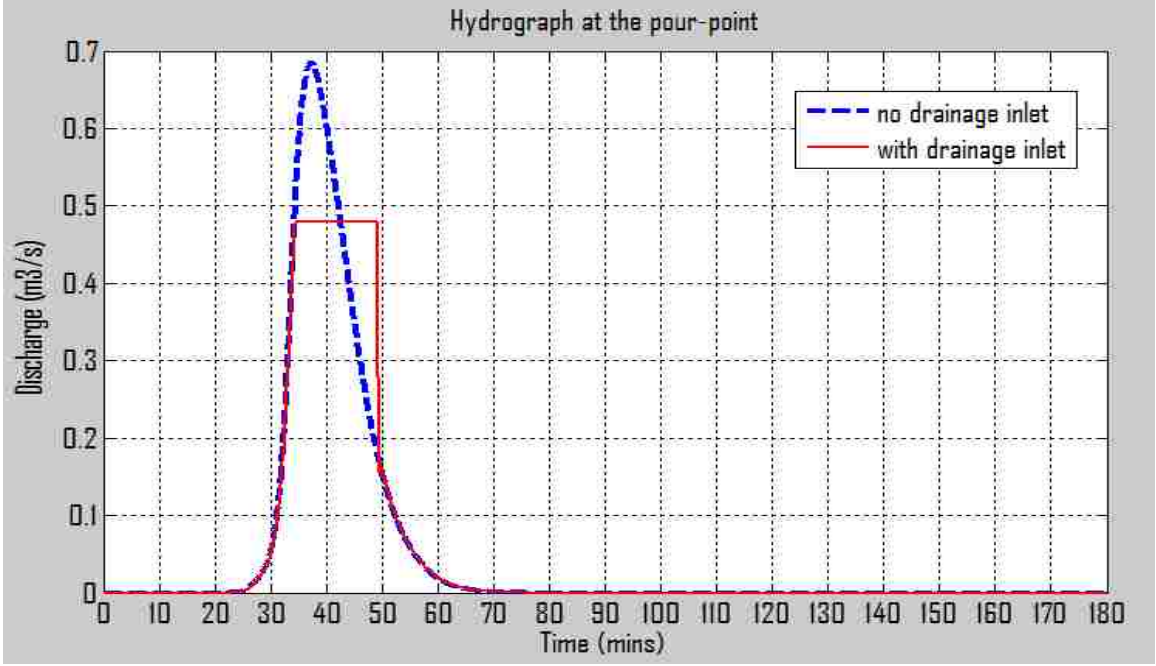

Figure 5.3-3: Runoff hydrograph at the pour-point for sparse vegetation without the drainage inlet.

Figure 5.3-5 shows the extent of inundation at peak flow. The model predicts that the inlet pixel is flooded to a maximum depth of 0.72 m at 39 mins.

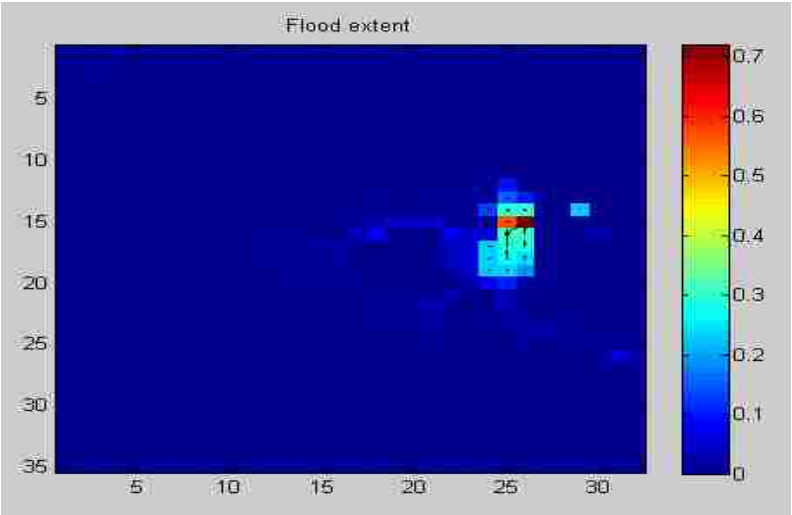

Figure 5.3-4: Inundation map at 39 mins (maximum flood depth of 0.72 m at drainage inlet pixel).

Scenario 3: The catchment area is covered with dense vegetation.

In this case, the landcover for the catchment area is considered to be dense vegetation by assigning the Manning's roughness coefficient value of 0.080 for all pixels within the catchment. Figure 5.3-5 shows the runoff hydrograph at the drainage inlet for the given rainfall event when the landcover of the catchment area is considered to be dense vegetation. It is observed that a peak flow of 0.35 m^3/s occurs at 47 mins. No flooding occurs in this case.

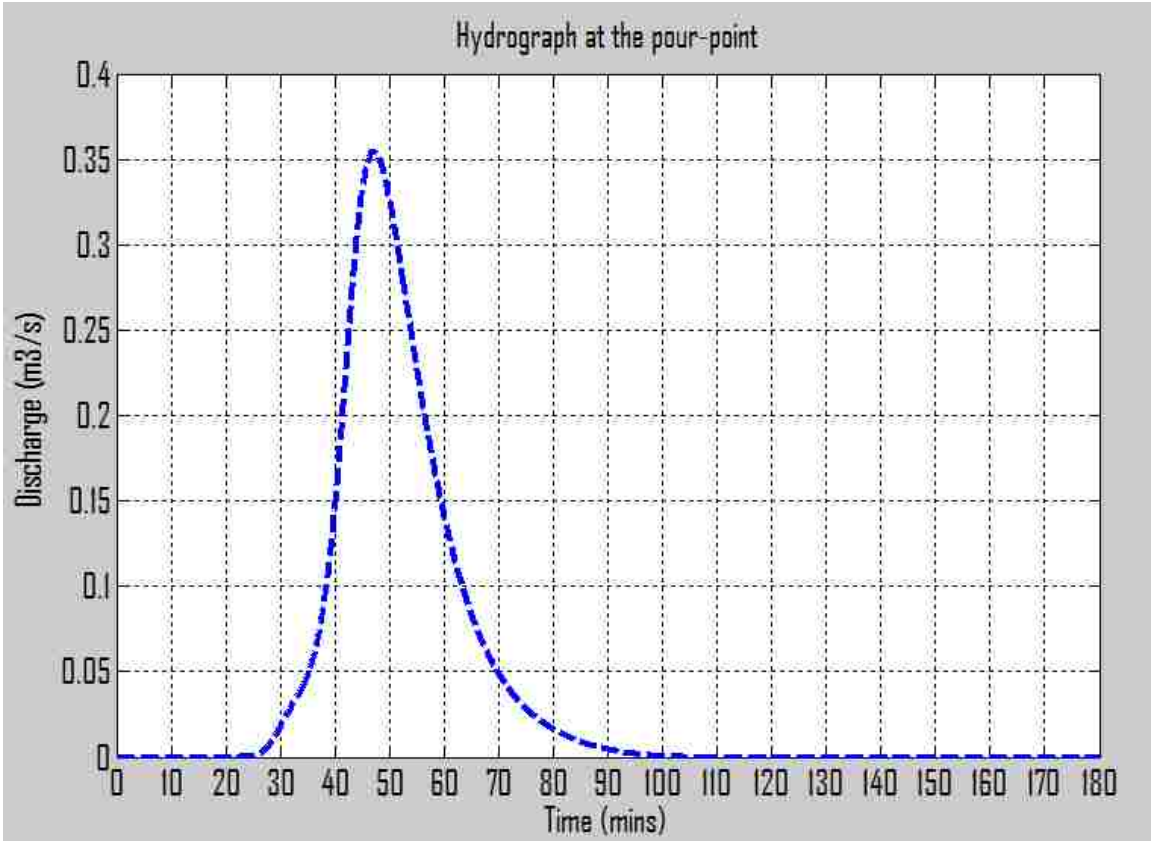

Figure 5.3-5: Runoff hydrograph at the pour-point for dense vegetation with/without the drainage inlet.

Scenario 4: The catchment area is covered by Bermuda grass

In this case, the landcover for the catchment area is considered to be Bermuda grass by assigning the Manning's roughness coefficient value of 0.41 for all pixels within the catchment. Figure 5.3-6 shows the runoff hydrograph at the drainage inlet for the given rainfall event when the landcover of the catchment area is considered to be Bermuda grass. It is observed that the peak flow of 0.026 m^3/s occurs at 87 mins. No flooding occurs in this case as well.

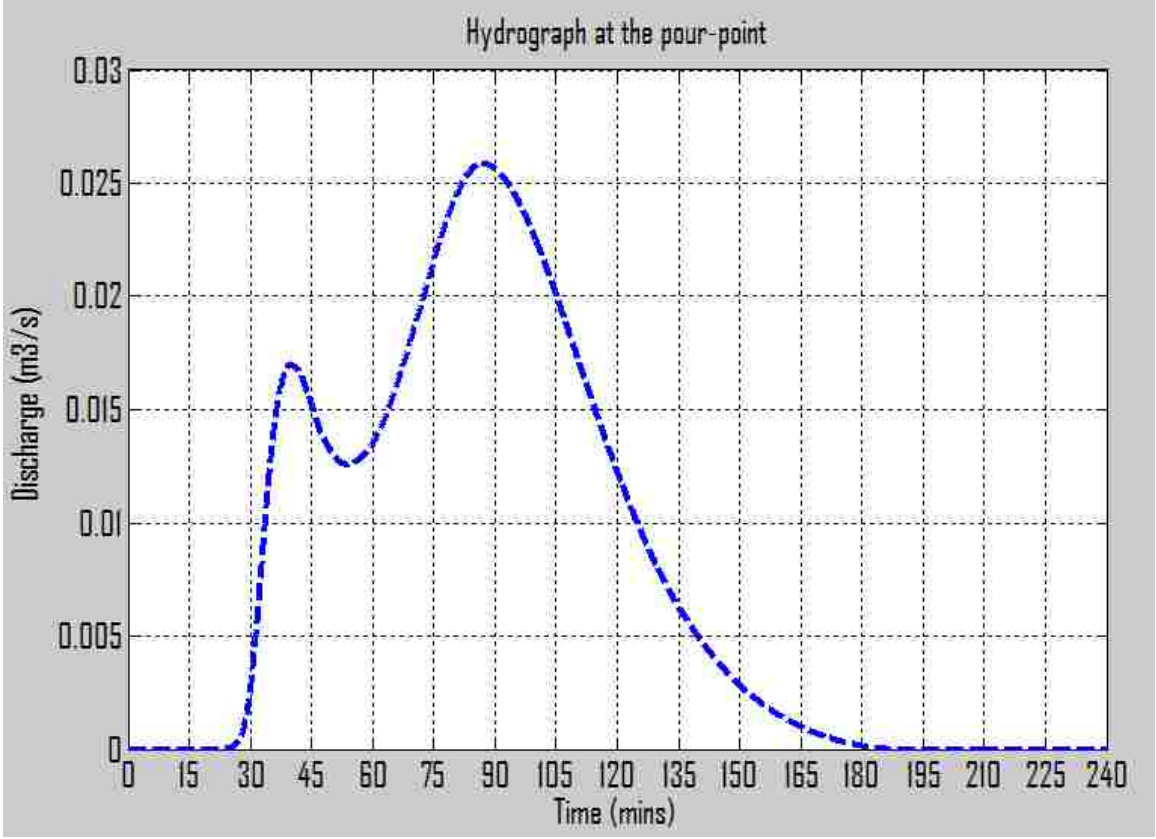

Figure 5.3-6: Runoff hydrograph at the pour-point for Bermuda grass (with and without the drainage inlet).

5.3.1) Discussion

Figure 5.3-9 shows the plot of the runoff hydrographs at the pour-point for all the landcover change scenarios. Table 5.3-1 shows the summary of the land cover change scenarios. For the first land cover i.e. asphalt, the total volume of runoff from the catchment for the rainfall event of Sep 11, 2012 is estimated to be 2656 m^3. For all the other land covers, the total volume of runoff from the catchment is estimated to be 456.76 m^3. It is as expected as the hydraulic conductivity of soil for all the other cases is 0.9018 cm/hr. However, it is observed that the time to peak and the peak flow for each landcover is different and depends on the Manning's roughness coefficient value. Asphalt has the highest peak flow value of 1.6 m^3/s and the lowest time to peak at 32 mins, while Bermuda grass has the lowest peak flow value of 0.026 m^3/s and the highest time to peak at 87 mins.

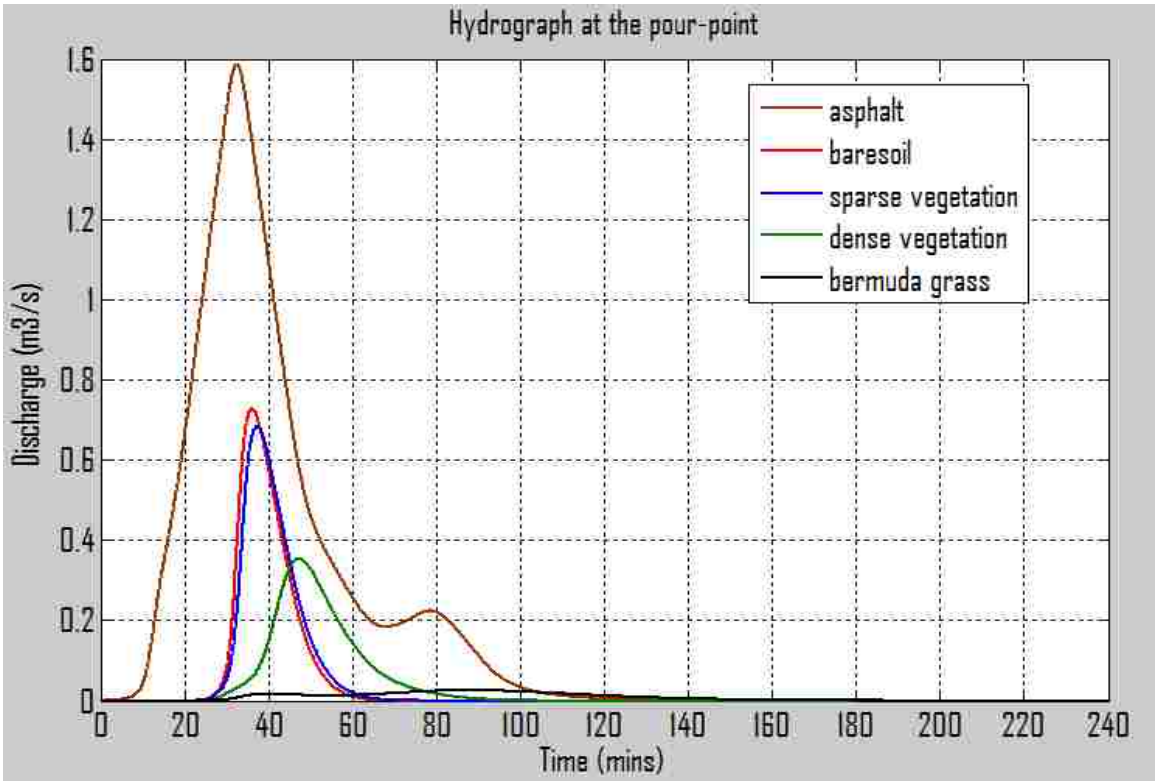

Figure 5.3-7: Plot of runoff hydrographs at the pour-point for all landcover scenarios.

This is as expected because Asphalt has the lowest value of Manning's roughness co-efficient, whereas Bermuda grass has the highest values of Manning's roughness coefficient. As per the Manning's equation, velocity of water in shallow flow is inversely proportional to the Manning's roughness coefficient.

Table 5.3-1: Summary of the landcover change scenarios

Landcover	Manning's roughness 'n'	Hydraulic Conductivity 'K' (cm/hr.)	Peak flow (m^3/s)	Time to peak (mins)	Peak flood depth (m)	Duration of flooding (mins)	Total runoff volume ($m^{3)}$
Asphalt	0.012	0.00001	1.6	32	0.96	103	2656
		Soil grp 'B'					
Bare Soil	0.018	0.9018	0.73	36	0.75	16	456.76
Sparse Veg.	0.023	0.9018	0.69	37	0.71	15	456.76
Dense Veg.	0.080	0.9018	0.036	47	-	-	456.76
Bermuda Grass	0.410	0.9018	0.026	87	-	-	456.76

From the results, it is observed that the volume of runoff from the catchment depends only upon the hydraulic conductivity of the soil group or landcover (if landcover is impervious). It is also observed that the time to peak and peak discharge depend on both the hydraulic conductivity

(to a lesser extent), and mainly, on the Manning's roughness co-efficient value of the landcover. It is also observed that no flooding would occur for the rainfall event of Sep 11, 2012 if the landcover of the study area is changed to dense vegetation or Bermuda grass.

5.4) Landcover treatment scenarios

The developed hydrologic model is tested for two landcover treatment scenarios to analyze the catchment's hydrologic response. In the first case, strips of areas covered with Bermuda grass (about 9% of the total catchment area) as shown in Figure 5.4-1 is considered. The values of Manning's roughness coefficient associated with 64 pixels were manually changed from 0.012 to

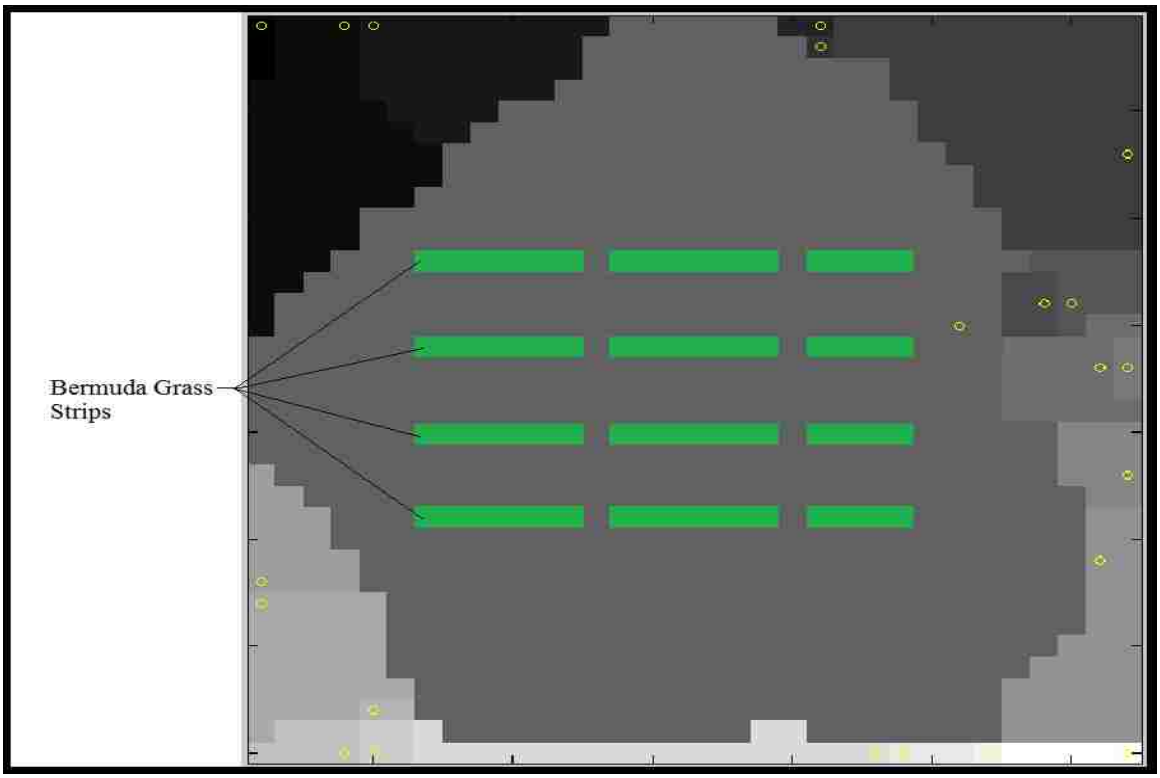

Figure 5.4-1: Landcover treatment scenario such that only 10% of the catchment area is covered with Bermuda grass.

0.35 in the first case while the values of 128 pixels were manually changed from 0.012 to 0.35 in the second case. Further, the value of hydraulic conductivity of pixels with Bermuda grass landcover was also manually changed from 0.00001 cm/hr. to 0.9018 in both cases, while no change was made for the hydraulic conductivity values of other pixels. Figure 5.4-2 shows the plot of the hydrographs for the two landcover treatment scenarios. It is observed that as the area covered by grass is increased, a peak runoff volume from the catchment decreases while the time to peak gets shifted towards right i.e. time to peak increases. Further, as the number of pixels in which infiltration can occur increases, it is observed that the overall runoff volume from the catchment decreases.

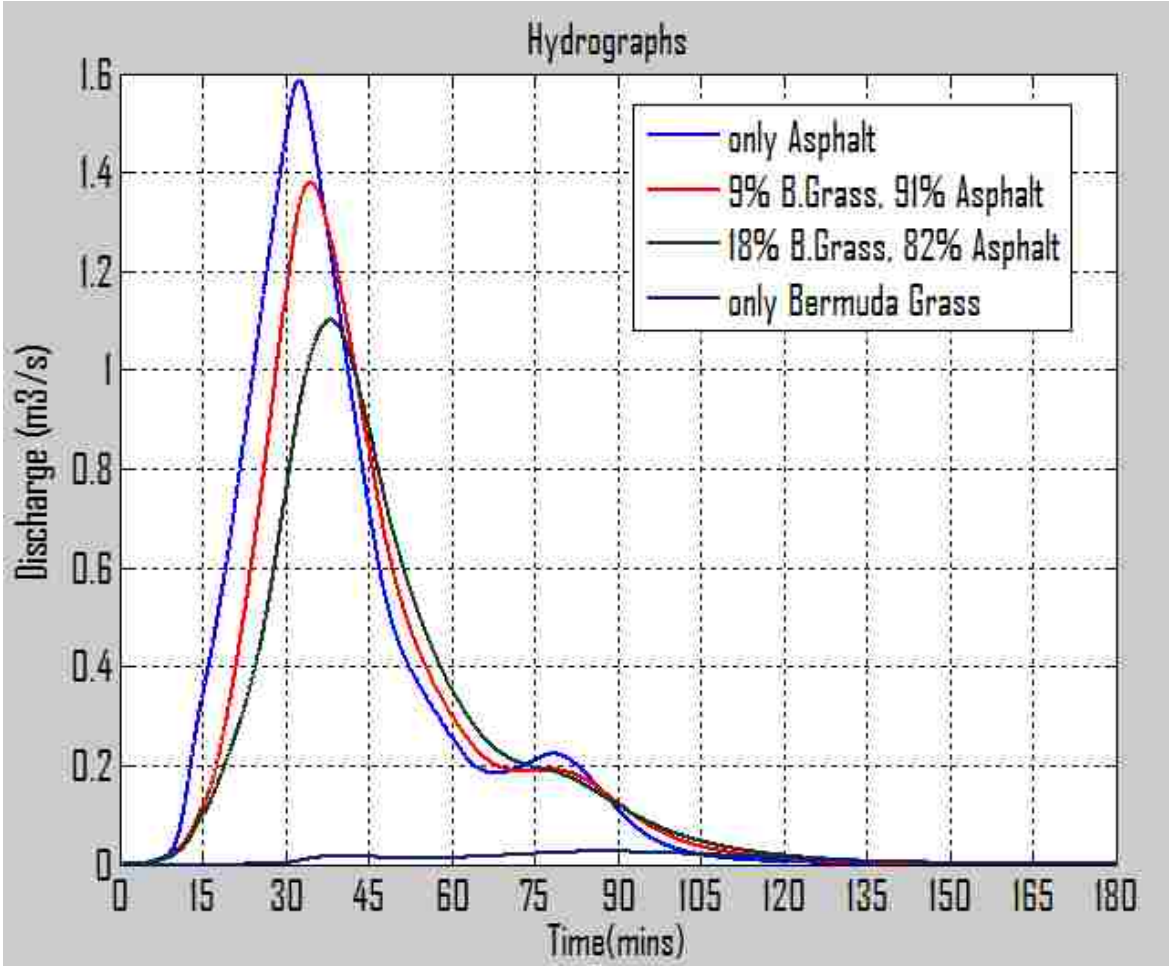

Figure 5.4-2: Hydrographs at the pour-point for different landcover treatment scenarios.

5.5) Summary of all results

From the results, it is concluded that the developed hydrologic model is capable of simulating rainfall-runoff events as well as modeling flood. The developed model was used to simulate the rainfall-runoff events of May 22, 2017 and May 24, 2017 over the study area containing Moores Run trib. catchment. 30-m resolution DEM was found to be the optimum DEM for the Moores Run study area to be used as an input in the developed hydrologic model. The model predicted the catchment area for Moores Run trib. catchment to be 0.5013 km^2, which is pretty close to its actual drainage area, 0.5434 km^2, provided by USGS. The error in estimation of catchment area is 7.75%. From calibration, the hydraulic conductivity for soil group D was found to be about 0.19 cm/hr., however more trials need to be conducted to ascertain this. The model was validated using the stream data for the rainfall event of April 17, 2017 over Moores Run trib. catchment. The average RMSE error for the predicted hydrographs in calibration was found to be 0.0071 m^3/s and the RMSE error for the predicted hydrograph as compared with the actual stream discharge data in validation was found to be 0.011 m^3/s. The developed model overpredicted the 'time-to-peak' in the predicted hydrographs for all the rainfall events even for the lowest possible values of Manning's roughness co-efficient found from literature review. The developed model also under-predicted the 'peak-runoff volume' for both two rainfall events. For the rainfall event of Sep 11, 2012 over the UNLV Parking-lots area, the developed model predicted the maximum depth of flooding to be 0.96 m, and the extent of flooding to be 70 m. Using photographic evidence, the error in maximum flood depth prediction by the model is estimated to be 11.46%, while the error in flood extent prediction is estimated to be 13%. From the land cover change analysis, it was observed that the total runoff volume from a catchment depends on hydraulic conductivity of

the soil group while the ‘time to peak’ and ‘peak discharge’ depend on both hydraulic conductivity and Manning’s roughness co-efficient of the landcover. Finally, from landcover treatment scenarios it is observed that volume of runoff from the catchment can be reduced by providing some grass strips within the Parking-lots area.

CHAPTER 6 – SUMMARY AND CONCLUSION

6.1) Summary

The hydrologic model developed in this research is developed in two stages: i) Rainfall-runoff model, and, ii) Flood model, and, the entire methodological approach can be divided into five components: i) Data preparation, ii) Modeling, iii) Simulation, iv) Validation, and, v) Error analysis. The first stage of the development of the hydrologic model consists of calculation of infiltration (dI), flow depth (dh), and, outflow from the cells (qo) as outputs, using rainfall (dR) as the input. The second stage of the development of the hydrologic model consists of simulation of the flooding process. For data preparation, ArcMap 10.1 is used to derive DEM, soil group data, and, landcover data of the study area, and the derived files are converted into 'Matlab' readable float files. For modeling and simulation, cumulative rainfall of a rainfall event is provided as the input into the model and the size of the time-step as well as the overall runtime are defined by the user. The rainfall for each time-step is interpolated by the model itself. The model uses DEM to delineate the watersheds within the study area and constructs hydrographs at the pour-points of each watersheds. For validation, hydrographs from selected watersheds are then compared with the actual stream-discharge data from the corresponding watersheds for the same rainfall event.

The developed hydrologic model is tested in two study area: i) Moores Run study in Baltimore, and, ii) UNLV Parking-lots study area in Las Vegas. The two sites are chosen because of the availability of all the necessary data for simulation and validation. The 'rainfall-runoff' modeling part of the model is calibrated over the Moores Run study area for the rainfall events of

May 22, 2017 and, May 24, 2017, and, validated for the rainfall event of April 17, 2017. Through calibration, the value of hydraulic conductivity 'K' for soil group D within the Moores Run study area is estimated to be around 0.19 cm/hr. However, more trials need to be conducted to determine and verify the exact value of 'K' for soil group D. The 'flood-modeling' part of the model is validated over the UNLV Parking-lots area for the flood event of Sep 11, 2012. Watershed hydrologic response to different land covers is also done. It is found that flow of water is significantly delayed over dense vegetation and grass as compared to other land covers. Further no flooding is observed for dense vegetation and grass. From landcover treatment scenario it is also found that flooding in the Parking-lots area could be reduced by providing strips of grassland within the catchment.

6.2) Conclusion

All the objectives for set out at the beginning of this research were met. The conclusions of this research are summarized as:

1. This research has developed a Green-Ampt infiltration equation based hydrologic model.
2. This research has also analyzed the watershed hydrologic response to various land covers.
3. The major findings of this research are:
    a. Green-Ampt infiltration equation based distributed parameter hydrologic models can be used to simulate 'rainfall-runoff' process from micro-watersheds.
    b. Manning's roughness co-efficient has no effect on the total volume of surface runoff from a catchment. However, peak flow and time to peak both depend on the Manning's roughness co-efficient of the landcovers within the catchment.

c. Higher the value of hydraulic conductivity of the soil groups within a catchment, lesser is the amount surface stormwater runoff from the area, and vice versa.

d. The value of hydraulic conductivity 'K' for soil group D within the Moores Run study area is estimated to be around 0.19 cm/hr. However, more trials need to be conducted to determine and verify the exact value of 'K' for soil group D.

6.3) Limitations

The limitations of this research are as follows:

1) The hydrologic model developed in this research is suitable for micro watersheds only.
2) The hydrologic model developed in this research is validated using stream discharge data from a single rainfall events only. The hydrologic model maybe further validated using stream discharge data from multiples rainfall events.
3) The hydrologic model developed in this research has limited computational capacity and limited computational memory.
4) The capacity of drainage inlet for UNLV Parking-lots area is assumed to be around 0.48 m^3/s (based on Urban Storm Drainage Criteria Manual, 2002). This needs to be verified.

6.4) Recommendations

The recommendations from this research are divided into two parts. Based on the literature review on the shortcomings of contemporary hydrologic models and the existing knowledge gap

in hydrological modeling, the following areas of research have been identified followed with some recommendations keeping in mind the future needs and technological advances:

- There is a need for hydrologic models to be flexible in terms of input requirements, discretization relating to the spatial and temporal scales, and, process parameterization. Flexibility is the most desirable characteristics for future hydrologic models as a flexible model structure allows for the selection of physical processes and inputs relevant for the case in hand and to make use of the available data, no matter the resolution.
- As computational capabilities are no longer a limitation (Elga et al., 2016), more meticulous and accurate physically-based formulations should be incorporated into future hydrologic models. The number of model parameters that need to be optimized should be minimized for the sake of avoiding uncertainty. Further, only measurable physical properties should be parameterized as the alternative processes to ascertain the values of unmeasurable physical properties might not exist. Future models also should incorporate the important processes of, 1) sub-surface hydrology and 2) pipe infiltration and exfiltration. The dissimilar and complex nature of urban subsoil to that of the subsoil in natural environments sometimes results in different physical behavior of water in urban subsoils, the theory behind which has not been fully understood and thus needs further research. The literature on the impacts of pipe infiltration and exfiltration on groundwater recharge and contamination is limited and also needs to be researched further.
- The possibilities of incorporating parallel computing for modeling and existing mobile communication technology for data collection needs to be explored further. Making use of the existing mobile towers, which are widely spread throughout the globe, can potentially bring down the cost of acquisition of the required data significantly. There is also a need to

incorporate parallel computing, heterogeneous core systems etc. into the existing hydrologic models. Vrught et al., (2005) demonstrated that considerable time saving for parameter estimation can be done, through parallel computing results as compared to the traditional sequential optimization runs. Incorporation of parallel computation techniques into hydrologic models offer immense possibilities to solve complex optimization problems in relative short amount of time.

- There is also a need to formulate new calibration and validation techniques, to deal with the uncertainties related to the use of parameters derived from remotely sensed data, high resolution temporal data that are used for predicting long term trends, and, other data, which have been acquired using newer techniques and have not been tested extensively. Also, methods for assessment of model structure uncertainty need to be developed so that model structure selection can be based on objective criteria rather than being pre-defined by the user. The current knowledge related to 'process interactions in the physical description of the urban hydrological system' is insufficient (Elga et al., 2015) and so, this field needs further research.
- Integration of several purpose-specific models into a general multi-purpose hydrologic model needs to be done. While some integrated hydrologic model do exist, there is still room for enhancement in the level of process detailing. These newer integrated hydrologic model should have a simple user interface that explains in detail as to what the user can and cannot do so that the user is required to have the least of hydrologic training. All in all, the future hydrologic models also need to be cost-effective, reliable and accurate while gravitating towards usability.

Based on the results and the shortcomings of the hydrologic model developed in this research the following recommendations are made:

1) The hydrologic model developed in this research can be used to estimate surface runoff from small urban catchments.
2) The hydrologic model developed in this research doesn't incorporate hydrologic component like sub-surface flow etc. Further, research needs to be done to incorporate components like contribution from sub-surface flow etc. into the developed model.
3) The computational memory space of the developed model needs to be increased to be able to handle data of highest resolutions. The computational speed of the developed model needs to be increased to be able to obtain results quicker than at the present.
4) The hydrologic model developed in this research can be used to determine the optimum landcover treatment solutions for flood reduction, for small urban watersheds.
5) The hydrologic model developed in this research can be used to determine the hydraulic conductivity of soil groups within a catchment provided the stream-discharge data at the pour-point of the catchment is available.

APPENDIX - I

Calculation of Cumulative Infiltration:

Within each time-step, the cumulative infiltration 'dI' into each cell is predicted using Green-Ampt model. Green-Ampt infiltration is physically based, provides an exact solution to an approximate theory and is widely accepted (Desborough and Pitman, 1998; Gusev and Nasonova, 1998). In Green Ampt method of infiltration estimation, instantaneous infiltration rate is defined as a function of hydraulic conductivity of the given soil (K) , soil suction head (ψ), and the initial amount of infiltrated water already present in the soil (ΔΘ) as given in equation (3). The method assumes piston flow (mixing of water doesn't occur and water moves down as a front) (Mein and Larsson, 1973). Infiltration into each cell is predicted using this model. The equation for infiltration rate is expressed as:

$$f_t = K\left(\frac{\psi.\Delta\Theta}{I_t} + 1\right) \ldots (3)$$

where f_t is the rate of infiltration in cm/hr. at time t, K is the hydraulic conductivity of the transmission zone in cm/hr., ψ is the wetting front suction head in cm (represented by the variable name 'psi' in the code), ΔΘ is the available soil moisture content (represented by the variable name 'dTh' in the code), and I_t (represented by the variable name 'F1' in the code) is the cumulative infiltration in cm (Smith, 1991).

Since $f = dI/dt$, a difference equation can be obtained from equation (3) as:

$$K.dt = \frac{I_t}{(\psi.\Delta\Theta/I_t + 1)} \ldots (4)$$

Integrating equation (4) we get,

$$\int_t^{t+\Delta t} K.dt = \int_t^{t+\Delta t} \frac{dI}{(\psi.\Delta\theta/I_t+1)} \ldots (5)$$

i.e. $K.\Delta t = I_{t+\Delta t} - I_t - \psi.\Delta\theta.\ln\frac{(I_{t+\Delta t}+\psi.\Delta\theta)}{(I_t+\psi.\Delta\theta)} \ldots (6)$

Rearranging equation (6) we get,

$$I_{t+\Delta t} - I_t - \psi.\Delta\theta.\ln\frac{(I_{t+\Delta t}+\psi.\Delta\theta)}{(I_t+\psi.\Delta\theta)} = K.\Delta t \ldots (7)$$

where, Δt is the time step in seconds $I_{t+\Delta t}$ and I_t represent cumulative values of infiltration at the end and the beginning of the time step, respectively.

Equation (7) doesn't have a closed form solution and hence needs be solved iteratively (Smith, 1991). Newton-Raphson method is used to solve for $I_{t+\Delta t}$ (represented by the variable name 'F2' in the code). To start the iteration process using Newton-Raphson method, an initial value of $I_{t+\Delta t}$ is required. So, an initial estimate for $I_{t+\Delta t}$ is made as:

$I_{t+\Delta t} = I_t + 1/2\ \Delta R \ldots (8)$ where, ΔR was the incremental rainfall in cm for the time step (represented by the variable name 'dR' in the code).

A function CIF (Cumulative infiltration function) is defined as:

$$= I_{t+\Delta t} - I_t - \psi.\Delta\theta.\ln\frac{(I_{t+\Delta t}+\psi.\Delta\theta)}{(I_t+\psi.\Delta\theta)} - K.\Delta t \ldots (9)$$

CIF gives the difference between the two sides (LHS and RHS) of equation (6). So, CIF is minimized, to make our estimated $I_{t+\Delta t}$ as close to the actual cumulative infiltration at the time step '$t+\Delta t$' as possible. Differentiating the function w.r.t. $I_{t+\Delta t}$ gives:

$$\frac{dCIF}{dI_{t+\Delta t}} = 1 - \frac{\psi.\Delta\theta}{I_{t+\Delta t}+\psi.\Delta\theta} \ldots (10)$$

A revised value of $I_{t+\Delta t\ \text{estimated}}$ is again evaluated using the Newton-Raphson procedure as

$$I^{new}_{t+\Delta t\ est} = I^{old}_{t+\Delta t\ est} - \frac{CIF(I^{old}_{t+\Delta t\ est})}{\frac{dCIF}{dI_{t+\Delta t}}(I^{old}_{t+\Delta t\ est})} \ldots (11)$$

The iteration is repeated until $I^{new}_{t+\Delta t\ est}$ *and* $I^{old}_{t+\Delta t\ est}$ were about the same given that

$| I^{new}_{\mathrm{t+\Delta t}\,est} - I^{old}_{\mathrm{t+\Delta t}\,est} | < tol$ . . . (12) where 'tol' is set to 0.001.

Once $I^{new}_{\mathrm{t+\Delta t}\,est}$ is close enough to $I^{old}_{\mathrm{t+\Delta t}\,est}$ i.e. the difference between them in less than 0.001, the iteration stops and $I^{new}_{\mathrm{t+\Delta t}\,est}$ is then considered to be the cumulative infiltration for time step ''$t + \Delta$t' .

Incremental difference in infiltration during each time step due to surface ponding is determined using equation (7). This incremental volume is subtracted from the rainfall volume added to each cell between the time't' and '$t + \Delta$t' to obtain the outflow into the next cell (Smith, 1991).

A comparison is made between f_t and the water in the cell available for infiltration i.e. current water depth, all adjacent cell inflows and the additional rainfall to the cell during the time interval. When the water inflow into the cell is smaller than f_t, all available water infiltrates into the ground and the cumulative infiltration is computed using equation 13 (Smith, 1991).

$I_{t+\Delta\mathrm{t}} = I_t + \Delta R + (\sum q_i * \Delta t)/A + h_t$ . . . (13)

Where 'A' is the surface area of the cell, $\sum q_i$ is the total inflow from the adjacent cells and h_t is the current water depth in the cell.

When f_t is smaller than the water inflow into the cell, ponding occurs and $I_{t+\Delta\mathrm{t}}$ is found using equation (7).

Thus, cumulative frequency $'I_{t+\Delta\mathrm{t}}'$ of each cell is calculated in the Green Ampt model for every time step.

Calculation of Overland Flow based on Continuity equation:

The stormwater surface runoff is produced from excess rainfall. Excess rainfall is computed using the combination of the Continuity equation and Manning's equation for shallow channels. At first the incremental infiltration for a time step is determined. Then, it is subtracted from the rainfall amount and the difference is considered as the outflow from the cell and inflow into the adjacent downstream cell.

The continuity equation for each cell is given by:

$$h_{t+\Delta t} = h_t + netrain + ((\sum q_i - q_o)/A).\Delta t \ldots (14)$$

Where $h_{t+\Delta t}$ and h_t are flow depths in the cell in meters at the end and the beginning of the time step respectively, A is the cell area, and netrain is the incremental rainfall minus the incremental infiltration (m) (Smith, 1991).

Outflow from each cell is computed using Manning's equation for wide channel flow:

$$q_o = (h_{t+\Delta t} - d)^{\frac{5}{3}} . S^{\frac{1}{2}} . \frac{1}{n} . cell \text{ width} \ldots (15)$$

Where d is the depression storage in meter, S is the cell slope in the direction of flow, cell width is cell dimension in meters perpendicular to flow and 'n' is the Manning's roughness coefficient (Smith, 1991).

Equation (15) is also solved iteratively to find the value of h_2. To solve for $h_{t+\Delta t}$, equation (14) is rearranged as:

$$\text{FDF} = -h_{t+\Delta t} + h_t + netrain + \frac{(\sum q_i - \sum q_o) * \Delta t}{A} - b^{\frac{5}{3}} . S^{\frac{1}{2}} . \frac{1}{nL} . \Delta t \ldots (16)$$

Where FDF (flow-depth function) is a function name, A is the cell area, L is the cell dimension in meters in the direction of flow, and b is equal to $(h_t + h_{t+\Delta t})/2 - d$, which represents

the average outflow depth during the time interval, $\sum q_i$ is the sum of the inflows into the cell and q_o is the outflow from the cell. FDF gives the difference between two sides of equation (14). So, FDF is minimized to make the estimated $h_{t+\Delta t}$ as close to the actual water depth in the cell at time step '$t + \Delta t$' as possible.

Differentiating FDF with $h_{t+\Delta t}$, we get:

$$\frac{dFDF}{dh_{t+\Delta t}} = -1 - \frac{5}{6} b^{\frac{2}{3}} slope^{\frac{1}{2}} \frac{1}{n.L} \Delta t \quad \ldots (17)$$

An initial estimate is made for $h_{t+\Delta t}$ as:

$$h_{t+\Delta t\ est} = h_t + 1/2.\ \Delta R \quad \ldots (18)$$

where $h_{t+\Delta t\ est}$ is the initial estimate of $h_{t+\Delta t}$. A revised estimate of the final output depth was computed using,

$$h^{new}_{h_{t+\Delta t}\ est} = h^{old}_{h_{t+\Delta t}\ est} - \frac{FDF\left(h^{old}_{h_{t+\Delta t}\ est}\right)}{\frac{dFDF}{dh_{h_{t+\Delta t}}}\left(h^{old}_{h_{t+\Delta t}\ est}\right)} \quad \ldots (19)$$

Where $FDF\left(h^{old}_{h_{t+\Delta t}\ est}\right)$ and $\frac{dFDF}{dh_{h_{t+\Delta t}}}\left(h^{old}_{h_{t+\Delta t}\ est}\right)$ are the function and its derivative evaluated at the previous value of the estimated depth. The iterations stop when $h^{old}_{h_{t+\Delta t}\ est}$ and $h^{new}_{h_{t+\Delta t}\ est}$ are close such that,

$$\left|h^{old}_{h_{t+\Delta t}\ est} - h^{new}_{h_{t+\Delta t}\ est}\right| < tolerance \quad \ldots (20)$$

where $tolerance$ is set to be 0.000001.

Thus, overland flow modeling based on Continuity equation gives the water depth in the cell for each time step from equation (14) and Manning's equation of roughness coefficient, equation (15) gives the outflow from each cell for each time step.

Newton-Raphson Method:

In numerical analysis, Newton–Raphson method, is an iterative process for finding successively better approximations to the roots (or zeroes) of a real-valued function $x: f(x) = 0$. This method is based on the knowledge of the tangent to the curve near the root.

Given a function f defined over the real x, its derivative f'.

Provided the function satisfies all the assumptions made in the derivation of the formula, a better approximation x1 is

$$x_1 = x_0 - \frac{f(x_0)}{f'(x_n)} \ldots (21)$$

Geometrically, $(x_1, 0)$ is the intersection with the x-axis of the tangent to the graph of f at $(x_0, f(x_0))$.

The process is repeated as

$$x_{n+1} = x_n - \frac{f(x_n)}{f'(x_n)} \ldots (22)$$

until a value within the given tolerance is reached.

The more iterations that are run, the closer dx will be to zero (0).

Time-step size estimation

The time step size in the developed model is estimated using the Courant-Friedrichs-Lewy (CFL) condition. For 1-D case, the CFL has the following form:

$$C = \frac{\mathrm{u}\,\Delta t}{\Delta x} \leq C_{max} \ldots (23)$$

where,

C is the Courant number, u is the magnitude of the velocity, Δt is the time-step, and, Δx is the length (cell-size). The magnitude of velocity for the developed model is determined by using Manning's roughness equation for shallow flow. To estimate the time-step size applicable for all trial simulations, the highest value of expected depth in the cell, the highest value of slope in the study area, and the lowest value of Manning's roughness co-efficient is used to calculate the highest possible magnitude of velocity. Considering 10-m resolution DEM to be the lowest resolution DEM of the study area and 5 m/s to be the highest velocity of the flow within a cell, for $\Delta t \leq C_{max} * \frac{\Delta x}{\mathrm{u}}$, where C_{max} = 1, it is observed that Δt should be less than or equal to 2s.

Development of the model:

The hydrologic model used in the research was first developed for a study area represented by just two cells, using the cell model as shown in figure 4.1-2. Later on it was expanded to deal with complex study area consisting of many cells and multiple watershed. The entire process for developing the hydrologic model is categorized into two stages and the evolution of model through those stages is explained below:

Stage 1:

The first stage of the development of the hydrologic model, developed in this research, consists of calculation of infiltration (dI), flow depth (dh), and, outflow from the cell (qo) as outputs, using rainfall (dR) as the input. The steps followed to develop the model are detailed below in chronological order.

- An artificial rainfall data of 5 mins resolution is created for an arbitrary sampling time. Cumulative rainfall data corresponding to each of the time-steps is then created from the artificial rainfall data.
- The resolution of the cell is defined. The entirety of the study area is defined as a matrix named 'DEM'. The matrix DEM, consists of the elevation values of the study area.
- A function called 'dem2fdir' is defined. The function 'dem2fdir' takes the 'DEM' as the input and gives the flow-direction (fdir) values as the output. Since the cell with the lowest elevation value doesn't have a flow direction, 'nan' is stored as its flow direction value. The flow direction for other cells is assigned as a single value from among 8 values depending on its direction. The function 'dem2fdir' also saves the index numbers of cells with 'nan' values for flow direction and defines them as either ditch pixels or pour-points. The boundary cells with 'nan' flow direction values are saved as pour-points while all the other cells with 'nan' flow direction values are saved as ditches. If multiple pour-points are encountered, then all the cells contributing the flow into the first pour-point are identified as cells of the first watershed and all cells contributing the flow into the second-pour point are identified as the cells of second watershed and so on.

It is difficult to assign a watershed for the ditch cells as their connectivity to the pour-point cannot be established based just on the flow direction into the neighboring cell. In such cases, the flow direction for the ditch cells is determined differently. To determine the pour-point associated

with a ditch cell, the elevations of the neighboring cells of the ditch cells are checked and the lowest neighbor of the ditch cell is identified. Then, the flow direction of that cell is determined for a case in which the ditch cell is supposed to be non-existent. If the flow direction from that cell for a non-existent ditch cell scenario, is again 'nan', then the first lowest neighbor of the ditch cell is supposed to be non-existent and flow direction for the second lowest neighbor is determined. The process is repeated until, the flow direction from one of the lowest neighbors of the ditch cell is into a cell that is not a direct neighbor of the ditch cell. The pour-point associated with that cell (non-direct lowest elevation neighbor of the ditch cell) is then considered to be the pour-point onto which the ditch cell will drain.

There arises a special case when a catchment doesn't have a pour-point but just ditches. However, analysis of such cases is beyond the scope of this research. Therefore, such cases are not taken into consideration for this research.

- A function called 'dem2slope' is defined. The function 'dem2slope' takes the 'DEM' as the input and gives the slope (So) values as the output. The slope for each cell is calculated using the equation (2).
- A function called 'fdir2conn' is defined. The function 'fdir2conn' takes 'fdir' values from step (3) as the input and gives a 'connectivity matrix' as the output. The connectivity matrix defines how the cells are connected with each other based on the flow direction. It is a matrix of array matrices, and, is of the same size as the 'DEM'. The array matrices within the cells of connectivity matrix are either empty or consists of index numbers of the cells of the DEM depending upon the connectivity of the cells of the DEM. E.g., in this case, the connectivity matrix consists of an empty array matrix at the first cell and an array matrix, [1], in the second cell, as the flow in occurring from the cell of index number 1 of the DEM to the cell of index

number 2, but there is no inflow into the cell of index number 1 from other cells. Hence, the cell of index number 1 is the ‘source cell’ for the cell of index number 2 of the DEM and the cell of index number 2 is the ‘target cell’ for the cell of index number 1 of the DEM. The model identifies source cells and target cells using the ‘fdir2conn’ function.

- A function called ‘cell_ordering’ is defined. The function ‘cell_ordering’ gives an array matrix as the output. The array matrix obtained as an output from the ‘cell_ordering’ function contains index numbers of all the cells of the DEM, in an order. The order of the index number of the cells of the DEM depends upon the count of cell-to-cell connectivity distance from the pour-point. The cell-to-cell connectivity distance from the pour-point refers to the number of cells that contribute in connecting the concerned cell to the pour-point. The cells with the farthest ‘cell-to-cell connectivity distance’ from the pour-point are identified and arranged at first. Among these cells, the cells are sorted in ascending order, based on their index number. Cells with decreasing cell-to-cell connectivity distance from the pour-point are identified and arranged in the next step and the sorting proceeds in a similar manner until the pour-point for the watershed is reached. Once the index number of the cells for the first watershed are sorted, the cells of the second watershed farthest from the second pour-point are identified and the index number of these cells are stored in the array matrix in ascending order. The process repeats until the index numbers for all the cells has been arranged and stored in the array matrix.
- The soil parameters used in equation 3, equation 14, and, equation 15, are defined with either their symbols or their abbreviated names behind the prefix ‘p.’ E.g., the variable name ‘p.psi’ is used to store the values of ‘wetting front suction head’. The units for the parameter are mentioned as comments within the code.

- All the parameters that are calculated using Newton-Raphson iteration are initialized with a value ‘0’, for the first time-step i.e. at ‘t= 0’.
- Three functions named ‘green-ampt_infiltration’, ‘mannings_depth_discharge’, and ‘cell_hydro_model’ are created. The function ‘green_ampt_infiltration’ takes five variables (F1, K, psi, dTh, dt) as input and gives two values stored in variables (dF, f) as the output using equations (9), (10), (11), and (12) for each time-step. The function ‘mannings_depth_discharge’ takes eight variables (h1, dR, dF, qi, So, n, L, dt) as input and gives three values stored in variables (h2, qo, dF) as the output using equation (16), (17), (18), (19), and, (20) for each time-step. The function ‘cell_hydro_model’ takes five variables along with all soil parameter variables (dR, qi, F1, h1, dt, p) as the input and gives three values stored in variables (F2, h2, qo) as the output using the ‘green-ampt filtration’ function and the ‘mannings_depth_discharge’ function for each time-step.
- The ‘qo’ value from the pour-points for each time-step is stored in a separate variable (D) while for all the other pixels ‘qo’ from one cell is considered to be the ‘qi’ into some other cell within the same time-step, based on it connectivity. ‘qo’ from ditch cells for each time-step is added to its ‘h2’ value as ‘h2 = h2 +qo’.
- A function called ‘water_filling’ is defined. The function ‘water_filling’ checks, whether or not, the sum of elevation of all the cells and their respective flow depths, is greater than or equal to or less than the sum of the elevation and the flow depth of the lowest neighboring cell. It then redistributes the excess flow depth in the cells into its lowest neighboring cell if the sum of the elevation and the flow depth in the cell, is greater than that of the neighboring cells. If there are multiple lowest neighboring cells i.e. if the sum of the elevation and flow depth of

the two or more neighboring cells are equal, then the excess flow depth of the cell is redistributed equally among the lowest neighboring cells.

- Two mass-balance checks are done at the end. The mass-balance check for each cell is done at the end of each time-step whereas the mass-balance check for the entire simulation process is done only once at the end. If both mass balance are satisfied then the model is considered to be working correctly.
- The value of 'D' for each pour-point is plotted for each time-step to obtain the discharge hydrograph for that pour-point.

The developed hydrologic model was run for multiple real rainfall events and their discharge hydrographs produced at the watershed pour-points are shown and discussed in the results chapter.

Stage 2:

The second stage of the development of the hydrologic model developed in this research consists of simulation of the flooding process. The hydrologic model developed in the first stage is capable of producing the discharge hydrograph for a watershed at its pour-point. In the hydrologic model developed in the first stage, the drainage capacity of the pour-point cell of the watershed is considered to be infinite, by default. However, in reality, the pour-point cells have a limit in capacity to drain the water. If the water flowing into the pour-point cell, within each time-step, exceeds the drainage capacity of the pour-point cell, flooding will occur. Flooding always starts from the pour-point cell and moves towards the upstream cells. The depth of flooding in the

flooded cells and the number of upstream cells flooded depends on the difference of volume of water flowing into the pour-point cell and the volume of water-flowing draining out of the pour-point cell during each time-step. In this research, the sum of the elevation and the flow-depth for all the flooded cells is assumed to be equal within each time-step. Hence, the flood model developed in this research can be considered a 'flat-flood model'.

The steps followed to incorporate the flood-mapping capability into the hydrologic model developed in the first stage are described below:

- The drainage capacity of the pour-points, identified in the step number (3) of Stage 1, is defined.
- The 'D' value of the pour-point cell during each time-step is then compared with the drainage capacity of the pour-point. If it is equal to or less than the drainage capacity of the pour-point, no flooding occurs. However, if it exceeds the drainage capacity of the pour-point, then the difference between the two is added into the existing flow-depth of the pour-point cell. The function 'water_filling' then checks, whether or not, the sum of elevation and the new flow depth of the pour-point cell, exceeds the sum of the elevation and the flow depth of the lowest neighboring cell, within that time-step, and if it does, then the excess flow-depth of the pour-point cell is redistributed into its neighboring cells.
- For all the time-steps in which, 'D' from the pour-point cell exceeds its drainage capacity, an image of all the flooded cells is saved.

There arises a special case when the flooding within a watershed reaches its boundary cells and the sum of the elevation and the flow depth of the boundary cells of the flooded watershed exceeds the sum of the elevation and the flow depth of the boundary cells of the adjacent watershed. In such cases, the excess depth of flow from the flooded watershed boundary cells

should drain into the pour-point of the adjacent watershed. However, analysis of such cases is beyond the scope of this research. Therefore, such cases are not taken into consideration for this research.

APPENDIX - II

Matlab Code for Moores Run Study area:

```
clear; clf;
% Setup the colormap
figure(1);
cm = (1:64)'/64; cmap2 = [0*cm cm cm];
colormap(cmap2);
% User Input of rainfall data for Moores Run study area
%April 17
rain.min=[0:10:10*18]; % (min) Sampling time %15 mins
rain.cum=[0 0.01 0.03 0.08 0.10 0.11 0.12 0.12 0.13 0.14 0.14 0.15 0.15 0.16
0.17 0.17 0.18 0.18 0.18]*2.54; %(cm) %April 17, 2017 %rain start at 1030am
%May 22
% rain.min=[0:10:10*13];
% rain.cum=[0 0.01 0.06 0.09 0.09 0.09 0.1 0.11 0.11 0.11 0.11 0.12 0.12
0.12]*2.54; %(cm) %April 25, 2017 %rain start at 0205am
%May 24
%rain.min=[0:10:10*31]; % (min) Sampling time %15 mins
%rain.cum=[0 0.01 0.02 0.02 0.02 0.03 0.03 0.04 0.04 0.05 0.05 0.05 0.06 0.08
0.10 0.12 0.12 0.12 0.12 0.13 0.13 0.13 0.14 0.14 0.14 0.14 0.14 0.14 0.15
0.16 0.16 0.16]*2.54; %(cm) %April 17, 2017 %rain start at 1030am
%Jun05
% rain.min=[0:10:10*20];
% rain.cum=[0 0.01 0.02 0.02 0.03 0.04 0.05 0.06 0.08 0.08 0.10 0.11 0.14
0.20 0.21 0.21 0.21 0.21 0.22 0.22 0.22]*2.54;
%% Region specification
load('dem30_noditches'); L=30;
%% Watershed and Hydrographic Ordering
O=cell_ordering(dem, L);
% By default ditches have zero discharge capacity and outlets have infinite
% It can be changed as follows
% O.pour.Q(2)=20;
So=O.slope; % Slope
%n=dem*0 + 0.014;
load('moores30_n1.mat');
K=dem*0+0.25; % cm/hr
%load('moores30_Kmin.mat');
%psi=dem*0 + 20.88; % cm
load('moores30_psi.mat');
dTh=dem*0 + 0.2163; % vol/vol
%% Flood Variable
fl.cov=cell(O.pour.N,1); % Coverage for each pour point
fl.bnd=cell(O.pour.N,1); % Boundary
fl.msk=[];
% Flooding will always start from the pourpoint
for o=O.pour.id
    fl.cov{o}=O.pour.ndx(o);
    fl.bnd{o}=O.con.rc{O.pour.ndx(o)};
```

```
end
% User Input about time-step and model run time
dt=1; % (sec) Time step size
tmax=6; % (sec) Maximum time of run
t=0:dt:tmax*3600; % (sec) Model run time
% Convert cummulative rain into intensity and resample it
rain.int=[0 diff(rain.cum)*60./diff(rain.min)]; % cm/hr (Rain intensity)
i=interp1(rain.min*60, rain.int, t); i(isnan(i))=0; % cm/hr (Resampled rain
intensity)
if abs(sum(i*dt/3600) - rain.cum(end)) > 1e-6; error('Incorrect rain'); end;
[R,C]=size(dem); % space dimensions
T=numel(t); % time dimentions
% Processing variables
F=ones(R,C,T)*1e-6;  % Infiltration
h=zeros(R,C,T);      % Depth
Q=zeros(R,C,T);      % Runoff
W=zeros(R,C,T);      % Inundation
D=zeros(O.pour.N,T); % Discharge
tic
for k=2:T % Time Loop
    % Rain
    dR=i(k) * dt/3600; % cm

    % Processing variables
    F1=F(:,:,k-1); F2=F1*0;
    h1=h(:,:,k-1); h2=h1*0;
    Qi=Q(:,:,k-1); Qi=Qi*0;
    fl.msk=0*dem;

    %% Run hydrological model on each cell from leaf to root
    for w=O.wsh.id % Pour point/watershed Loop
        for c=O.wsh.ndx{w} % Each cell loop

           % physical characteristics
            p.L=L; p.So=So(c); p.n=n(c);

            % soil properties
            p.K=K(c); p.psi=psi(c); p.dTh=dTh(c);

            [F2(c), h2(c), qo]=cell_hydro_model(dR, Qi(c), F1(c), h1(c), dt,
p);

            fc=O.con.fc(c);
            if ~isnan(fc)
                Qi(fc)=Qi(fc)+qo;
            else
                id=O.pour.ind(c);
                if qo < O.pour.Q(id)
                   D(id,k)=qo;
                else
                   D(id,k)=O.pour.Q(id);
                   h2(c) = h2(c) + (qo-O.pour.Q(id))*dt/L/L;
                   qo=D(id,k);
                end
            end
```

```
            % Cell mass balance
            Ci=dR + 100*Qi(c)*dt/L/L; Co=(F2(c)-F1(c)) + 100*qo*dt/L/L;
dC=100*(h2(c)-h1(c));
            %disp(sprintf('Cell[%d]: %.6f - %.6f - (%.6f) = %.6f', c, Ci, Co,
dC, Ci-Co-dC));
            if abs(Ci-Co-dC) > 1e-6; error('Cell Mass Imbalance'); end

        end % Each cell loop

        %% Flooding within watershed from cell overflowing
        while(1) % Flood spreading loop
            %% Level all the previously known flooded cells
            cov=fl.cov{w};
            h2(cov)=water_filling(dem(cov), sum(h2(cov)));

            %% Compare with the boundary cells and stop if needed
            hd=dem+h2; %imagesc(hd+50, [0 100]);
            bnd=fl.bnd{w};
            ind=hd(cov(1)) > hd(bnd);
            if ~any(ind); break; end;

            %% Update the flooded and boundary cells
            fld=bnd(ind);
            fl.cov{w}=[cov fld];
            fl.bnd{w}=bnd(~ind);
            for b=fld
                fl.bnd{w}=[fl.bnd{w} O.con.rc{b}];
            end
        end % Flood spreading loop
        fl.msk(fl.cov{w})=1;
    end % Pour point/watershed Loop
    %% Inter-watershed overflow
    % If a border pixel is flooded then it should overflow into the
    % neighboring watershed
    ov=find(O.wsh.bnd.*fl.msk);
    win=-1:1;
    hd=dem+h2;
    for o=ov'
        [r,c]=ind2sub([R,C],o);
        if (r == 1 | r == R | c == 1 | c == C)
            disp('WARNING: Boundary pixel is flooded. Ignoring');
            continue;
        end
        [Wc, Wr]=meshgrid(c+win, r+win);
        ind=sub2ind([R,C], Wr, Wc);
        bnd=O.wsh.msk(ind);
        box=hd(ind);
        box=box(2,2)-box;
        box(bnd == bnd(2,2) | box < 0)=nan;
        ndx=ind(~isnan(box(:)));
        if isempty(ndx); continue; end;
        ndx=[ind(2,2), ndx(1)];
        h2(ndx)=water_filling(dem(ndx), sum(h2(ndx)));
    end
    F(:,:,k)=F2;
```

```
    h(:,:,k)=h2;
    Q(:,:,k)=Qi;
    w2=h2; w2(~fl.msk)=0;
    W(:,:,k)=w2;
    % Image Mass Balance
    In=dR*R*C/100;
    Out=sum(sum(F2-F1))/100 + sum(D(:,k))*dt/L/L;
    dS=sum(sum(h2-h1));
    %disp(sprintf('Image[%d] %.3f - %.3f - (%.3f) = %.3f', k, In, Oout, dS,
In-Out-dS));
    if abs(In-Out-dS) > 1e-6; error('Image Mass Imbalance'); end

    % Plotting
    [X,Y]=meshgrid([1:C]*L, [1:R]*L);
    subplot(2,3,1);
    bar(t/3600,i,1); xlim([0 tmax]); title('Rain Intensity');
    hold on; plot(t([k k])/3600, ylim, 'k-'); hold off
    subplot(2,3,2);
    imagesc(O.wsh.msk); title('Watershed Mask');
    hold on; quiver(O.u, O.v, 1, 'w');
    plot(O.pour.c, O.pour.r, 'ko', 'MarkerSize', 5); hold off;
    %h2(O.wsh.msk ~= 3)=nan;
    %Qi(O.wsh.msk ~= 3)=nan;
    subplot(2,3,3); imagesc(h2); title('Flood extent'); colorbar;
    hold on; quiver(Qi.*O.u, Qi.*O.v, 1, 'k'); hold off
    %bar3stacked(h2, dem);
    subplot(2,3,4); %mesh(dem); hold on; surface(dem+h2); hold off;
    surf(X, Y, dem+h2, h2); caxis([0 0.01]);
    camlight left;
    lighting phong;
    title('3D View'); view(136, 60); axis tight; zlim([0 200]);

    subplot(2,3,5); plot(t/60, D(14,:)'); title('Hydrographs');
    xlabel('Time(mins)'); ylabel('Discharge (m3/s)');
    subplot(2,3,6); quiver(Qi.*O.u, Qi.*O.v, 3, 'k'); title('Runoff');
    set(gca, 'ydir', 'reverse');
    pause(0.001);

 disp(k);
end % Time Loop
toc
% Final Mass Balance
In=sum(i*dt/3600)*R*C/100;
Out=sum(sum(F(:,:,k)))/100 + sum(sum(D))*dt/L/L;
dS=sum(sum(h(:,:,k)));
disp(sprintf('Final: %.3f - %.3f - (%.3f) = %.3f', In, Out, dS, In-Out-dS));
if abs(In-Out-dS) > 1e-3; error('Final Mass Imbalance'); end
```

Matlab code for UNLV Parking-lots Study area:

```
clear; clf;
```

```
% Setup the colormap
figure(1);
cm = (1:64)'/64; cmap2 = [0*cm cm cm];
colormap(cmap2);
% User Input of rainfall data
rain.min=[0:15:15*8]; % (min) Sampling time
rain.cum=[0 0.25 1 1.2 1.27 1.38 1.38 1.38 1.38]*2.54; % (cm) Cummulative
rainfall
%% Region specification
load('lot10_dem.mat'); L=10;
dem(15,26)=590.80;
%% Watershed and Hydrographic Ordering
O=cell_ordering(dem, L);
% By default ditches have zero discharge capacity and outlets have infinite
% It can be changed as follows
O.pour.Q(9)=0.48;
So=O.slope; % Slope
n=dem*0 + 0.012;
K=dem*0 + 0.0001; % cm/hr
psi=dem*0 + 16.68; % cm
dTh=dem*0 + 0.2163; % vol/vol
%% Flood Variable
fl.cov=cell(O.pour.N,1); % Coverage for each pour point
fl.bnd=cell(O.pour.N,1); % Boundary
fl.msk=[];
% Flooding will always start from the pourpoint
for o=O.pour.id
    fl.cov{o}=O.pour.ndx(o);
    fl.bnd{o}=O.con.rc{O.pour.ndx(o)};
end
% User Input about time-step and model run time
dt=1; % (sec) Time step size
tmax=3; % (sec) Maximum time of run
t=0:dt:tmax*3600; % (sec) Model run time
% Convert cummulative rain into intensity and resample it
rain.int=[0 diff(rain.cum)*60./diff(rain.min)]; % cm/hr (Rain intensity)
i=interp1(rain.min*60, rain.int, t); i(isnan(i))=0; % cm/hr (Resampled rain
intensity)
if abs(sum(i*dt/3600) - rain.cum(end)) > 1e-6; error('Incorrect rain'); end;
[R,C]=size(dem); % space dimensions
T=numel(t); % time dimentions
% Processing variables
F=ones(R,C,T)*1e-6;  % Infiltration
h=zeros(R,C,T);      % Depth
Q=zeros(R,C,T);      % Runoff
W=zeros(R,C,T);      % Inundation
D=zeros(O.pour.N,T); % Discharge
tic
for k=2:T % Time Loop
    % Rain
    dR=i(k) * dt/3600; % cm
    % Processing variables
    F1=F(:,:,k-1); F2=F1*0;
    h1=h(:,:,k-1); h2=h1*0;
    Qi=Q(:,:,k-1); Qi=Qi*0;
    fl.msk=0*dem;
    %% Run hydrological model on each cell from leaf to root
```

```
    for w=O.wsh.id % Pour point/watershed Loop
        for c=O.wsh.ndx{w} % Each cell loop
           % physical characteristics
            p.L=L; p.So=So(c); p.n=n(c);
            % soil properties
            p.K=K(c); p.psi=psi(c); p.dTh=dTh(c);
            [F2(c), h2(c), qo]=cell_hydro_model(dR, Qi(c), F1(c), h1(c), dt,
p);
            fc=O.con.fc(c);
            if ~isnan(fc)
                Qi(fc)=Qi(fc)+qo;
            else
                id=O.pour.ind(c);
                if qo < O.pour.Q(id)
                   D(id,k)=qo;
                else
                   D(id,k)=O.pour.Q(id);
                   h2(c) = h2(c) + (qo-O.pour.Q(id))*dt/L/L;
                   qo=D(id,k);
                end
            end
            % Cell mass balance
            Ci=dR + 100*Qi(c)*dt/L/L; Co=(F2(c)-F1(c)) + 100*qo*dt/L/L;
dC=100*(h2(c)-h1(c));
            %disp(sprintf('Cell[%d]: %.6f - %.6f - (%.6f) = %.6f', c, Ci, Co,
dC, Ci-Co-dC));
            if abs(Ci-Co-dC) > 1e-6; error('Cell Mass Imbalance'); end
        end % Each cell loop
        %% Flooding within watershed from cell overflowing
        while(1) % Flood spreading loop
            %% Level all the previously known flooded cells
            cov=fl.cov{w};
            h2(cov)=water_filling(dem(cov), sum(h2(cov)));
            %% Compare with the boundary cells and stop if needed
            hd=dem+h2; %imagesc(hd+50, [0 100]);
            bnd=fl.bnd{w};
            ind=hd(cov(1)) > hd(bnd);
            if ~any(ind); break; end;
            %% Update the flooded and boundary cells
            fld=bnd(ind);
            fl.cov{w}=[cov fld];
            fl.bnd{w}=bnd(~ind);
            for b=fld
                fl.bnd{w}=[fl.bnd{w} O.con.rc{b}];
            end
        end % Flood spreading loop
        fl.msk(fl.cov{w})=1;
    end % Pour point/watershed Loop
    %% Inter-watershed overflow
    % If a border pixel is flooded then it should overflow into the
    % neighboring watershed
    ov=find(O.wsh.bnd.*fl.msk);
    win=-1:1;
    hd=dem+h2;
    for o=ov'
        [r,c]=ind2sub([R,C],o);
        if (r == 1 | r == R | c == 1 | c == C)
```

```
            disp('WARNING: Boundary pixel is flooded. Ignoring');
            continue;
        end
        [Wc, Wr]=meshgrid(c+win, r+win);
        ind=sub2ind([R,C], Wr, Wc);
        bnd=O.wsh.msk(ind);
        box=hd(ind);
        box=box(2,2)-box;
        box(bnd == bnd(2,2) | box < 0)=nan;
        ndx=ind(~isnan(box(:)));
        if isempty(ndx); continue; end;
        ndx=[ind(2,2), ndx(1)];
        h2(ndx)=water_filling(dem(ndx), sum(h2(ndx)));
    end
    F(:,:,k)=F2;
    h(:,:,k)=h2;
    Q(:,:,k)=Qi;
    w2=h2; w2(~fl.msk)=0;
    W(:,:,k)=w2;
    % Image Mass Balance
    In=dR*R*C/100;
    Out=sum(sum(F2-F1))/100 + sum(D(:,k))*dt/L/L;
    dS=sum(sum(h2-h1));
    %disp(sprintf('Image[%d] %.3f - %.3f - (%.3f) = %.3f', k, In, Oout, dS,
In-Out-dS));
    if abs(In-Out-dS) > 1e-6; error('Image Mass Imbalance'); end
    % Plotting
    [X,Y]=meshgrid([1:C]*L, [1:R]*L);
    subplot(2,3,1);
    bar(t/3600,i,1); xlim([0 tmax]); title('Rain Intensity');
    hold on; plot(t([k k])/3600, ylim, 'k-'); hold off
    subplot(2,3,2);
    imagesc(O.wsh.msk); title('Watershed Mask');
    hold on; quiver(O.u, O.v, 1, 'w');
    plot(O.pour.c, O.pour.r, 'ko', 'MarkerSize', 5); hold off;
    %h2(O.wsh.msk ~= 3)=nan;
    %Qi(O.wsh.msk ~= 3)=nan;
    subplot(2,3,3); imagesc(h2); title('Flood extent'); colorbar;
    hold on; quiver(Qi.*O.u, Qi.*O.v, 1, 'k'); hold off
    %bar3stacked(h2, dem);
    subplot(2,3,4); %mesh(dem); hold on; surface(dem+h2); hold off;
    surf(X, Y, dem+h2, h2); caxis([0 0.01]);
    camlight left;
    lighting phong;
    title('3D View'); view(136, 60); axis tight; zlim([0 200]);

    subplot(2,3,5); plot(t/60, D(9,:)'); title('Hydrographs');
    xlabel('Time(mins)'); ylabel('Discharge (m3/s)');
    subplot(2,3,6); quiver(Qi.*O.u, Qi.*O.v, 3, 'k'); title('Runoff');
    set(gca, 'ydir', 'reverse');
    pause(0.001);
    disp(k);
end % Time Loop
toc
% Final Mass Balance
In=sum(i*dt/3600)*R*C/100;
Out=sum(sum(F(:,:,k)))/100 + sum(sum(D))*dt/L/L;
```

```
dS=sum(sum(h(:,:,k)));
disp(sprintf('Final: %.3f - %.3f - (%.3f) = %.3f', In, Out, dS, In-Out-dS));
if abs(In-Out-dS) > 1e-3; error('Final Mass Imbalance'); end
```

REFERENCES

Abbott, M. B., Bathurst, J. C., Cunge, J. A., O'Connell, P. E., & Rasmussen, J. (1986). An introduction to the European Hydrological System—Systeme Hydrologique Europeen,"SHE", 1: History and philosophy of a physically-based, distributed modelling system. Journal of hydrology, 87(1), 45-59.

Abbott, M. B., Bathurst, J. C., Cunge, J. A., O'connell, P. E., & Rasmussen, J. (1986). An introduction to the European Hydrological System—Systeme Hydrologique Europeen,"SHE", 2: Structure of a physically-based, distributed modelling system. Journal of hydrology, 87(1), 61-77.

Abedin, S. J. H. (2014). GIS Framework for Spatiotemporal Mapping of Urban Flooding and Analyze Watershed Hydrological Response to Land Cover Change.

Ahmad, S., Kalra, A., & Stephen, H. (2010). Estimating soil moisture using remote sensing data: A machine learning approach. Advances in Water Resources, 33(1), 69-80.

Ahmad, S., & Prashar, D. (2010). Evaluating municipal water conservation policies using a dynamic simulation model. Water Resources Management, 24(13), 3371-3395.

Ahmad S. and Simonovic S. P. (2001), Modeling human behavior for evacuation planning: a system dynamics approach, in "Bridging the Gap", Proceedings of the ASCE world water and environmental resources congress, edt. Don Phelps and Gerald Shelke, Orlando, FL., 20 pp. https://doi.org/10.1061/40569(2001)462

Ahmad, S., & Simonovic, S. P. (2004). Spatial system dynamics: new approach for simulation of water resources systems. Journal of Computing in Civil Engineering, 18(4), 331-340.

Ahmad, S., & Simonovic, S. P. (2006). An intelligent decision support system for management of floods. Water Resources Management, 20(3), 391-410.

Ahmad, S., & Simonovic, S. P. (1999). Comparison of one-dimensional and two-dimensional hydrodynamic modeling approaches for Red river basin.

Bach, P. M., Rauch, W., Mikkelsen, P. S., McCarthy, D. T., & Deletic, A. (2014). A critical review of integrated urban water modelling–Urban drainage and beyond. Environmental Modelling & Software, 54, 88-107.

Barnes, H. H. (1967). Roughness characteristics of natural channels (No. 1849). US Govt. Print. Off.,.

Beven, K. J.(2001): Rainfall-runoff Modelling, The Primer. John Wiley&Sons Ltd, 360.

Beven, K. J., & Kirkby, M. J. (1979). A physically based, variable contributing area model of basin hydrology/Un modèle à base physique de zone d'appel variable de l'hydrologie du bassin versant. Hydrological Sciences Journal, 24(1), 43-69.

Britto, Brittany. "Heavy rains cause flash flooding across Baltimore region, stranding drivers and knocking out power to thousands". The Baltimore Sun. Retrieved 31 July 2016.

Burnash, R. J., Ferral, R. L., & McGuire, R. A. (1973). A generalized streamflow simulation system, conceptual modeling for digital computers.

Carpenter, T. M., & Georgakakos, K. P. (2006). Intercomparison of lumped versus distributed hydrologic model ensemble simulations on operational forecast scales. *Journal of Hydrology*, *329*(1), 174-185.

CCRFCD (2013). History of Flooding in Clark County. Retrieved from: http://gustfront.ccrfcd.org/pdf_arch1/Flood%20Event%20Reports/History%20of%20Flooding.pdf

Chen, J., Hill, A. A., & Urbano, L. D. (2009). A GIS-based model for urban flood inundation. *Journal of Hydrology, 373*(1), 184-192.

Chen, W., & Chau, K. W. (2006). Intelligent manipulation and calibration of parameters for hydrological models. International Journal of Environment and Pollution, 28(3-4), 432-447.

Chow, V. T. (1959). Open-channel hydraulics. McGraw-Hill, New York.

Crawford, N. H., & Linsley, R. K. (1966). Digital Simulation in Hydrology'Stanford Watershed Model 4.

Dawadi, S., & Ahmad, S. (2012). Changing climatic conditions in the Colorado River Basin: implications for water resources management. Journal of Hydrology, 430, 127-141.

Dawdy, D. R., & Vanoni, V. A. (1986). Modeling alluvial channels. Water Resources Research, 22(9S).

De Roo, A. P. J., Wesseling, C. G., & Van Deursen, W. P. A. (2000). Physically based river basin modelling within a GIS: the LISFLOOD model. Hydrological Processes, 14(11-12), 1981-1992.

Delleur, J. W. (2003). The evolution of urban hydrology: past, present, and future. Journal of hydraulic engineering, 129(8), 563-573.

Desborough, C. E., & Pitman, A. J. (1998). The BASE land surface model. Global and Planetary Change, 19(1), 3-18.

DeVantier, B. A., & Feldman, A. D. (1993). Review of GIS applications in hydrologic modeling. Journal of Water Resources Planning and Management, 119(2), 246-261.

Diskin, M. H., & Simon, E. (1979). The relationship between the time bases of simulation models and their structure. Water Resource Bulletin, Vol. 15, No. 6, pp. 1716-1732.

Ellis, J. B., & Viavattene, C. (2014). Sustainable Urban Drainage System Modeling for Managing Urban Surface Water Flood Risk. Clean–Soil, Air, Water, 42(2), 153-159.

Ewen, J., Parkin, G., & O'Connell, P. E. (2000). SHETRAN: distributed river basin flow and transport modeling system. Journal of hydrologic engineering, 5(3), 250-258.

Feyen, L., Barredo, J. I., & Dankers, R. (2009). Implications of global warming and urban land use change on flooding in Europe. Water & Urban Development Paradigms-Towards an integration of engineering, design and management approaches, 217-225.

Forsee, W. J., & Ahmad, S. (2011). Evaluating urban storm-water infrastructure design in response to projected climate change. Journal of Hydrologic Engineering, 16(11), 865-873.

Fletcher, T., & Burns, M. (2012). Urban stormwater runoff: a new class of environmental flow problem. PLoS ONE [P], 7(9), 1-10.

Freeze, R. A., & Harlan, R. L. (1969). Blueprint for a physically-based, digitally-simulated hydrologic response model. Journal of Hydrology, 9(3), 237-258.

Genovese, E. (2006). A methodological approach to land use-based flood damage assessment in urban areas: Prague case study. Technical EUR Reports, EUR, 22497.

Gomes-Pereira, L.M., Wicherson, R.J., 1999. Suitability of laser data for deriving geographical information — a case study in the context of management of fluvial zones. ISPRS Journal of Photogrammetry and Remote Sensing 54 (2–3), 105–114.

Gusev, Y. M., & Nasonova, O. N. (1998). The land surface parameterization scheme SWAP: Description and partial validation. Global and Planetary Change, 19(1), 63-86.

Hardy, R. J. (2005). Modelling granular sediment transport over water-worked gravels. Earth Surface Processes and Landforms, 30(8), 1069-1076.

Hessel, R., Jetten, V., & Guanghui, Z. (2003). Estimating Manning's n for steep slopes. Catena, 54(1), 77-91.

Hunter, N. M., Bates, P. D., Horritt, M. S., & Wilson, M. D. (2007). Simple spatially-distributed models for predicting flood inundation: a review.*Geomorphology*, *90*(3), 208-225.

Hunter, N. M., Bates, P. D., Horritt, M. S., & Wilson, M. D. (2007). Simple spatially-distributed models for predicting flood inundation: a review. Geomorphology, 90(3), 208-225.

Hunter, N. M., Horritt, M. S., Bates, P. D., Wilson, M. D., & Werner, M. G. (2005). An adaptive time step solution for raster-based storage cell modelling of floodplain inundation. Advances in Water Resources, 28(9), 975-991.

Huong, H.T.L.; Pathirana, A. Urbanization and Climate Change Impacts on Future Urban Flood Risk in Can Tho City, Vietnam. *Hydrol. Earth Syst. Sci. Discuss.* 2011, *8*, 10781–10824.

Li, J., Maddox, R. A., Gao, X., Sorooshian, S., & Hsu, K. (2003). A numerical investigation of storm structure and evolution during the July 1999 Las Vegas flash flood. Monthly weather review, 131(9), 2038-2059.

Joyce, J. M., & Scott, M. S. (2005). An assessment of Maryland's vulnerability to flood damage. Maryland Department of the Environment. Accessed October, 11, 2010.

Kale, R. V., & Sahoo, B. (2011). Green-Ampt infiltration models for varied field conditions: A revisit. Water resources management, 25(14), 3505.

Khan, S., Hong, Y., Wang, J., Yilmaz, K. K., Gourley, J. J., Adler, R. F., & Irwin, D. (2011). Satellite remote sensing and hydrologic modeling for flood inundation mapping in Lake Victoria Basin: Implications for hydrologic prediction in ungauged basins. Geoscience and Remote Sensing, IEEE Transactions on, 49(1), 85-95.

Kilgore, J. L. (1997). Development and evaluation of a GIS-based spatially distributed unit hydrograph model (Doctoral dissertation, Virginia Polytechnic Institute and State University).

Knapp, H. V., Durgunoglu, A., & Ortel, T. W. (1991). A review of rainfall-runoff modeling for stormwater management. Illinois State Water Survey.

Kouwen, N. (2009). WATFLOOD-SPL9 Hydrological Model and Flood Forecasting System-Manual. Univ. of Waterloo, Ontario, Canada.

Laurenson, E. M. and R. G. Mein, 1983. RORB — Version 3 Runoff Routing Program User Manual. Department of Civil Engineering, Monash University, Australia.

Liang, X., Lettenmaier, D. P., & Wood, E. F. (1996). One-dimensional statistical dynamic representation of subgrid spatial variability of precipitation in the two-layer variable infiltration capacity model. Journal of Geophysical Research: Atmospheres, 101(D16), 21403-21422.

Liang, X., Wood, E. F., & Lettenmaier, D. P. (1996). Surface soil moisture parameterization of the VIC-2L model: Evaluation and modification. Global and Planetary Change, 13(1-4), 195-206.

Lim, K. J., Engel, B. A., Muthukrishnan, S., & Harbor, J. (2006). Effects of initial abstraction and urbanization on estimated runoff using CN technology. JAWRA Journal of the American Water Resources Association, 42(3), 629-643.

Manning, Mary, 1999, Nevadans pleased with federal aid for flood damage: Las Vegas Sun, July 21, 1999, p. 1A, 5 A.

Marlow, Jarvis, "Taming the waters that taketh from the devil's playground: A history of flood control in Clark County, Nevada, 1955-2010" (2011). UNLV Theses/Dissertations/Professional Papers/Capstones. Paper 950

McPherson, M.B., and F.C. Zuidema. 1977. Urban Hydrological Modeling and Catchment Research: International Summary, ASCE Urban Water Resources Research Program, Technical Memorandum No. IHP-13, New York, NY.

Mein, R. G., & Larson, C. L. (1973). Reply to "Comments on 'Modeling infiltration during a steady rain'by Russell G. Mein and Curtis L. Larson". *Water Resources Research, 9*(5), 1478-1478.

Melone, F., Barbetta, S., Diomede, T., Peruccacci, S., Rossi, M., Tessarolo, A., & Verdecchia, M. (2005). Review and selection of hydrological models–Integration of hydrological models and meteorological inputs. Resulting from WP1, Action, 13.

Metacalf and Eddy, Inc., University of Florida and Water Resources Engineers, Inc., 1971. Storm water management model, Vol. 1, final report. Water Pollution Control Research Series 11024 DOC 07/71, U.S. Environmental Protection Agency, Washington, D.C.

Mitchell, V. G., & Diaper, C. (2005). UVQ: A tool for assessing the water and contaminant balance impacts of urban development scenarios. Water science and technology, 52(12), 91-98.

Moore, R. J., & Clarke, R. T. (1981). A distribution function approach to rainfall runoff modeling. Water Resources Research, 17(5), 1367-1382.

Morris, E. M. (1980). Forecasting flood flows in grassy and forested basins using a deterministic distributed mathematical model.

Mulvaney, T. J. (1851). On the use of self-registering rain and flood gauges in making observations of the relations of rainfall and flood discharges in a given catchment. Proceedings of the institution of Civil Engineers of Ireland, 4(2), 18-33.

Ntelekos, A. A., Oppenheimer, M., Smith, J. A., & Miller, A. J. (2010). Urbanization, climate change and flood policy in the United States. Climatic Change, 103(3), 597-616.

O'Donnell, T. (1966). Methods of computation in hydrograph analysis and synthesis. In Proc. Tech. Meeting no. 21, TNO (pp. 65-102).

Palacios-Vélez, O. L., Gandoy-Bernasconi, W., & Cuevas-Renaud, B. (1998). Geometric analysis of surface runoff and the computation order of unit elements in distributed hydrological models. Journal of hydrology, 211(1), 266-274.

Pereira, L. G., & Wicherson, R. J. (1999). Suitability of laser data for deriving geographical information: A case study in the context of management of fluvial zones. ISPRS Journal of Photogrammetry and Remote Sensing, 54(2), 105-114.

Pilgrim, D.H. 1986. Bridging the Gap between Flood Research and Design Practice. Water Resources Research 22 (9): 165-176.

Ponce, V. M., & Hawkins, R. H. (1996). Runoff curve number: Has it reached maturity?. Journal of hydrologic engineering, 1(1), 11-19.

Price, R. K. (2011). Urban hydroinformatics: data, models, and decision support for integrated urban water management. IWA publishing.

Purkey, B.W., Duebendorfer, E.M., Smith, E.I., Price, J.G., and Castor, S.B., 1994, Geologic tours in the Las Vegas area: Nevada Bureau of Mines and Geology Special Publication 16, 156 p.

Randerson, D. (1976). Meteorological analysis for the Las Vegas, Nevada, flood of 3 July 1975. Monthly Weather Review, 104(6), 719-727.

Rawls, W. J., Brakensiek, D. L., & Miller, N. (1983). Green-Ampt infiltration parameters from soils data. Journal of hydraulic engineering, 109(1), 62-70.

Refsgaard, J. C., & Storm, B. (1995). Mike she. Chapter 23 in computer models of watershed hydrology, 809-846. VP Singh ed. Water Resources Pub., Highlands Ranch, CO.

Rockwood, D. M. (1968). Application of Streamflow Synthesis and Reservoir Regulation-" SSARR"-Program to the Lower Mekong River. US Army Corps of Engineers.

Sagarika, S., Kalra, A., & Ahmad, S. (2014). Evaluating the effect of persistence on long-term trends and analyzing step changes in streamflows of the continental United States. Journal of Hydrology, 517, 36-53.

Salvadore, E., Bronders, J., & Batelaan, O. (2015). Hydrological modelling of urbanized catchments: A review and future directions. Journal of hydrology, 529, 62-81.

Schoenmann. Joe, 1999. Flood damage to cost millions. A government team is on its way to assess whether southern Nevada qualifies for federal disaster aid: Las Vegas Review Journal, July 9, 1999, p. 1A, 6A.

Seggelke, K., Brown, R., & Krebs, P. (2005). Integrated approaches in urban storm drainage: where do we stand? Environmental management, 35(4), 396-409.

Shafer, J. M., & Skaggs, R. L. (1983). Identification and characterization of watershed models for evaluation of impacts of climate change on hydrology (No. PNL-SA-11924). Pacific Northwest Lab., Richland, WA (USA).

Shamsi, U. M. (1996). Storm-water management implementation through modeling and GIS. Journal of Water Resources Planning and Management, 122(2), 114-127.

Sherman, L. K. (1932). Streamflow from rainfall by the unit-graph method. Eng. News Record, 108, 501-505.

Singh, V. P. (1989). Hydrologic Systems, Watershed Modeling Vol. II.

Singh, V. P. (1995). Computer models of watershed hydrology. Water Resources Publications.

Singh, V. P., & Woolhiser, D. A. (2002). Mathematical modeling of watershed hydrology. Journal of hydrologic engineering, 7(4), 270-292.

Skinner, B.J., and Porter, S.C., 1992, The dynamic Earth An introduction to physical geology, (2d ed.): John Wiley, 203 p.

Smith, B. K. (2015). Flooding and heavy rainfall in small urban watersheds (Order No. 3718567). Available from ProQuest Dissertations & Theses Global. (1716373936).

Smith, M. B. (1993). A GIS-based distributed parameter hydrologic model for urban areas. *Hydrological processes*, *7*(1), 45-61.

Song, X., Zhan, C., Kong, F., & Xia, J. (2011). Advances in the study of uncertainty quantification of large-scale hydrological modeling system. Journal of Geographical Sciences, 21(5), 801-819.

Sterman, J. D. (2000). Business dynamics: systems thinking and modeling for a complex world (No. HD30. 2 S7835 2000).

Sugawara, M. (1967). Runoff analysis and water-balance analysis by a series storage type model.

Sugawara, M. (1995). Tank model. Computer models of watershed hydrology.

Sugawara, M., Watanabe, I., Ozaki, E., & Katsugama, Y. (1984). Tank model with snow component. Research Notes of the National Research Center for Disaster Prevention No. 65. Science and Technolgoy, Ibaraki-Ken, Japan.

Sui, D. Z., & Maggio, R. C. (1999). Integrating GIS with hydrological modeling: practices, problems, and prospects. Computers, environment and urban systems, 23(1), 33-51.

Sun, Y., Solomon, S., Dai, A., & Portmann, R. W. (2007). How often will it rain?. Journal of Climate, 20(19), 4801-4818.

Todini, E. 1988. Rainfall-Runoff Modeling-Past, Present, and Future. Journal of Hydrology 100:341-352.

United Nations, 2010. World population prospects: The 2009 revision, New York, sn.

USDA (1997). Special Report: History of Flooding, Clark County, Nevada, 1905-1975. Retrieved from: http://gustfront.ccrfcd.org/pdf_arch1/Flood%20Event%20Reports/History%20of%20Flooding.pdf

Vallet, R. (1996). Habuba Kebira: ou la naissance de l'urbanisme. Paléorient, 45-76.

Venkatesan AK, Ahmad S, Johnson W and Batista JR (2011a), Salinity Reduction and Energy Conservation in Direct and Indirect Potable Water Reuse, Desalination, 272 (1-3):120-127.

Venkatesan AK, Ahmad S, Johnson W and Batista JR (2011b), System Dynamics Model to Forecast Salinity Load to the Colorado River Due to Urbanization within the Las Vegas Valley, Science of the Total Environment 409(13): 2616-2625.

Vojinovic, Z., & Seyoum, S. D. (2008). Integrated urban water systems modelling with a simplified surrogate modular approach. In 11th International Conference on Urban Drainage (pp. 1-7).

Vrugt, J. A., Gupta, H. V., Bouten, W., & Sorooshian, S. (2003). A Shuffled Complex Evolution Metropolis algorithm for optimization and uncertainty assessment of hydrologic model parameters. Water Resources Research, 39(8).

Werner, M. G. F. (2004). Spatial flood extent modelling. A performance based comparison (Doctoral dissertation, TU Delft, Delft University of Technology).

Wigmosta, M. S., Vail, L. W., & Lettenmaier, D. P. (1994). A distributed hydrology-vegetation model for complex terrain. Water resources research, 30(6), 1665-1679.

Williams, J. R., & Hann, R. W. (1972). Hymo, A problem-oriented computer language for building hydrologic models. Water Resources Research, 8(1), 79-86.

Wooding, R. A. (1965). A hydraulic model for the catchment-stream problem: I. Kinematic-wave theory. Journal of hydrology, 3(3-4), 254-267.

Wooding, R. A. (1965). A hydraulic model for the catchment-stream problem: II. Numerical solutions. Journal of hydrology, 3(3-4), 268-282.

Woolhiser, D. A., & Liggett, J. A. (1967). Unsteady, one-dimensional flow over a plane—The rising hydrograph. Water Resources Research, 3(3), 753-771.

Woodward, D. E., Hawkins, R. H., Jiang, R., Hjelmfelt, Jr, A. T., Van Mullem, J. A., & Quan, Q. D. (2003). Runoff curve number method: examination of the initial abstraction ratio. In World Water & Environmental Resources Congress 2003 (pp. 1-10).

Zhang, D., Shi, L., Chang, H., & Yang, J. (2010). A comparative study of numerical approaches to risk assessment of contaminant transport. Stochastic Environmental Research and Risk Assessment, 24(7), 971-984.

Zhao, R. J. (1977). Flood forecasting method for humid regions of China. East China College of Hydraulic Engineering, Nanjing, China.

CURRICULUM VITAE

Graduate College

University of Nevada, Las Vegas

Roshan Poudel

Degrees:

Bachelor of Science, Civil Engineering (Specialization: Hydropower),

2013

Kathmandu University, Nepal

Thesis Title:

SURFACE HYDROLOGIC MODELING AND ANALYZING

WATERSHED HYDROLOGICRESPONSE TO LANDCOVER

CHANGE

Thesis Examination Committee:

Chairperson, Dr. Haroon Stephen, Ph. D

Committee Member, Dr. Sajjad Ahmad, Ph. D

Committee Member, Dr. Jacimaria Batista, Ph. D

Graduate Faculty Representative, Dr. Ashok Singh, Ph. D